INORGANIC-ORGANIC HYDROGEL SCAFFOLDS FOR TISSUE ENGINEERING

A Dissertation

by

BRENNAN MARGARET BAILEY

Submitted to the Office of Graduate Studies of
Texas A&M University
in partial fulfillment of the requirements for the degree of

DOCTOR OF PHILOSOPHY

Chair of Committee,	Melissa A. Grunlan
Committee Members,	Elizabeth Cosgriff-Hernandez
	Mariah Hahn
	Mike McShane
Chair of Materials Science and Engineering Faculty,	Ibrahim Karaman

August 2013

Major Subject: Materials Science and Engineering

ABSTRACT

Analogous to the extracellular matrix (ECM) of natural tissues, properties of a tissue engineering scaffold direct cell behavior and thus regenerated tissue properties. These include both physical properties (e.g. morphology and modulus) and chemical properties (e.g. hydrophobicity, hydration and bioactivity). Notably, recent studies suggest that scaffold properties (e.g. modulus) may be as potent as growth factors in terms of directing stem cell fate. Thus, 3D scaffolds possessing specific properties modified for optimal cell regeneration have the potential to regenerate native-like tissues. Photopolymerizable poly(ethylene glycol) diacrylate (PEG-DA)-based hydrogels are frequently used as scaffolds for tissue engineering. They are ideal for controlled studies of cell-material interactions due to their poor protein adsorption in the absence of adhesive ligands thereby making them "biological blank slates". However, their range of physical and chemical properties is limited. Thus, hydrogel scaffolds which maintain the benefits of PEG-DA but possess a broader set of tunable properties would allow the establishment of predictive relationships between scaffold properties, cell behavior and regenerated tissue properties.

Towards this goal, this work describes a series of unique hybrid inorganic-organic hydrogel scaffolds prepared using different solvents and also in the form of continuous gradients. Properties relevant to tissue regeneration were investigated including: swelling, morphology, modulus, degradation rates, bioactivity, cytocompatibility, and protein adhesion. These scaffolds were based on the

incorporation of hydrophobic, bioactive and osteoinductive methacrylated star polydimethylsiloxane ($PDMS_{star}$-MA) ["inorganic component"] into hydrophilic PEG-DA ["organic component"]. The following parameters were varied: molecular weight (M_n) of PEG-DA (M_n = 3k & 6k g/mol) and $PDMS_{star}$-MA (M_n = 1.8k, 7k, 14k), ratio of $PDMS_{star}$-MA to PEG-DA (0:100 to 20:80), total macromer concentration (5 to 20 wt%) and utilizing either water or dichloromethane (DCM) fabrication solvent. The use of DCM produced solvent induced phase separation (SIPS) resulting in scaffolds with macroporous morphologies, enhanced modulus and a more homogenous distribution of the $PDMS_{star}$-MA component throughout. These hybrid hydrogel scaffolds were prepared in the form of continuous gradients such that a single scaffold contains spatially varied chemical and physical properties. Thus, cell-material interaction studies may be conducted more rapidly at different "zones" defined along the gradient. These gradients are also expected to benefit the regeneration of the osteochondral interface, an interfacial tissue that gradually transitions in tissue type. The final aspect of this work was focused on enhancing the osteogenic potential of PDMS via functionalization with amine and phosphonate. Both amine and phosphonate moieties have demonstrated bioactivity. Thus, it was expected that these properties will be enhanced for amine and phosphonate functionalized PDMS. The subsequent incorporation of these PDMS-based macromers into the previously described PEG-DA scaffold system is expected to be valuable for osteochondral tissue regeneration.

DEDICATION

To My Parents

Times in my life when I have felt inadequate for the objectives set before me you have provided wisdom and encouraged me towards completion and success.

ACKNOWLEDGEMENTS

First, I would like to acknowledge and thank my committee chair, Dr. Melissa Grunlan, for her guidance throughout both my undergraduate and graduate studies. It is a result of her enthusiastic interest in polymeric biomaterials that I originally took notice of and had the opportunity to perform research in this area. Specifically, I would like to thank her for the opportunities she has provided for me, assuring me I was capable of completing the research herein, and encouraging me towards a successful career in biomaterials research.

Next, I would like to thank my committee members, Dr. Elizabeth Cosgriff-Hernandez, Dr. Mariah Hahn, and Dr. Mike McShane for their guidance and support throughout the course of this research. I genuinely appreciate the countless letters of recommendation, the time spent listening to presentations and reading through proposals, and the numerous words of encouragement.

I want to thank my family and friends for enduring many frustrating times and creating many fun memories with me throughout my studies and my life. I would also like to thank my colleagues and the department faculty and staff for making my time at Texas A&M University a great experience. Financial support from the Office of Graduate Studies Dissertation Fellowship is also gratefully acknowledged.

Dany Munoz-Pinto and Mariah Hahn are acknowledged for the LDH assay studies, cytocompatibility and cell adhesion and spreading studies.

Funding from NIH/NIBIB (1R03EB015202) NIH/NIBIB (1R21HL089964-01) is gratefully acknowledged. FESEM acquisition was supported by the National Science Foundation (DBI-0116835), the Vice President for Research (VPR) Office, and the Texas Engineering and ExperimentStation (TEES).

TABLE OF CONTENTS

Page

ABSTRACT ii

DEDICATION iv

ACKNOWLEDGEMENTS v

TABLE OF CONTENTS vii

LIST OF FIGURES ix

LIST OF TABLES xiii

CHAPTER I INTRODUCTION 1

1.1. Background 1
1.2. Approach 5
1.3. Innovation 11

CHAPTER II TUNING PEG-DA HYDROGELS VIA SOLVENT-INDUCED PHASE SEPARATION (SIPS) 14

2.1. Overview 14
2.2. Introduction 15
2.3. Materials and Methods 18
2.4. Results and Discussion 22
2.5. Conclusions 29

CHAPTER III $PDMS_{star}$-PEG HYDROGELS PREPARED VIA SOLVENT-INDUCED PHASE SEPARATION (SIPS) AND THEIR POTENTIAL UTILITY AS TISSUE ENGINEERING SCAFFOLDS 31

3.1. Overview 31
3.2. Introduction 32
3.3. Materials and Methods 36
3.4. Results and Discussion 45
3.5. Conclusions 60

CHAPTER IV CONTINUOUS GRADIENT SCAFFOLDS FOR RAPID SCREENING OF CELL-MATERIAL INTERACTIONS AND INTERFACIAL TISSUE REGENERATION 62

4.1. Overview 62
4.2. Introduction 65
4.3. Materials and Methods 68
4.4. Results and Discussion 72
4.5. Conclusions 83

CHAPTER V SYNTHESIS OF AMINATED AND PHOSPHONATED POLY(DIMETHYL SILOXANE) METHACRYLATE FOR ENHANCED BIOACTIVITY AND OSTEOINDUCTIVITY 85

5.1. Introduction 85
5.2. Materials and Methods 88
5.3. Results and Discussion 91
5.4. Conclusions 92

CHAPTER VI CONCLUSIONS AND FUTURE DIRECTIONS 94

6.1. Conclusions 94
6.2. Future Directions 96

REFERENCES 102

APPENDIX 122

LIST OF FIGURES

Page

Figure 1.2. Scaffolds fabricated herein contain a broad range of spatially varied chemical and physical properties and thus, will be beneficial towards the rapid assessment of cell-material interactions and the ultimate regeneration of interfacial tissues. 6

Figure 2.1. Reported hydrogel fabrication via SIPS and resulting enhanced porous structure. 14

Figure 2.2. Macroscopic images of conventional PEG-DA hydrogels fabricated from an aqueous precursor solution [left] and PEG-DA hydrogels fabricated via SIPS with a DCM precursor solution (and subsequently dried and hydrated) [right]. (PEG-DA: M_n = 6k g/mol; 10 wt% concentration). 22

Figure 2.3. SEM images of PEG-DA hydrogels fabricated via SIPS. (Scale bars = 100 μm).....24

Figure 2.4. Swelling ratio of PEG-DA hydrogels fabricated with 3.4k g/mol (left) and 6k g/mol (right) PEG-DA from a DCM precursor solution (i.e. via SIPS) or from an aqueous precursor solution. Statistical significance was determined by student‟s t-test where (*): $p < 0.05$ and (#): $p > 0.05$. 26

Figure 2.5. Storage modulus of PEG-DA 3k g/mol (left) and PEG-DA 6k g/mol (right) fabricated in either DCM or H_2O at various wt% concentrations. 27

Figure 2.6. Swelling ratio as a function of degradation time under basic conditions (0.05 M NaOH) of PEG-DA hydrogels fabricated with 3.4k g/mol (left) and PEG-DA 6k g/mol (right) via SIPS at various wt% concentrations. [ ] = hours to complete dissolution. ( ) = hours to complete dissolution for analogous conventional hydrogels (i.e. prepared from aqueous precursor solutions).....29

Figure 3.1. Reported $PDMS_{star}$-PEG hydrogel fabrication via SIPS and resulting dissolution and distribution of PDMS. 32

Figure 3.2. Precursor solutions [top] and corresponding hydrogels [bottom] formed from an aqueous precursor solution (left) and via SIPS (right) (i.e. with a DCM precursor solution followed by subsequent drying and hydration) with 6k g/mol PEG-DA.....46

Figure 3.3. SEM images of $PDMS_{star}$-PEG hydrogels fabricated via SIPS. (scale bars = 50 μm).....48

Figure 3.4. CLSM images of hydrated $PDMS_{star}$-PEG hydrogels prepared with different wt% ratios of $PDMS_{star}$-MA:PEG-DA from a DCM precursor solution (i.e. via SIPS). PDMS-enriched regions stained with hydrophobic dye (Nile Red). (scale bars = 250 μm) 49

Figure 3.5. Swelling ratio of $PDMS_{star}$-PEG hydrogels fabricated with 3.4k g/mol (left) and 6k g/mol (right) PEG-DA from a DCM precursor solution (i.e. via SIPS) or from an aqueous precursor solution. Statistical significance was determined by student‟s t-test where (*): $p < 0.05$ and (#): $p > 0.05$.....51

Figure 3.6. Storage modulus (G‟) of $PDMS_{star}$-PEG hydrogels fabricated with 3.4k g/mol (left) and 6k g/mol (right) from a DCM precursor solution (i.e. via SIPS) [solid lines] or from an aqueous precursor solution [dashed lines]. 52

Figure 3.7. Swelling ratio under basic conditions (0.05 M NaOH) of $PDMS_{star}$-MA:PEG-DA hydrogels fabricated via SIPS with 3.4k g/mol (left) and 6k g/mol (right) PEG-DA. [ ] = hours to complete dissolution and ( ) = hours to complete dissolution of analogous hydrogel (i.e. fabricated from aqueous precursor solutions).....54

Figure 3.8. Swelling ratio under basic conditions (0.05 M NaOH) of $PDMS_{star}$-MA:PEG-DA hydrogels fabricated via SIPS with 3.4k g/mol (left) and 6k g/mol (right) PEG-DA. ( ) = hours to complete dissolution. 54

Figure 3.9. SEM images (following exposure to SBF for 2 weeks) of hydrogels fabricated with either 3.4k (top) or 6k g/mol (bottom) PEG-DA from a DCM precursor solution (i.e. via SIPS) with (right column) and without PDMS (left column) (scale bars = 50 μm). 56

Figure 3.10. X-ray Diffraction of PDMS:PEG (3.4k and 6k g/mol) hydrogels soaked in SBF - revealing the formation of HAp within hydrogels when PDMS is incorporated (dotted line) and absence of HAp when no PDMS is incorporated (solid line). 56

Figure 3.11. Cell spreading for PDMS-PEG hydrogels prepared without [top] and with [bottom] RGDS (cell-adhesive peptide). PEG Control = PEG-DA hydrogel (3.4k g/mol) prepared from an aqueous precursor solution. [Scale bars = 50 μm].....59

Figure 3.12. Relative LDH activity (24 hr) of $PDMS_{star}$-PEG hydrogels fabricated with 3.4k g/mol PEG-DA from a DCM precursor solution (i.e. via SIPS) with varying wt% ratio $PDMS_{star}$-MA:PEG-DA. PEG Control = PEG-DA hydrogel (3.4k g/mol) prepared from an aqueous precursor solution. All formulations were statistically similar versus each other (ANOVA, $p < 0.05$). 60

Figure 4.1. Gradient fabrication and compositions. The fabrication method (top) and eight resulting scaffolds possessing continuous gradients (bottom) based on a gradual transition in: (a) the wt% ratio of $PDMS_{star}$-MA to PEG-DA macromers, (b) the total wt% macromer concentration, (c) the M_n of PEG-DA and (d) the M_n of $PDMS_{star}$-MA. A constant wt% ratio of $PDMS_{star}$-MA to PEG-DA was maintained for b-d. Each scaffold was fabricated in both DI-H_2O and DCM to vary PDMSstar-MA distribution, scaffold porosity and modulus. Note, when fabricated from a DCM precursor solution, the resulting network was dried (i.e. DCM removal) and hydrated with water before testing. 64

Figure 4.2. Properties of PDMSstar:PEG gradient scaffolds. These scaffolds (depicted in Figure 4.1.a) were formed with a gradual transition from high (top) to low (bottom) amounts of $PDMS_{star}$-MA using both DI-H_2O and DCM as the fabrication solvent. The total macromer concentration (10 wt%) and M_n of both $PDMS_{star}$-MA (7k g/mol) and PEG-DA (3.4k g/mol) were held constant. For gradient scaffolds prepared from an aqueous and DCM precursor solution, respectively: (a, e) CLSM images of $PDMS_{star}$-MA distribution and scaffold porosity, (b, f) SEM images of HAp formation following exposure to SBF (i.e. "bioactivity") and (c, d) swelling and modulus. 76

Figure 4.3. Right: SEM of HAp formation on (a) $PDMS_{star}$:PEG gradient (fabricated in DI-H_2O); zone 1 and (b) PEG-DA M_n gradient (fabricated in DI-H_2O); zone 4. Left: XRD of "a" and "b" exhibit characteristic HAp peaks of 31.7, 45.5, and 56.5. 77

Figure 4.4. Properties of total wt% macromer concentration gradient scaffolds. These scaffolds (depicted in Figure 4.1.b) were produced with a gradual transition from low (top) to high (bottom) total wt% macromer concentrations. A constant 9:91 wt% ratio of $PDMS_{star}$-MA (7k g/mol) to PEG-DA (3.4k g/mol) was maintained. For gradient scaffolds prepared from an aqueous and DCM precursor solution, respectively: (a, e) CLSM images of $PDMS_{star}$-MA distribution and scaffold porosity, (b, f) SEM images of HAp formation following exposure to SBF (i.e. "bioactivity") and (c, d) swelling and modulus 79

Figure 4.5. Properties of PEG-DA M_n gradient scaffolds. These scaffolds (depicted in Figure 4.1.c) were produced with a gradual transition from low (3.4k g/mol) (top) to high (6k g/mol) (bottom) PEG-DA M_n with a constant 9:91 wt% ratio of $PDMS_{star}$-MA (7k g/mol) to PEG-DA. For gradient scaffolds prepared from an aqueous and DCM precursor solution, respectively: (a, e) CLSM images of $PDMS_{star}$-MA distribution and scaffold porosity, (b, f) SEM images of HAp formation following exposure to SBF (i.e. "bioactivity") and (c, d) swelling and modulus. 81

Figure 4.6. Properties of $PDMS_{star}$-MA M_n gradient scaffolds. These scaffolds (depicted in Figure 4.1.d) were produced with a gradual transition from low (top) to high (bottom) $PDMS_{star}$-MA M_n with a constant 9:91 wt% ratio of $PDMS_{star}$-MA to PEG-DA (3.4k g/mol). For gradient scaffolds prepared from an aqueous and DCM precursor solution, respectively: (a, e) CLSM images of $PDMS_{star}$-MA distribution and scaffold porosity, (b, f) SEM images of HAp formation following exposure to SBF (i.e. "bioactivity") and (c, d) swelling and modulus. 83

Figure 5.1. Amine and phosphonate functionalized PDMS-MA described herein for subsequent incorporation into PEG-DA hydrogels towards enhanced bioactivity and osteoinductivity of tissue engineering scaffolds. 88

Figure 5.2. (a) Platinum catalyzed hydrosilylation of D_4^{H1} with allyl amine to yield D_4^{NH2} and (b) base catalyzed ring opening polymerization of D_4^{NH2} to yield silane terminated, amine functionalized PDMS ($Poly(D_4^{NH2})$). 90

Figure 6.1. Methacrylated $Poly(D_4^{NH2})$ and $Poly(D_4^{P})$ can be subsequently incorporated into the "gradient platform technology" established in Chapter IV allowing for rapid screening and potentially the fabrication of more native-like osteochondral interface. Amine and phosphonate moieties on PDMS are expected to enhance properties of PEG-DA hydrogel scaffolds, including bioactivity. 97

Figure 6.2. Hydrosilylation of D_4^{NH2} with allyl methacrylate to yield an amine functionalized polymer capable of photo-crosslinking into a PEG-DA hydrogel scaffold. 98

Figure 6.3. (a) Platinum catalyzed hydrosilylation of $Poly(D_4^{NH2})$ with DEVP to yield a phosphonate functionalized polymer and (b) platinum catalyzed hydrosilylation of $Poly(D_4^{P})$ to yield a phosphonate functionalized polymer capable of photo-crosslinking within a PEG-DA hydrogel. 100

LIST OF TABLES

Page

Table 3.1. Sol Content of SIPS and analogous conventional hydrogels. 47

Table 3.2. Hydrogel Swelling Ratio and Adsorption of BSA Protein. 50

CHAPTER I

INTRODUCTION

1.1. Background

1.1.1. Osteochondral Defects

Osteochondral Defects (OCDs) are areas of joint damage affecting both the cartilage and underlying subchondral bone (**Figure 1.1**) [1, 2]. These defects, which can result from injury and/or disease often lead to excruciating pain and an advanced form of osteoarthritis [1, 3-6].

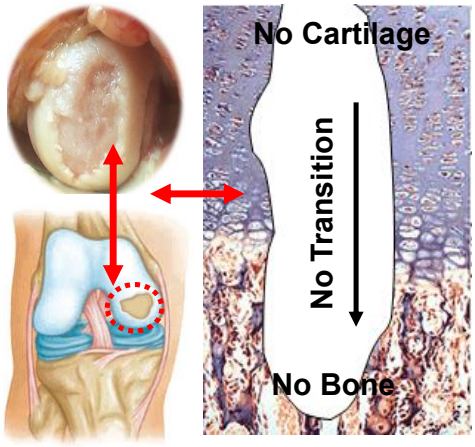

Figure 1.1. Osteochondral defects are characterized by a loss of bone and cartilage tissue as well as the transition between these tissues. These defects (shown here in the medial femoral condyle) are both painful and progressive.

A common example of an OCD resulting from injury is "post-traumatic osteoarthritis" which affects approximately 5.6 million people in the United States

across all age groups [7-14]. OCDs in younger patients present an exceptionally difficult clinical problem due to the undesirable utilization of treatments such as joint replacement or joint fusion which limit activity [15, 16]. This is also the case for OCDs resulting from osteochondral dissecans (i.e. disease) and sickle cell disease,[17] where the majority of those affected are physically active adolescents [18]. Osteochondral dissecans is a disease resulting in the deterioration of articular cartilage and thus a loss of lubrication and support in the joint. Cartilage is avascular and has poor intrinsic healing capabilities; therefore, loss of the cartilage-bone interface within a joint will lead to further bone deterioration, agonizing pain, and potentially osteoarthritis [19, 20]. Noting the prevalence of OCDs, the inability of cartilage to naturally repair, and the problems associated with long-term presence of these defects, the definite need for an osteochondral defect replacement or treatment option can be seen.

1.1.2. Current Treatments of OCDs

Smaller OCDs across articular cartilage-bone interface are generally treated by arthroscopic drilling, abrasion, or microfracturing [20, 21]. However, these mainly produce fibrocartilage at the defect site which is biomechanically inferior to articular cartilage and thus deteriorates over time [20, 22, 23]. Much research has focused on new techniques that fill defects with tissues that more closely mimic native osteochondral tissue. These treatments include autograft procedures,[24-27] such as the osteochondral autograft transfer system (OATS), where osteochondral cylindrical plugs are removed from a joint area of minor load and press-fitted into pre-drilled holes at the defect site

[28]. Another common autograft treatment involves periosteal/perichondrial transplantation to full-thickness defects [29]. However, autografts are limited in supply and often result in severe donor site morbidity, as well as graft delamination and endochondral ossification. The alternative use of allografts often results in failure due to infection and rejection [30-33]. Another treatment option is joint fusion, where pieces of bone or metal implants are used to stimulate fusion of the bones. However, this limits motion and is prone to infection and ultimately deterioration [34]. "Autologous chondrocyte transfer" (ACT) is another biological approach based on the implantation of a suspension of cultured autologous chondrocytes beneath a tightly sealed periosteal flap [35-37]. However, the use of ACT carries a number of limitations, essentially related to the complexity of the surgical procedure and the biological response of the periosteum [38-40]. Due to the limitations associated with the aforementioned treatments, OCDs ultimately necessitate replacement of the entire joint. Annually in the US, >500,000 total knee replacements (TKRs) are performed at a cost of >$11 billion [41, 42]. Despite it"s prevelence, TKR is generally not effective as it results in chronic knee pain and stiffness, bleeding into the knee joint, and nerve damage and is also quite costly [42-47]. In general, current biological and replacement treatments show limited success as they do not consistently result in long-term repair.

1.1.3. Tissue Engineering of OCDs

Tissue engineering is an alternative approach for OCD repair that may avoid many of the limitations associated with current treatments [48]. A three-dimensional

scaffold is utilized to create an environment in which living cells can proliferate, differentiate, and ultimately produce a new extracellular matrix (ECM) [49]. Specifically, it has been shown that through defined scaffold cues, MSCs are able to acquire characteristics of cells derived from embryonic mesoderm, including osteoblasts (bone cells) and chondrocytes (cartilage cells) [50-52]. Regeneration of interfacial tissues is particularly complex. Conventionally, regeneration of the osteochondral interface has been attempted by connecting (via fibrin glue, sutures, or press fitting) two compositionally homogenous scaffolds designed to individually promote either bone or cartilage tissue growth [53-58]. However, the resulting individual tissues are not mechanically representative of the respective native tissues [59]. Finally, the inability of the scaffold to securely bind to the defect site results in a lack of cell infiltration and ultimate graft delamination [60, 61]. Thus, an improved approach to regenerate the osteochondral interface in which the engineered bone and cartilage tissues are joined via an interface characterized by a gradual transition in properties and interpenetration is necessary.

Natural and synthetic polymers have been used to construct scaffolds for tissue engineering [62-64]. One major advantage that synthetic polymers have over natural polymers is their ability to offer superior control and range of chemical and physical properties [65-67]. The use of synthetic hydrogels as tissue engineering scaffolds has been the subject of extensive research [67-69]. Hydrogels are highly hydrated polymer networks consisting primarily of hydrophilic polymers which are crosslinked through chemical bonds or physical interactions [70-73]. Hydrogels are ideal for use as tissue

engineering scaffolds due to their superior biocompatibility which minimizes inflammation, thrombosis, and tissue damage, as well as their high diffusivity and elasticity which is analogous to many tissues [67-69]. It has been found that non-specific chemical and physical properties of scaffolds directly influence the properties (e.g. mechanical) of the regenerated tissue [74]. Altering the chemical nature of the scaffold, (e.g. bioactivity, chemical functionality, and hydrophilicity [75, 76]) as well as physical properties (e.g. scaffold morphology [77-84] and modulus [74, 85-87]) is known to influence cell behavior. Thus, a hydrogel scaffold that guides cellular behavior by nature of its physical and chemical properties could be designed to produce a gradual transition in regenerative tissue properties as an effective tool for tissue engineering the osteochondral interface.

1.2. Approach

1.2.1. Overview

The two main obstacles hindering the regeneration of a native-like osteochondral interface are (1) deficient knowledge of the optimal scaffold properties which independently promote the regeneration of native-like bone and cartilage tissue and (2) the lack of a gradual transition and integration between these tissues. It is hypothesized that these challenges will be addressed by the inorganic-organic hydrogel scaffolds reported herein.

Herein, a series of "hybrid" 3D hydrogel scaffolds were prepared based on combining an inorganic and organic macromer and using both aqueous and organic

fabrication solvents. Scaffold physical and chemical properties were controlled by altering molecular weight (M_n) of PEG-DA (M_n = 3k & 6k g/mol) and $PDMS_{star}$-MA (M_n = 1.8k, 7k, 14k), ratio of $PDMS_{star}$-MA to PEG-DA (0:100 to 20:80), total macromer concentration (5 to 20 wt%) and utilizing either water (DI-H_2O) or dichloromethane (DCM) as the fabrication solvent. The subsequent preparation of these hybrid hydrogel scaffolds in the form of continuous gradients will allow for rapid assessment of cell-material interactions and is also expected to benefit the regeneration of interfacial tissues which gradually transition between tissue types (**Figure 1.2**). The final aspect of this work was focused on the functionalization of a PDMS macromer with phosphonate and amine groups towards enhancing PEG-DA scaffold bioactivity and osteoinductivity.

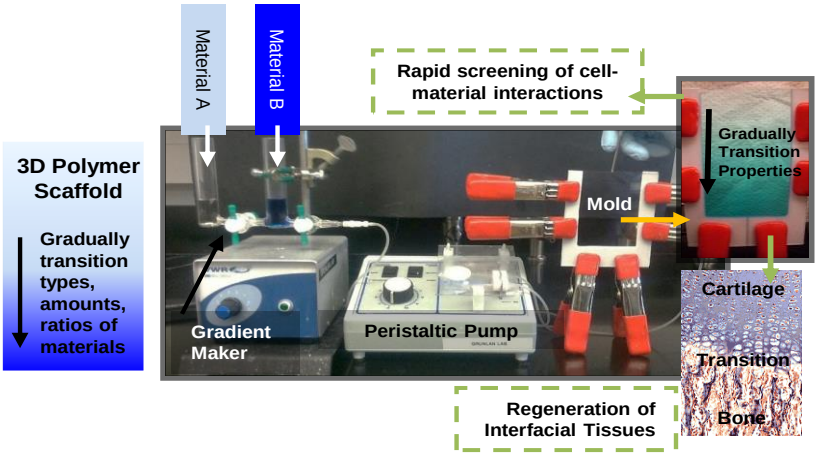

Figure 1.2. Scaffolds fabricated herein contain a broad range of spatially varied chemical and physical properties and thus, will be beneficial towards the rapid assessment of cell-material interactions and the ultimate regeneration of interfacial tissues.

1.2.2. PEG-DA Hydrogels as Tissue Engineering Scaffolds

The resistance to protein and cell adhesion of PEG-DA hydrogels in the absence of precisely introduced adhesive ligands makes them particularly useful to study cell-material interactions [88-92]. However, their range of physical, as well as chemical properties is limited, thus restricting their utility for such studies. Accordingly, the aim of the research herein is the fabrication of a series of hydrogel scaffolds which maintain the benefits of PEG-DA but possess a broader range of tunable properties. In addition, a method to gradually transition these properties within a single hydrogel scaffold is presented. These gradient scaffolds will allow for a more rapid assessment of the relationship between scaffold properties, cell behavior and regenerated tissue properties. The ability to gradually transition the properties of a single scaffold is also expected to benefit the regeneration of the osteochondral interface, an interfacial tissue that gradually transitions in tissue type.

1.2.3. Modification of PEG-DA Hydrogel Properties via Solvent Induced Phase Separation (SIPS)

An organic fabrication solvent was employed as a tool to extend the physical properties of PEG-DA hydrogels [93]. Using a solvent-based precursor solution in substitution of the conventional aqueous precursor solution has been reported to promote a phase separation of the growing polymer chains during photocure. This results in polymer rich networks surrounding polymer lean domains (i.e. pores) [93-95] and thus a macroporous morphologies. Macroporous hydrogels have shown particular utility to

enhance tissue engineering outcomes [79, 82, 84, 96, 97]. Furthermore, increased pore size has been shown to enhance degradation rates [98]. Thus, pore size can be used to design scaffolds that ideally degrade at a rate corresponding with tissue regeneration [99]. Thus, PEG-DA hydrogels prepared via SIPS exhibited macroporous morphologies [93, 100]. In addition, SIPS resulted in increased modulus but did not necessarily effect total swelling compared to analogous water-fabricated hydrogels. Thus, within this library of scaffolds pairs of hydrogels were identified whose modulus and hydration or morphology and hydration were uncoupled. Such scaffolds would permit independent study of these properties on cell behavior. Furthermore, the tunable porosity, modulus and degradation rates of these scaffolds are expected to enhance their utility as environments for tissue regeneration as well as provide a means to study these effects on cell behavior.

1.2.4. Modification of PEG-DA Hydrogel Properties via Incorporation of Methacrylated Star Poly(dimethyl siloxane) ($PDMS_{star}$-MA)via SIPS

Inorganic, hydrophobic $PDMS_{star}$-MA was incorporated into organic PEG-DA hydrogel scaffolds to extend the range of physical properties and chemical properties [100]. This was expected given the unique properties of $PDMS_{star}$-MA: (1) low glass transition temperature (Tg = -127 ˚C), (2) hydrophobicity and (3) inorganic nature.

When incorporated into a PEG-DA hydrogel, the flexibility of low T_g $PDMS_{star}$-MA is expected to alter mechanical properties. The hydrophobicity of $PDMS_{star}$-MA renders it insoluble in H_2O but soluble in DCM such that fabrication via SIPS alters its

distribution throughout the PEG-DA matrix [100, 101]. In addition, scaffold hydrophobicity has also been shown to influence osteogenic differentiation [102-104]. Previous studies have demonstrated that the incorporation of inorganic silicon-containing materials into organic scaffolds enhances their bioactivity [105-107]. Munoz-Pinto et al. demonstrated that $PDMS_{star}$-PEG scaffolds guide mesenchymal stem cells toward osteogenic differentiation with increased amounts of the bone cell marker, osteocalcin being observed with increased amounts of $PDMS_{star}$-MA [108]. Thus, $PDMS_{star}$-PEG hydrogels prepared via SIPS can be used to alter scaffold physical and chemical properties including modulus and osteoinductivity.

1.2.5. Fabrication of $PDMS_{star}$-PEG Hydrogels as Continuous Gradients

These hybrid $PDMS_{star}$-PEG hydrogels were then fabricated in the form of continuous gradients (such that a single scaffold contains spatially varied chemical and physical properties) in both DI-H_2O and DCM (**Figure 1.2**) [109]. Three-dimensional continuous gradients have been reported [110-113]. Recently, Chatterjee and co-workers used a gradient maker to produce continuous gradient hydrogel scaffolds based on an organic macromer [poly(ethylene glycol)-diacrylate, PEG-DA] and an aqueous fabrication solvent [114]. In this study, this method has been applied to prepare "hybrid" continuous gradient hydrogel scaffolds based on combining an inorganic and organic macromer and using both aqueous and organic fabrication solvents. Their rapid production and achievable range of properties not only allow for rapid screening of cell-material interactions, but would also prove useful towards the regeneration of interfacial

tissues which require scaffolds comprised of spatially organized material compositions [114, 115]. Given the bioactivity and osteoinductivity of $PDMS_{star}$-MA, these hybrid scaffolds are of particular interest for bone and osteochondral tissue engineering.

1.2.6. Chemical Functionalization of PDMS towards Enhanced Bioactivity and Ostoeinductivity

The final aspect of this work is focused on further enhancing the bioactivity and osteoinductivity of PDMS macromer via functionalization with amine and phosphonate groups. Well-defined (2D) models have been used to study the effects of amine and phosphonate on cell behavior [116-119]. Keselowsky et al. demonstrated that surfaces grafted with amine groups up-regulated osteoblast-specific gene expression, alkaline phosphatase enzymatic activity, and matrix mineralization [117]. The positive charge on these functional groups at neutral pH may explain this phenomenon [117]. Increasing phosphonate content of graft copolymers on the surface of biomaterials increased osteoblast-like cell adhesion and proliferation [120]. Also, the addition of pendant phosphorous-containing groups to polymers has shown to result in more complete mineralization and at a faster rate *in vitro* [121, 122]. Phosphorous-based scaffolds are of particular interest for bone tissue regeneration given the ideal osteoinductive environment they are able to provide [123-125]. Saltzman et al. found that the adhesion and growth of osteoblast-like cells within acrylamide gels increased with increasing phosphonate content [123]. While, Anseth et al. incorporated pendant phosphate groups

into PEG hydrogels and found that this increased both the rate and degree of mineralization within the hydrogel even in the absence of hMSCs [126].

Thus, it was hypothesized that amine and phosphonate functionalized PDMS will exhibit enhanced bioactivity and osteoinductivity. The subsequent incorporation of these PDMS-based macromers into the previously described PEG-DA scaffold system is expected to provide a method to study their effect on cell behavior in a 3D environment. These scaffolds are also anticipated to be valuable for osteochondral tissue regeneration.

1.3. Innovation

1.3.1. Manipulation of PEG-DA Hydrogel Properties via SIPs and PDMS$_{star}$

Grunlan and co-workers were the first to incorporate PDMS$_{star}$-MA into PEG-DA hydrogel scaffolds [127]. These were limited to those prepared with an aqueous precursor solution and prepared as "single composition" hydrogels. Munoz-Pinto et al. demonstrated that these scaffolds guide MSCs toward osteogenic differentiation with increased amounts of the bone cell marker, osteocalcin being observed with increased amounts of PDMS $_{star}$-MA [108]. Unique to the proposed research is the use of SIPS to fabricate PEG and PDMS$_{star}$-PEG hydrogel scaffolds with macroporous morphologies and controlled distribution of the inorganic component. Until now, SIPS has only been utilized to prepare macroporous poly(*N*-isopropylacrylamide) (PNIPAAm) hydrogels [94, 95]. Macroporous hydrogels have shown particular utility to enhance tissue engineering outcomes as they allow for cell ingrowth and enhanced degradation rates [79, 82, 84, 96-98]. However, conventional PEG-DA hydrogels (i.e. fabricated by the

photopolymerization of aqueous precursor solutions) are generally limited in their size and amount of native pores (i.e. approximately 5–10 μm pore size for a M_n = 3.4k to 6k),[128] whereas a pore size of 100-250 μm is considered ideal for bone tissue regeneration [129, 130]. In addition to producing macropores, SIPS alters the distribution of the inorganic, hydrophobic $PDMS_{star}$-MA due to its improved solubility in DCM versus water. As $PDMS_{star}$-MA is bioactive and osteoinductive, its controlled redistribution within the PEG-DA matrix is significant. The homogeneous redistribution is also expected to alter the way in which $PDMS_{star}$-MA impacts scaffold physical properties due to the distinct properties it possesses (i.e. low T_g, hydrophobic, inorganic).

1.3.2. Fabrication of $PDMS_{star}$-PEG Scaffolds as Continuous Gradients

Novel gradient hydrogel scaffolds were subsequently fabricated based on the wt% ratio of the $PDMS_{star}$-MA to PEG-DA macromer, the total wt% concentration of macromer in the precursor solution (water or DCM), and the molecular weight (M_n) of both PEG-DA and $PDMS_{star}$-MA. A previously reported continuous gradient making strategy was utilized to rapidly prepare scaffolds with gradually transitioning chemical and physical properties that will be subsequently characterized [114]. The approach presented herein offers a method for the systematic and rapid examination of scaffold-mediated MSC response over a broad range of properties, as well as, a method for the regeneration of a native-like osteochondral interface.

1.3.3. Phosphonate and Amine Functionalized PDMS-MA

Much research has revealed the osteoinductivity and/or bioactivity of silicon [102-104], phosphonates [116, 121, 125] and amines [117, 118]. Herein, amine functionalized PDMS macromer were prepared. Also, a rational and protocol were given for the synthesis of phosphonate functionalized PDMS. Their subsequent methacrylation will allow for incorporation into PEG-DA hydrogel scaffolds via photo-crosslinking. It is expected that these novel macromers combined with previously described fabrication processes (i.e. SIPS and continuous gradients) will provide a platform for the rapid assessment of a broad range of properties. These studies are anticipated to result in the establishment of an ideal environment for bone, cartilage, and bone – cartilage interfacial tissue regeneration.

CHAPTER II

TUNING PEG-DA HYDROGEL PROPERTIES VIA SOLVENT-INDUCED PHASE SEPARATION (SIPS)*

2.1. Overview

Poly(ethylene glycol) diacrylate (PEG-DA) hydrogels are widely utilized to probe cell-material interactions and ultimately for a material-guided approach to tissue regeneration. In this study, PEG-DA hydrogels were fabricated via solvent-induced phase separaration (SIPS) to obtain hydrogels with a broader range of tunable physical properties including morphology (i.e. porosity), swelling and modulus (G,,) (**Figure 2.1**).

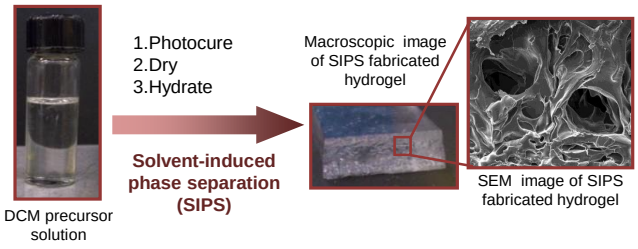

Figure 2.1. Reported hydrogel fabrication via SIPS and resulting enhanced porous structure.

*Reprinted with permission from "Tuning PEG-DA hydrogel properties via solvent-induced phase separation (SIPS)" by Bailey BM, Hui V, Fei R, Grunlan MA, 2011. J Mater Chem, 21, 18776-82, Copyright [2011] by The Royal Society of Chemistry. **http://pubs.rsc.org/en/content/articlelanding/2011/JM/c1jm13943f**

In contrast to conventional PEG-DA hydrogels prepared from an aqueous precursor solution, the reported SIPS protocol utilized a dichloromethane (DCM) precursor solution which was sequentially photopolymerized, dried and hydrated. Physical properties were further tailored by varying the PEG-DA wt% concentration (5 wt% - 25 wt%) and M_n (3.4k and 6k g/mol). SIPS produced PEG-DA hydrogels with a macroporous morphology as well as increased G,, values versus the corresponding conventional PEG-DA hydrogels. Notably, since the total swelling was not significantly changed versus the corresponding conventional PEG-DA hydrogel, pairs or series of hydrogels represent scaffolds in which morphology and hydration or G,, and hydration are uncoupled. In addition, PEG-DA hydrogels prepared via SIPS exhibted enhanced degradation rates.

2.2. Introduction

As with the extracellular matrix (ECM) in natural tissues, the physical properties of tissue engineering scaffolds mediate cell behavior including regeneration [131-135]. Most notable are scaffold morphology (e.g. porosity) [77, 78, 81, 136-139] and modulus [74, 86, 87, 140]. Thus, regeneration of tissues which closely resemble native tissues may be accomplished through a material property-guided approach. Towards this goal, scaffolds whose physical properties can be precisely tuned over a broad range are essential.

Poly(ethylene glycol) diacrylate (PEG-DA) hydrogels have been widely utilized as scaffolds for the regeneration of diverse tissues [90, 91, 98, 141-144]. They are

particularly useful to probe cell-material interactions due to their resistance to protein and cell adhesion in the absence of the controlled introduction of adhesive ligands [88-92]. The limited range of physical properties which may be obtained for PEG-DA hydrogels restricts their utility to study material-guided cell behavior. For instance, hydrogel mechanical properties may be tuned over a limited range by altering the weight % (wt%) concentration of PEG-DA in the precursor solution or the crosslink density as determined by PEG-DA number average molecular weight (M_n) [98, 145]. However, these changes simultaneously alter swelling behavior and so limit the ability to uncouple modulus and swelling and thus the impact of each on the cellular response [146]. Hydrogel scaffold morphology including porosity is also known to influence cell behavior [77, 147-150]. Macroporous hydrogels have shown particular utility to enhance tissue engineering outcomes [79, 97, 151]. Furthermore, increased pore size has been shown to be useful to enhance degradation rates [82, 152]. In order to increase their pore size range, several strategies have been used to produce PEG-DA hydrogels with macroporous morphologies, including: salt leaching [153, 154], cryogelation [155, 156], and gas foaming [157]. However, each method is associated with specific limitations such as difficulty leaching poragens (salt leaching), high temperatures or low pressures (gas foaming), and extremely low temperatures (cryogelation) [64, 158].

To successfully produce functional tissues, it is highly desirable that the scaffold degrade at a rate which parallels regeneration [64, 67, 99]. Because of the stability of ether bonds and limited number of hydrolytically unstable ester crosslinks, PEG-DA hydrogels do not readily degrade under physiological conditions [159]. A variety of

synthetic strategies have been reported to enhance degradation of PEG-DA hydrogels, including incorporation of polyester segments [160-162], crosslinking to form labile bonds [163-165] and introduction of enzymatically unstable peptides [89, 166]. However, these alter the scaffold chemistry which is known to illicit changes in cell behavior [76, 167, 168].

Solvent-induced phase separation (SIPS) has been utilized to prepare macroporous poly(*N*-isopropylacrylamide) (PNIPAAm) hydrogels [94, 95]. During SIPS, a solvent system is utilized which promotes phase separation of the growing polymer chain and network during cure. In this study, PEG-DA hydrogels were formed via SIPS by photocuring dichloromethane (DCM) precursor solutions rather than aqueous precursor solutions as is used to formed conventional PEG-DA hydrogels. Precursor solutions were formed with DCM at various wt% concentrations (5 wt% - 25 wt%) and M_n"s (3.4k and 6k g/mol) of PEG-DA and subsequently dried and hydrated. These concentrations and M_n"s represent those typically utilized to prepare PEG-DA scaffolds for tissue engineering studies. The resulting macroporous morphology, swelling behavior, modulus, and degradation behavior was related to composition and compared to analogous conventional PEG-DA hydrogels fabricated from aqueous precursor solutions.

2.3. Materials and Methods

2.3.1. Materials

Allyl methacrylate, acryloyl chloride, triflic acid, 2,2-dimethyl-2-phenyl-acetophenone (DMAP), 1-vinyl-2-pyrrolidinone (NVP), triethylamine (Et_3N), $MgSO_4$, K_2CO_3, hexamethyldisilazane (HMDS) and solvents were obtained from Sigma Aldrich. HPLC grade toluene and CH_2Cl_2 and NMR grade $CDCl_3$ were dried over 4Å molecular sieves. Poly(ethylene glycol) (PEG) [PEG-6000; MW = 5000-7000 g/mol and PEG-3400; MW = 3000-3700 g/mol per manufacturer‟s specifications] were obtained from BioChemika. The precise M_n‟s of PEG-3400 (3393 g/mol) and PEG-6000 (6143 g/mol) were back-calculated from ^{1}H NMR end-group analysis of the corresponding diacrylated products.

2.3.2. PEG-DA Synthesis

PEG-DA (3.4k g/mol or 6k g/mol) were prepared as previously reported [127]. PEG-3400 (23.5 g, 7.0 mmol), Et_3N (1.95 mL, 14.0 mmol) and acryloyl chloride (2.27 mL, 28.0 mmol) were reacted to obtain PEG-DA (15.2 g, 63% yield). ^{1}H NMR (δ, ppm): 3.62 (s, 297H, -OCH_2CH_2), 5.81 (dd, 2H, *J* = 10.5 and 1.2 Hz, -CH=CH_2), 6.13 (dd, 2H, *J* = 17.4 and 10.5 Hz, -CH=CH_2), 6.40 (dd, 2H, *J* = 17.3 and 1.5 Hz, -CH=CH_2). By ^{1}H NMR end-group analysis, M_n of PEG-DA (3.4k g/mol) was determined to be 3393 g/mol (~3400 g/mol). PEG-6000 (24 g, 4.0 mmol), Et_3N (1.12 mL, 8.0 mmol) and acryloyl chloride (1.30 mL, 16.0 mmol) were reacted to obtain PEG-DA (31 g, 63% yield). ^{1}H NMR (*δ*, ppm): 3.61 (s, 547H, -OCH_2CH_2), 5.81 (dd, 2H, *J* = 10.4 and 1.5 Hz, -

C*H*=C*H*$_2$), 6.13 (dd, 2H, *J* = 16.8 and 10.5 Hz, -CH=C*H*$_2$), 6.40 (dd, 2H, *J* = 17.3 and 1.5 Hz, CH=C*H*$_2$). By ^{1}H NMR end-group analysis, M_n of PEG-DA (6k g/mol) was determined to be 6143 g/mol (~6000 g/mol).

2.3.3. NMR

^{1}H NMR spectra were obtained on a Mercury 300 300 MHz spectrometer operating in the Fourier transform mode. Five percent (w/v) $CDCl_3$ solutions were used to obtain spectra. Residual $CHCl_3$ served as an internal standard.

2.3.4. Hydrogel Preparation

PEG-DA hydrogels formed via SIPS were prepared from DCM-based precursor solutions whereas conventional PEG-DA hydrogels were prepared from aqueous precursor solutions. Precursor solutions were prepared at concentrations of 5, 10, 15, 20, and 25 wt% PEG-DA (M_n = 3.4k or 6k g/mol) in DCM or deionized (DI) water. 10 μL of photoinitiator solution (30 wt% solution of DMAP in NVP) was added per one mL of the precursor solution. Solutions were vortexed for one minute following both the addition of polymer and the subsequent addition of the photoinitiator solution. Planar hydrogel sheets (1.5 mm thick) were prepared by pipetting the precursor solution between two clamped microscope slides (75 x 50 mm) separated by Teflon spacers and exposing the mold to longwave UV light (UV-Transilluminator, 6 mW/cm^2, 365 nm) for a total of 6 min with rotation to the alternate side after 3 min. After removal from the mold, the water-based hydrogel sheets were rinsed with DI water and soaked in a Petri

dish containing DI water (60 mL) for 2 days with daily water changes to remove catalyst impurities. The DCM-based sheets were rinsed with DCM then air dried for 30 min to permit evaporation of DCM and subsequently placed in a Petri dish containing DI water (60 mL) to remove any remaining DCM. During the first hour of soaking, the water was changed every 15 min and thereafter daily for 2 days. All hydrogels were permitted to soak in DI water for a total of 72 hr prior to testing.

2.3.5. Sol Content

Five discs (13 mm diameter) were punched from a single hydrogel sheet with a die. After air-drying for 30 min, each disc was placed in an open scintillation vial and dried at room temperature (RT) in a vacuum oven (30 in. Hg, 24 hr). Dried discs were then weighed (W_{d1}), returned to the vial and 10 mL DCM was added to each. The vials were capped and placed on a rocker table (250 rpm) for 48 hr to remove sol (i.e. uncrosslinked material). The discs were subsequently removed and weighed (W_{d2}). Sol Content is defined as: $sol\ content = [(W_{d1} - W_{d2})/ W_{d1}]*100$.

2.3.6. Morphology

Water-swollen hydrogels discs (13 mm diameter) were flash frozen in liquid nitrogen for 1 min and immediately lyophilized for 24 hr (Labconco Centri Vap Gel Dryer System). Specimen cross-sections were subjected to Pt/Pd-sputter coating and viewed with a field emission scanning electron microscope (FEI Quanta 600 FE-SEM) at an accelerated electron energy of 10 keV.

2.3.7. Equilibrium Swelling

Three discs (13 mm diameter) were punched from a single sheet with a die. Each disc was placed in a sealed vial containing 20 mL DI water for 48 hr at RT, removed, blotted with filter paper to remove surface water, and weighed (W_s). Equilibrium swelling ratio is defined as: *swelling ratio* = $(W_s - W_d)/W_d$, where W_s is the weight of the water-swollen hydrogel and W_d is the weight of the vacuum dried hydrogel (30 in. Hg, 60 ºC, 24 hr).

2.3.8. Dynamic Mechanical Analysis (DMA)

Three discs (13 mm diameter) were prepared as above. Storage modulus (G‟) of each disc was measured in the compression mode with a dynamic mechanical analyzer (TA Instruments Q800) equipped with parallel-plate compression clamp with a diameter of 40 mm (bottom) and 15 mm (top). A water-swollen disc (13 mm diameter) was blotted with a Kim Wipe, clamped between the parallel plates and silicone oil placed around the exposed hydrogel edge to prevent dehydration. Following equilibration at 25 °C (5 min), the samples were tested in a multi-frequency-strain mode (1 to 30 Hz).

2.3.9. Degradation

Six hydrogel discs (8 mm diameter) were prepared as above. After soaking in DI water for 3 hr, an initial swollen weight was recorded. Three discs were each placed into a well plate (secured with Parafilm and covered with foil) containing 1 mL 0.05M NaOH and maintained at 37 ºC on a rocker table at 50 rpm. The NaOH solution was exchanged

every 12 hr. Swollen weights were recorded at regular intervals (W_s) until the hydrogel exhibited a loss in weight with a corresponding loss in mechanical integrity. The time required for the disc to completely dissolve was also recorded. The remaining three hydrogel discs were vacuum dried (30 in. Hg, 60 ºC, 24 hr) and their weights recorded (W_d). S ratio (SR) is defined as: s*welling ratio* = $(W_s - W_d)/W_d$. Results reported are based on the average of the three individual specimens.

2.4. Results and Discussion

2.4.1. Hydrogel Fabrication

Both the hydrogels formed via SIPS and the conventional hydrogels were transparent (**Figure 2.2**). However, the cross-section of PEG-DA hydrogels formed by SIPS displayed a sponge-like or coarser texture. To verify the efficacy of photocrosslinking, sol content values of hydrogels were measured (Supplemental Table S1). Sol contents of PEG-DA hydrogels fabricated from DCM precursor solutions (~3-9%) and aqueous precursor solutions (~1-9%) were similarly low.

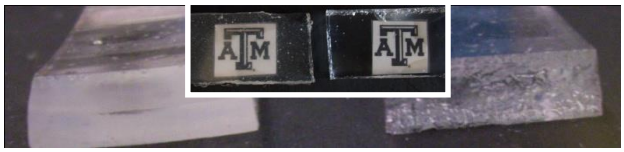

Figure 2.2. Macroscopic images of conventional PEG-DA hydrogels fabricated from an aqueous precursor solution [left] and PEG-DA hydrogels fabricated via SIPS with a DCM precursor solution (and subsequently dried and hydrated) [right]. (PEG-DA: M_n = 6k g/mol; 10 wt% concentration).

2.4.2. Morphology

Conventional PEG-DA hydrogels photopolymerized from aqueous precursor solutions at typical concentrations cannot be imaged via SEM as they collapse during the freezing/freeze-drying process [151]. In contrast, SEM images of PEG-DA hydrogels prepared via SIPS were obtained and revealed open porous structures (**Figure 2.3**). During SIPS, phase separation of the growing polymer chains and network from the solvent leads to polymer rich as well as polymer lean domains (i.e. pores) which upon hydration, fill with water. Depending on the extent as well as rate of phase separation prior to a final three-dimensional structure determined by significant crosslinking, the porosity will vary somewhat. A macroporous morphology was observed when PEG-DA hydrogels were prepared at concentrations between 10 and 25 wt%. Notably, for the hydrogel series based on 3.4k PEG-DA, higher wt% concentrations produced increasingly larger pores. At the same wt% concentration, hydrogels based on 6k PEG-DA exhibited a different morphology versus the corresponding hydrogel based on 3.4k PEG-DA. Thus, SIPS is useful to achieve macroporous morphologies which may be tuned by PEG-DA wt% concentration as well as M_n.

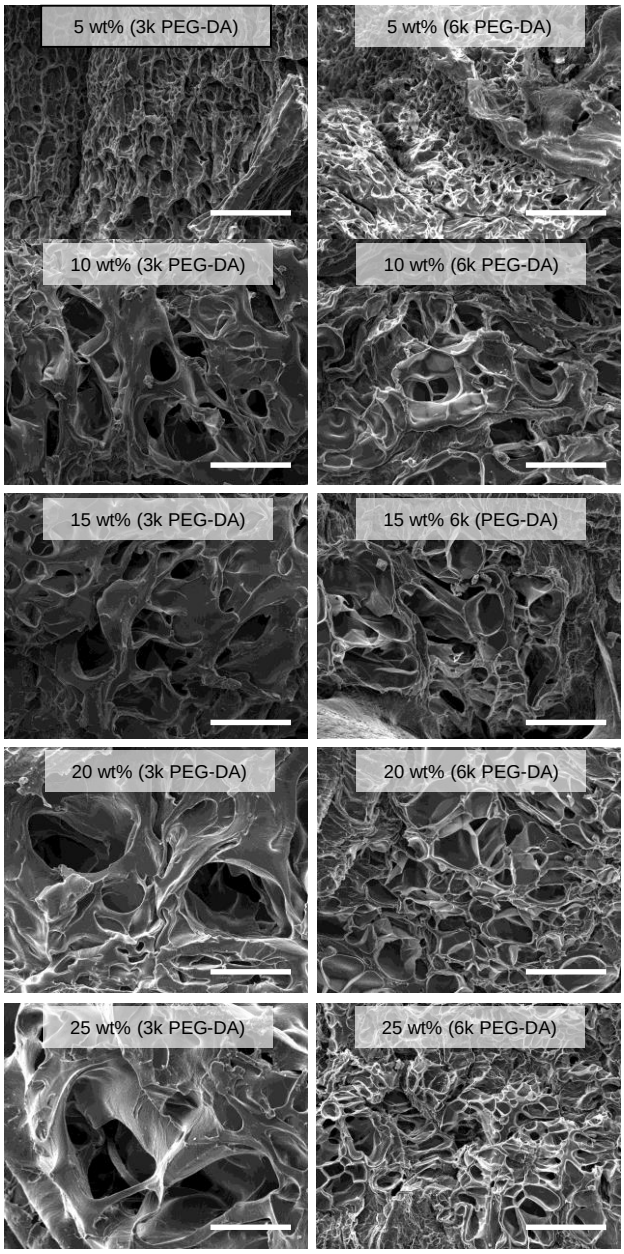

Figure 2.3. SEM images of PEG-DA hydrogels fabricated via SIPS. (Scale bars = 100 μm)

2.4.3. Equilibrium Swelling

PEG-DA hydrogels formed via SIPS generally exhibited similar swelling to the analogous conventional PEG-DA hydrogel (**Figure 2.4**). The exceptions are hydrogels formed at very low (5 wt%) concentrations which produced substantially lower swelling for hydrogels prepared by SIPS. For a given PEG-DA M_n at a concentration between 10-25 wt%, rather similar and, in some cases, statistically similar swelling ratios were achieved when prepared via SIPS versus from an aqueous precursor solutions. This was somewhat unexpected given the macroporous morphology of hydrogels prepared via SIPS (**Figure 2.3**) which is typically associated with enhanced water uptake [94, 154]. The lack of swelling increase for PEG-DA hydrogels prepared via SIPS may be attributed to reduced water uptake in the polymer-rich regions of the hydrogels. Thus, SIPS changes the distribution of water rather than the total water uptake in the resulting PEG-DA hydrogels. In addition, certain pairs of PEG-DA hydrogels prepared via SIPS at different concentrations also exhibit quite similar swelling ratios (e.g. 6k g/mol at 15 and 20 wt%). Hydrogel swelling (i.e. hydration) is an important scaffold property given its impact on cell behavior in terms of local environment and diffusion of waste and nutrients [67]. Thus, the impact of scaffold morphology on cell behavior decoupled from total hydration may be studied by utilizing series of PEG-DA scaffolds formed via SIPS and conventional PEG-DA hydrogels.

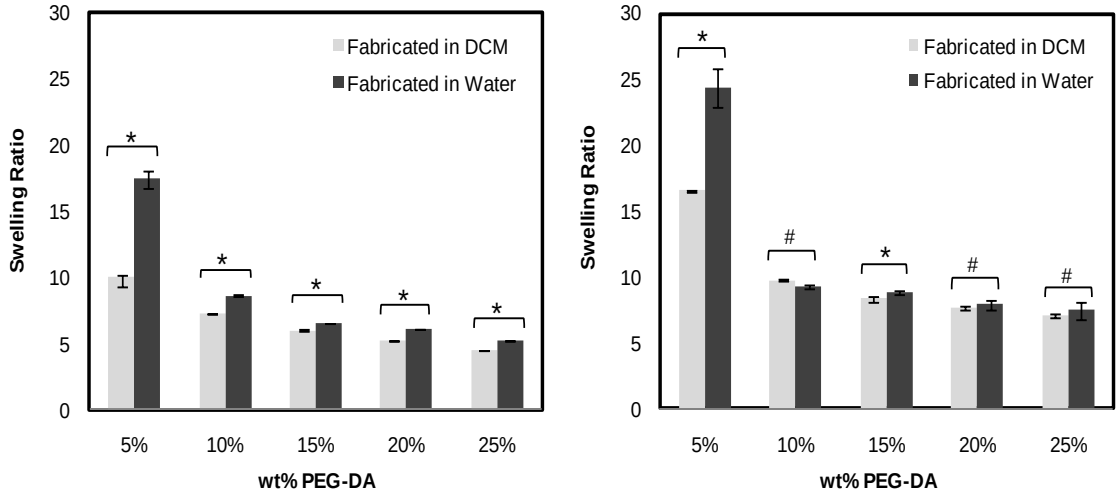

Figure 2.4. Swelling ratio of PEG-DA hydrogels fabricated with 3.4k g/mol (left) and 6k g/mol (right) PEG-DA from a DCM precursor solution (i.e. via SIPS) or from an aqueous precursor solution. Statistical significance was determined by student‟s t-test where (*): $p < 0.05$ and (#): $p > 0.05$.

2.4.4. Modulus

During DMA, hydrogel stiffness was measured in terms of the storage modulus (G‟) as a function of frequency of the applied strain in compression (**Figure 2.5**). For a given PEG-DA M_n at a specific concentration (5-25 wt%), G‟ was substantially higher for hydrogels fabricated via SIPS compared those fabricated from aqueous precursor solutions. As previously observed [98, 145] for conventional PEG-DA hydrogels, G‟ increased with increasing crosslink density (i.e. reducing PEG-DA M_n) or increasing PEG-DA concentration. The same compositional changes to PEG-DA hydrogels fabricated via SIPS similarly produced an increase in G‟. For conventional PEG-DA hydrogels, increased crosslink density or concentration produces a concomitant decrease in swelling such that the impact of G‟ on cell behavior may not be uncoupled from the

effect of hydration [146]. From the series of PEG-DA hydrogels formed via SIPS and aqueous precursor solutions, a pair or more of hydrogels with similar hydration (**Figure 2.4**) but different G‟ (**Figure 2.5**) are available. Thus, PEG-DA hydrogels prepared via SIPS affords the opportunity to study the influence of modulus on cell behavior decoupled from hydration.

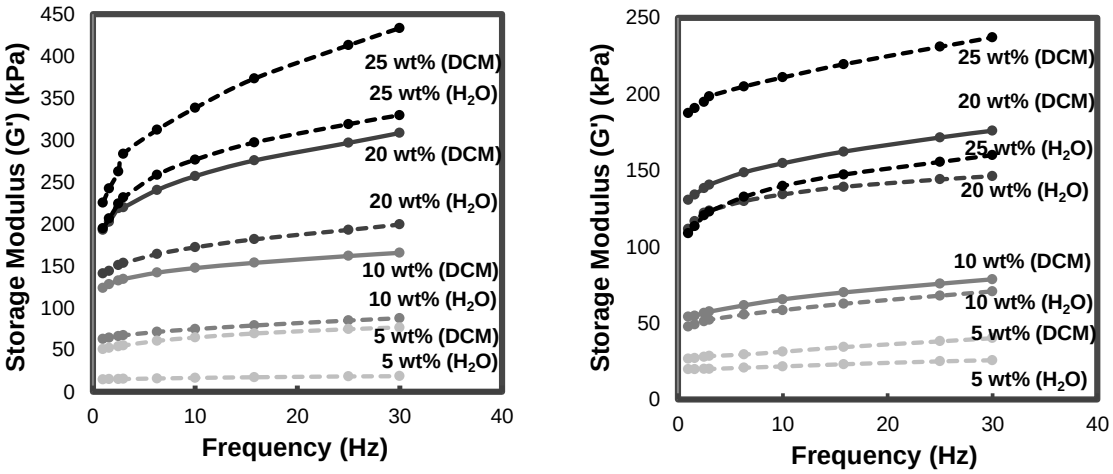

Figure 2.5. Storage modulus of PEG-DA 3k g/mol (left) and PEG-DA 6k g/mol (right) fabricated in either DCM or H_2O at various wt% concentrations.

2.4.5. Degradation

Increased pore size has been related to faster degradation rates [82, 152] and thus represents a strategy to tailor degradation without changing the chemical composition of the scaffold material. Because SIPS produces macroporous PEG-DA hydrogels at 10-25 wt% concentrations (**Figure 2.3**), it was anticipated that its degradation rate would be

faster than the corresponding conventional PEG-DA prepared from aqueous precursor solutions. PEG-DA hydrogels were subjected to hydrolytic degradation under accelerated (basic) conditions (**Figure 2.6**). Degradation was measured in terms of the time to achieve maximum swelling before loss of mechanical integrity and also in terms of time to completely dissolve [160]. For solid aliphatic polyester films, hydrolytic degradation rate increases with film thickness due to an autocatalytic effect of more slowly diffusing acidic degradation products [169]. In the same way, the degradation rate of aliphatic polyester porous materials is increased with larger pore size and hence higher pore wall thickness [170]. In the case of PEG-DA hydrogels, hydrolysis of labile ester bonds releases poly(acrylic acid) (PAA) kinetic chains [171] which similarly may induce autoacceleration if diffusion its limited. Thus, the enhanced rate of degradation of PEG-DA hydrogels prepared via SIPS versus conventional hydrogels is attributed to the larger pore size and thicker pore wall of the former. As expected, for PEG-DA hydrogels prepared via SIPS, lower wt% concentrations led to shorter dissolution times. Also, at the same wt% concentration, the degradation rate was higher for hydrogels fabricated from 6k g/mol PEG-DA M_n (i.e. hydrogel crosslink density) versus 3.4k PEG-DA. The effect of concentration and M_n were similarly observed for conventional PEG-DA hydrogels. Given the limited susceptibility to hydrolysis of PEG-DA hydrogels, their fabrication by SIPS to produce enhanced degradation rates without alterations to its chemical nature is a useful to study cell behavior and ultimately tissue regeneration.

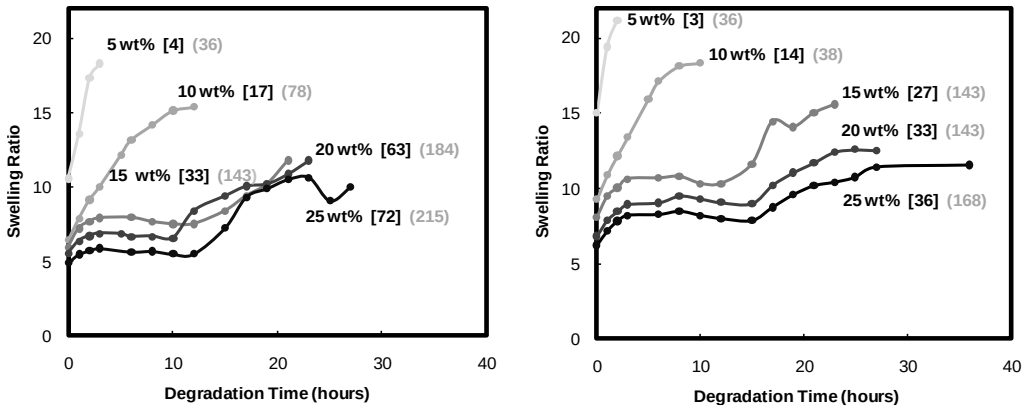

Figure 2.6. Swelling ratio as a function of degradation time under basic conditions (0.05 M NaOH) of PEG-DA hydrogels fabricated with 3.4k g/mol (left) and PEG-DA 6k g/mol (right) via SIPS at various wt% concentrations. [ ] = hours to complete dissolution. ( ) = hours to complete dissolution for analogous conventional hydrogels (i.e. prepared from aqueous precursor solutions).

2.5. Conclusions

PEG-DA hydrogels with broader, tunable physical properties which furthermore are uncoupled (i.e. not dependent on one another) would be extremely useful to study cell-material interaction and ultimately improve tissue regeneration. Towards this goal, PEG-DA hydrogels were formed via SIPS with 3.4k and 6k g/mol PEG-DA at various wt% concentrations (5-25 wt%). While conventional PEG-DA hydrogels are fabricated from an aqueous precursor solution, the reported SIPS protocol utilized a DCM precursor solution followed by drying and hydration after photopolymerization. When prepared via SIPS, PEG-DA hydrogels displayed a macroporous morphology (10-25 wt%) but did not exhibit increased total swelling versus the corresponding conventional hydrogel. Thus, certain series of hydrogels represent scaffolds in which morphology and

hydration are uncoupled. In addition, PEG-DA hydrogels prepared via SIPS exhibited a substantial increase in modulus (G‟) versus the corresponding conventional hydrogel. In this case, a particular series of hydrogels represent scaffolds in which hydration and modulus are uncoupled. Lastly, because of the larger pore size, PEG-DA hydrogels fabricated via SIPS exhibited an increased degradation rate under accelerated conditions. Thus, PEG-DA hydrogels formed via SIP, particularly when combined with conventional PEG-DA hydrogels, form a useful library of scaffolds to study the influence of physical properties on cell behavior and ultimately regenerate tissues.

CHAPTER III

$PDMS_{STAR}$-PEG HYDROGELS PREPARED VIA SOLVENT-INDUCED PHASE SEPARATION (SIPS) AND THEIR POTENTIAL UTILITY AS TISSUE ENGINEERING SCAFFOLDS*

3.1. Overview

Inorganic-organic hydrogels based on methacrylated star polydimethylsiloxane ($PDMS_{star}$-MA) and diacrylated poly(ethylene glycol) (PEG-DA) macromers were prepared via solvent-induced phase separation (SIPS). The macromers were combined in a dichloromethane (DCM) precursor solution and sequentially photopolymerized, dried and hydrated (**Figure 3.1**). The chemical and physical properties of the hydrogels were further tailored by varying the number average molecular weight (M_n) of PEG-DA (M_n = 3.4k and 6k g/mol) as well as the weight % (wt%) ratio of $PDMS_{star}$-MA (M_n = 7k g/mol) to PEG-DA from 0:100 to 20:80. Compared to analogous hydrogels fabricated from aqueous precursor solutions, SIPS produced hydrogels with a macroporous morphology, a more even distribution of $PDMS_{star}$-MA, increased modulus and enhanced degradation rates.

*Reprinted with permission from "$PDMS_{star}$-PEG hydrogels prepared via solvent-induced phase separation (SIPS) and their potential utility as tissue engineering scaffolds" by Brennan M. Bailey, Ruochong Fei, Dany Munoz-Pinto, Mariah S. Hahn, and Melissa A. Grunlan, 2012. Acta Biomaterialia, 8, 4324-4333, Copyright [2012] by Acta Materialia Inc. Published Elsevier Ltd.

The morphology, swelling ratio, mechanical properties, bioactivity, non-specific protein adhesion, controlled introduction of cell-adhesion, and cytocompatibility of the hydrogels were characterized. As a result of their tunable properties, this library of hydrogels is useful to study material-guided cell behavior and ultimate tissue regeneration.

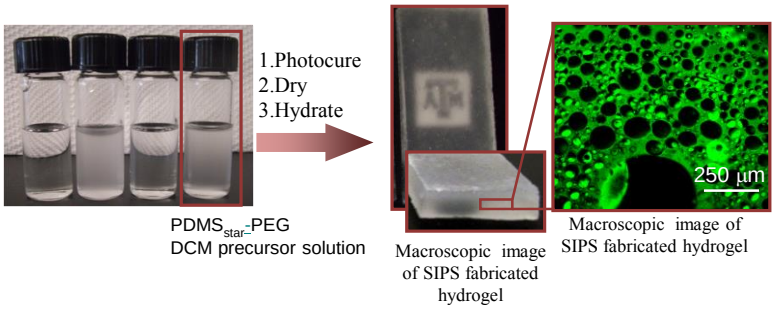

Figure 3.1. Reported PDMS$_{star}$-PEG hydrogel fabrication via SIPS and resulting dissolution and distribution of PDMS.

3.2. Introduction

In tissue engineering, the properties of the three dimensional scaffold guide cell behavior and ultimate tissue regeneration [131-135]. Physical properties of scaffolds known to impact cell behavior include modulus [74, 86, 87, 140] and morphology (e.g. porosity) [77-79, 81, 82, 84, 136, 137, 139, 172]. In addition, scaffold chemical properties influence cell behavior including bioactivity,[105, 106, 173] chemical functionality,[76] hydrophobicity,[102, 104, 174] and related hydration (i.e. swelling) [87, 175]. Therefore, a library of scaffolds having precisely tunable physical and

chemical properties over a broad range would be a valuable tool to probe material-guided cell behavior and enable the regeneration of functional tissues.

Poly(ethylene glycol) diacrylate (PEG-DA) hydrogels are extensively utilized as scaffolds for the regeneration of numerous types of tissues [90, 91, 98, 141-144]. Their resistance to protein and cell adhesion in the absence of cell adhesive ligands makes them particularly useful to study cell-material interactions [88-92]. Thus, changes in cell behavior may be related to an associated material property change. However, PEG-DA hydrogels display a limited range of physical as well as chemical properties restricting their utility for such studies. For instance, the modulus of PEG-DA hydrogels may be tuned over a somewhat narrow range by altering the crosslink density (i.e. PEG-DA number average molecular weight, M_n) or the weight percent (wt%) concentration of PEG-DA in the aqueous precursor solution [98, 145]. However, these alterations simultaneously produce changes in swelling thereby restricting the ability to uncouple the effect of modulus and swelling on cellular response [176]. While morphological changes in general alter cell behavior,[177-179] a macroporous hydrogel morphology has shown particular utility in tissue regeneration [79, 97, 151]. PEG-DA (M_n = 3.4k and 6k g/mol) hydrogels fabricated by the photopolymerization of aqueous precursor solutions exhibit pores smaller than ~5-10 μm [128]. Several strategies have been explored to produce macroporous PEG-DA hydrogels, including: salt leaching,[153, 154] gas foaming [157] and cryogelation [155, 156]. However, difficulty leaching porogens (salt leaching), high temperatures or low pressures (gas foaming), and extremely low temperatures (cryogelation) [158] limits these techniques.

In general, the chemical nature of hydrogel scaffolds has been shown to have a significant impact on cell behavior [168, 180-183]. Alterations to the chemical nature of PEG-DA hydrogels have been largely limited to those that increase the rate of degradation. For instance, polyester segments [160, 184] and enzymatically unstable peptides [89, 166] have been introduced to enhance the otherwise limited degradation rate of PEG-DA hydrogels. The impact of chemical functionality incorporated into PEG-DA hydrogels on cell behavior has been explored only to a limited extent [76]. Previous studies have demonstrated that the incorporation of inorganic silicon-containing materials into organic scaffolds enhances their bioactivity [105-107]. In addition, scaffold hydrophobicity has also been shown to influence osteogenic differentiation [102-104]. Previously, hydrogels were formed by introduction of an inorganic, hydrophobic methacrylated star polydimethylsiloxane ($PDMS_{star}$-MA) into PEG-DA hydrogels [101]. The insolubility of the $PDMS_{star}$-MA in the aqueous precursor solutions produced hydrogels comprised of discrete $PDMS_{star}$-enriched microparticles distributed throughout the PEG-DA hydrogel matrix. $PDMS_{star}$-MA content altered mechanical behavior without significant changes to hydration. Furthermore, previous study showed that these PDMS-PEG hydrogel scaffolds demonstrated the ability to guide mesenchymal stem cells (MSCs) towards osteogenic differentiation with increased levels of $PDMS_{star}$-MA [108].

Recently, PEG-DA hydrogels were prepared via solvent induced phase separation (SIPS) which involved photopolymerization of a dichloromethane (DCM) precursor solution followed by sequentially drying and hydration [93]. During SIPS, a

solvent system is utilized which promotes phase separation of the growing polymer chain and network during cure [94, 95]. Compared to PEG-DA hydrogels fabricated from an aqueous precursor solution, hydrogels were macroporous and exhibited increased modulus values and enhanced degradation rates. Herein, the introduction of variable levels $PDMS_{star}$-MA into PEG-DA hydrogels fabricated via SIPS to produce bioactive, macroporous $PDMS_{star}$-PEG hydrogel scaffolds with enhanced modulus values and degradation rates is reported. In contrast to $PDMS_{star}$-PEG hydrogels fabricated from an aqueous solvent, the improved solubility of $PDMS_{star}$-MA in the DCM fabrication solvent enables its more homogeneous distribution throughout the hydrogel. A series of $PDMS_{star}$-PEG hydrogels were prepared via SIPS (i.e. from DCM precursor solutions) at 10 wt% total macromer concentration but with variable wt% ratios of $PDMS_{star}$-MA (7k g/mol) to PEG-DA (3.4k and 6k g/mol) [0:100, 1:99, 10:90 and 20:80]. The effect of hydrogel composition on physical and chemical properties, including equilibrium swelling (i.e. hydration), morphology, compressive modulus, degradation, bioactivity, protein resistance, controlled introduction of cell adhesion and cytocompatibility were assessed. Properties of $PDMS_{star}$-PEG hydrogels fabricated via SIPS were compared to analogous hydrogels fabricated from an aqueous precursor solution.

3.3. Materials and Methods

3.3.1. Materials

Pt-divinyltetramethyldisiloxane complex (Karstedt‟s catalyst, 2 wt% in xylene), tetrakis(dimethylsiloxy)silane (tetra-SiH), and octamethylcyclotetrasiloxane (D_4) were obtained from Gelest. Allyl methacrylate, acryloyl chloride, triflic acid, 2,2-dimethyl-2-phenyl-acetophenone (DMAP), 1-vinyl-2-pyrrolidinone (NVP), triethylamine (Et_3N), $MgSO_4$, K_2CO_3, hexamethyldisilazane (HMDS), N3013 Nile Red (Nile Blue A Oxazone), NaOH, and solvents were obtained from Sigma Aldrich. HPLC grade toluene, CH_2Cl_2, and NMR grade $CDCl_3$ were dried over 4Å molecular sieves. Poly(ethylene glycol) (PEG) [PEG-6000; MW = 5000-7000 g/mol and PEG-3400; MW = 3000-3700 g/mol per manufacturer‟s specifications] were obtained from BioChemika. The M_n of PEG-3400 (3371 g/mol) and PEG-6000 (6072 g/mol) were back-calculated from ^1H NMR end-group analysis of the corresponding diacrylated products. Phosphate buffered solution (PBS, pH = 7.4, without calcium and magnesium), HEPES, Dulbecco‟s Modified Eagle Medium (DMEM), fetal bovine serum (FBS), PSG solution (10,000 U/mL penicillin, 10000 mg/L streptomycin, and 29.2 mg/mL L-glutamine), and PSA solution (10,000 U/mL penicillin, 10,000 mg/L streptomycin, and 25 mg/L amphotericin) were obtained from Mediatech. Peptide RGDS was obtained from American Peptide. Acryloyl PEG-succinimidyl valerate (acryloyl-PEG-SVA, 3.4 kDa) was obtained from Laysan Bio Inc. Mouse smooth muscle precursor cells (10T1/2) were obtained from American Type Culture Collection (ATCC).

3.3.2. $PDMS_{star}$-MA Synthesis

$PDMS_{star}$-MA was prepared as previously reported [185]. First, D_4 (29.9 g, 100.8 mmol), tetra-SiH (1.1 g, 3.3 mmol), triflic acid (60 μL), and HMDS (0.15 g, 0.93 mmol) were reacted. In this way, $PDMS_{star}$-SiH (24.9 g, 80% yield) was obtained as a colorless liquid, M_n/M_w = 7600/18,800 g/mol, PDI = 2.5. ^{1}H NMR (δ, ppm): 0.064-0.113 (bm, 1174H, SiC*H*$_3$), 4.7 (m, 4H, Si*H*). IR (ν): 2125 cm-1 (Si-H). Next, $PDMS_{star}$-SiH (7.0 g, 0.92 mmol), allyl methacrylate (0.26 g, 2.1 mmol), toluene (30 mL), and Karstedt‟s catalyst (100 μL) were reacted to obtain $PDMS_{star}$-MA (6.37 g, 88% yield) as a colorless liquid, M_n/M_w = 8300/22,000 g/mol, PDI = 2.6. ^{1}H NMR (δ, ppm): 0.045-0.127 (bm, 1673H, SiC*H*$_3$), 0.559 (m, 8H, -Si*CH*$_2$CH$_2$CH$_2$), 1.67 (m, 8H, -SiCH$_2$*CH*$_2$CH$_2$), 1.92 (m, 12H, -C(CH$_2$)*CH*$_3$), 4.10 (m, 8H, -SiCH$_2$CH$_2$*CH*$_2$), 5.57 (m, 4H, -C(*CH*$_2$)CH$_3$), 6.11 (m, 4H, -C(*CH*$_2$)CH$_3$). IR (*v*): no Si-H peak.

3.3.3. PEG-DA Synthesis

PEG-DA (3.4k and 6k g/mol) were prepared as previously reported [101]. PEG-3400 (23.5 g, 7.0 mmol), Et_3N (1.95 mL, 14.0 mmol) and acryloyl chloride (2.27 mL, 28.0 mmol) were reacted to obtain PEG-DA (15.2 g, 63% yield). ^{1}H NMR (δ, ppm): 3.62 (s, 297H, -O*CH*$_2$*CH*$_2$), 5.81 (dd, 2H, *J* = 10.5 and 1.2 Hz, -CH=C*H*$_2$), 6.13 (dd, 2H, *J* = 17.4 and 10.5 Hz, -CH=C*H*$_2$), 6.40 (dd, 2H, *J* = 17.3 and 1.5 Hz, -CH=C*H*$_2$). By ^{1}H NMR end-group analysis, M_n of PEG-DA (3.4k g/mol) was determined to be 3393 g/mol (∼3400 g/mol). PEG-6000 (24 g, 4.0 mmol), Et_3N (1.12 mL, 8.0 mmol) and acryloyl chloride (1.30 mL, 16.0 mmol) were reacted to obtain PEG-DA (31 g, 63% yield). ^{1}H

NMR (δ, ppm): 3.61 (s, 547H, -OCH_2CH_2), 5.81 (dd, 2H, J = 10.4 and 1.5 Hz, -CH=CH_2), 6.13 (dd, 2H, J = 16.8 and 10.5 Hz, -CH=CH_2), 6.40 (dd, 2H, J = 17.3 and 1.5 Hz, -CH=CH_2). By ^{1}H NMR end-group analysis, M_n of PEG-DA (6k g/mol) was determined to be 6143 g/mol (~6000 g/mol).

3.3.4. NMR

^{1}H NMR spectra were obtained on a Mercury 300 300 MHz spectrometer operating in the Fourier transform mode. Five percent (w/v) $CDCl_3$ solutions were used to obtain spectra. Residual $CHCl_3$ served as an internal standard.

3.3.5. Hydrogel Preparation

$PDMS_{star}$-PEG hydrogels formed via SIPS were prepared from DCM-based precursor solutions and analogous hydrogels were prepared from aqueous precursor solutions at the same concentrations for comparison. First, PEG-DA (3.4k or 6k g/mol) was added to either DCM or DI-H_2O at 10 wt% total concentration in solvent. $PDMS_{star}$-MA (7k g/mol) was then added at the following wt% ratios of $PDMS_{star}$-MA to PEG-DA: 0:100, 1:99, 10:90 and 20:80. 10 μL of photoinitiator solution (30 wt% solution of DMAP in NVP) was subsequently added per one mL of the precursor solution. Solutions were vortexed for one minute following each addition. Planar hydrogel sheets (1.5 mm thick) were prepared by pipetting the precursor solution between two clamped microscope slides (75 x 50 mm) separated by Teflon spacers and exposing the mold to longwave UV light (UV-Transilluminator, 6 mW/cm^2, 365 nm) for a total of 6 min with

rotation to the alternate side after 3 min. After removal from the mold, the water-based hydrogel sheets were rinsed with DI water and soaked in a Petri dish containing DI water (60 mL) for 2 days with daily water changes to remove impurities. The DCM-based sheets were rinsed with DCM then air dried for 30 min to permit evaporation of DCM and subsequently placed in a Petri dish containing DI water (60 mL) to remove impurities and any remaining DCM. During the first hour of soaking, the water was changed every 15 min and thereafter daily for 2 days. All hydrogels were permitted to soak in DI water for 72 hr prior to testing.

3.3.6. Sol Content

Three discs (13 mm diameter) were punched from a single hydrogel sheet with a die. After air-drying (30 min), each disc was placed in an open scintillation vial and dried at room temperature (RT) in a vacuum oven (14.7 psi, 24 hr). Dried discs were then weighed (W_{d1}), placed in a new vial and 10 mL DCM was added to each. The vials were capped and placed on a rocker table (250 rpm) for 48 hr to remove sol (i.e. uncrosslinked material). The discs were subsequently removed, air dried for 30 min, placed in an open vial, dried again at RT in a vacuum oven (30 in. Hg, 24 hr) and finally weighed (W_{d2}). Sol Content is defined as: sol content = $[(W_{d1} - W_{d2})/W_{d1}] \times 100$.

3.3.7. Morphology

3.3.7.1. Scanning Electron Microscopy

Water-swollen hydrogels discs (13 mm diameter) were flash frozen in liquid nitrogen for 1 min and immediately lyophilized for 24 hr (Labconco Centri Vap Gel Dryer System). Specimen cross-sections were subjected to Pt-sputter coating and viewed with a field emission scanning electron microscope (FEI Quanta 600 FE-SEM) at an accelerated electron energy of 10 keV.

3.3.7.2. Confocal Laser Scanning Microscopy (CLSM)

For a given hydrogel, a disc (8 mm diameter, 1.5 mm thickness) was punched from a hydrogel sheet with a die. A Nile Red solution was prepared as follows: 75 μL of a Nile Red solution (20 mg per mL of methanol) was dissolved in 8 mL of DI water and combined with 120 mL of PBS. Each hydrogel disc was sequentially soaked for 24 h in 60 mL of the aforementioned Nile Red solution and then soaked for 3 days in 60 mL of PBS (exchanged daily). With each disc placed on a glass microscope slide and DI water dropped onto the disc to maintain hydration, images were captured with CLSM using a Leica TCS SP5 confocal microscope (Leica Microsystems, Bannockburn, IL; excitation filter of 488 nm and emission filter 490-570 nm). Images were obtained from 3 μm sections in the z-direction. Images were assigned green for contrast.

3.3.8. Equilibrium Swelling

Three discs (13 mm diameter) were punched from a single hydrogel sheet with a die. Each disc was placed in a sealed vial containing 20 mL DI water and placed on a rocker table (250 rpm) for 48 hr at RT. Discs were then removed, blotted with filter paper to remove surface water, and weighed (W_s). Equilibrium swelling ratio (SR) is defined as: $SR = (W_s - W_d)/W_d$, where W_s is the weight of the water-swollen hydrogel and W_d is the weight of the vacuum dried hydrogel (30 in. Hg, 60 ºC, 24 hr).

3.3.9. Dynamic Mechanical Analysis (DMA)

Three discs (13 mm diameter) were prepared as above. Storage modulus (G‟) of each disc was measured in the compression mode with a dynamic mechanical analyzer (TA Instruments Q800) equipped with parallel-plate compression clamp with a diameter of 40 mm (bottom) and 15 mm (top). A water-swollen disc (13 mm diameter) was blotted with a Kim Wipe, clamped between the parallel plates and silicone oil placed around the exposed hydrogel edge to prevent dehydration. Following equilibration at 25 °C (5 min), the samples were tested in a multi-frequency-strain mode (1 to 25 Hz).

3.3.10. Degradation

Six hydrogel discs (8 mm diameter) were prepared as above. After soaking in DI water for 3 hr, an initial swollen weight (W_s) was recorded. Three discs were each placed into a well of a 24-well plate containing 1 mL 0.05M NaOH, the well plate covered with Parafilm and foil and maintained at 37 ºC on a rocker table at 50 rpm. The

NaOH solution was exchanged every 12 hr. Swollen weights (W_s) were recorded at regular intervals until the hydrogel exhibited an increase in swelling with a corresponding loss in mechanical integrity. The time required for the disc to completely dissolve was also recorded. The remaining three hydrogel discs were vacuum dried (30 in. Hg, 60 ºC, 24 hr) and their weights recorded (W_d). Swelling ratio (SR) is defined as: $SR = (W_s - W_d)/W_d$.

3.3.11. Bioactivity

3.3.11.1. Hydrogel Preparation

A hydrogel sheet with 0:100 and 10:90 wt% $PDMS_{star}$-MA to PEG-DA (6 k g/mol) was prepared via SIPS as above. A disc (13 mm diameter) was punched from each sheet and each disc placed into a sealed centrifuge tube containing 40 mL of 1.5X simulated body fluid (SBF)[186] at 37 °C. After two weeks, the hydrogel discs were removed and prepared for SEM imaging as above.

3.3.11.2. X-ray Diffraction Spectroscopy

Powder X-ray diffraction data was collected on a Bruker D8 diffractometer fitted with LynxEYE detector (CuKa; 40kV, 40 mA; Bragg Brentano geometry; scan range: 5 - 70 degrees; step size: 0.05 degrees; step time: 1 s).

3.3.12. Nonspecific Protein Adhesion

The adhesion of Alexa Fluor 555 dye conjugate of bovine serum albumin (AF-555 BSA; MW = 66 kDa; Molecular Probes, Inc.) onto hydrogels was studied by fluorescence microscopy. For a given hydrogel, three hydrogel discs (14 mm diameter, 1.5 mm thickness) were punched from a single hydrogel sheet and placed in PBS (15 min) to ensure hydration. Immediately prior to transferring to a 24-well plate, discs were gently blotted with filter paper to remove PBS on the surface. Of the three discs, two discs were each placed in wells containing 1.5 mL of BSA (0.1 mg/mL of PBS) and the third disc was placed in a well containing 1.5 mL of PBS. Hydrogel discs were maintained in the dark at RT for 3 h. Next, from both the top and bottom surfaces of the discs, the BSA solution was carefully removed via aspiration and both sides of the disc were rinsed with fresh PBS 3 times for 1 h each time to permit the diffusion of unadsorbed protein out of the hydrogels before imaging. No measurable internal fluorescence signal was detected following rinsing. Each of these discs was returned to a well containing 1.5 mL of fresh PBS for imaging.

A Zeiss Axiovert 200 optical microscope equipped with an A-Plan 5X objective (Axiocam HRC Rev. 2), and filter cube (excitation filter of 546 (12 nm [band-pass] and emission filter 575-640 nm [bandpass]) was used to obtain fluorescent images on three randomly selected regions of each hydrogel surface. The fluorescent light source was permitted to warm up for 30 min prior to image capture. Linear operation of the camera was ensured and constant exposure time used during the image collection to permit quantitative analyses of the observed fluorescent signals. The fluorescence microscopy

images were analyzed using ImageJ, which yielded the mean and standard deviation of the fluorescence intensity within a given image. For a given hydrogel composition, the average fluorescence intensity of the two discs exposed to AF-555 BSA was subtracted from that of the disc maintained only in PBS to ensure correction for of any fluorescence signal from the material itself. The background corrected fluorescence intensities for each hydrogel were then used to quantify AF-555 BSA levels adsorbed by comparison against a calibration curve constructed from the measured fluorescence intensities of AF-555 BSA standard solutions. Standard solutions were prepared at 0, 0.005, 0.01, 0.02, and 0.04 mg/mL AF-555 BSA in PBS and each placed into an individual well.

3.3.13. Controlled Introduction of Cell Adhesion and Spreading

Hydrogel sheets were prepared with and without acrylate-derivatized cell-adhesive peptide RGDS in the DCM precursor solutions. RGDS-modified hydrogel sheets (50 x 40 x 1 mm) were fabricated at different wt% ratios of $PDMS_{star}$-MA to PEG-DA (3.4k g/mol) [0:100, 1:99, 10:90 and 20:80] via SIPS as above but with 1 μmol/mL (post-swelling) of acrylate-derivatized RGDS in the DCM precursor solutions. Acryloyl-PEG-RGDS was prepared by reacting acryloyl-PEG-SVA (3.4 kDa) with RGDS.[187] A PEG-DA hydrogel fabricated in water ("PEG Control") was similarly formed with acrylate-derivatized RGDS from an aqueous precursor solution. The DCM-based sheets were first air dried for 24 hr. Both the water-based and dried DCM-based sheets were sterilized with two changes of ethanol/water (70/30; 24 h) and transferred into sterile Petri dishes where they were washed twice with sterile DI water (24 hr) and

finally rinsed twice with Dulbecco‟s PBS (pH = 7.2) supplemented with 1% PSA (24 hr). Four (8 mm diameter) discs were punched from each sample and transferred into a 48 well plate. 10T ½ cells were seeded onto the hydrogel surfaces at 10,000 cells/cm^2. After being maintained for 24 hr at 37 °C with 5% CO_2 in DMEM (without phenol red) supplemented with 10% heat-inactivated FBS and 1% PSG, cell adhesion and spreading was examined at 24 h using a bright field microscopy (Zeiss Axiovert).

3.3.14. Cytocompatibility

Hydrogel sheets prepared for cell adhesion and spreading studies were likewise prepared for cytocompatiblity tests. Hydrogel cytocompatiblity was assessed by measuring lactate dehydrogenase (LDH) levels released by 10T ½ cells 24 hr following cell seeding. Following the aforementioned sterilization protocol, four 8 mm hydrogel discs per sample type were transferred to separate wells of a 48 well plate. Harvested 10T ½ cells were seeded onto the hydrogel surfaces at 6000 cells/cm^2. After being maintained for 24 hr at 37 °C as above, the media surrounding each specimen was collected for LDH measurements following manufacturer (Roche) protocol.

3.4. Results and Discussion

3.4.1. Hydrogel Fabrication

Figure 3.2 shows the appearance of precursor solutions and the corresponding hydrogel. As was previously observed,[93] pure PEG-DA hydrogels fabricated via SIPS were similarly transparent compared to the corresponding PEG-DA hydrogel (i.e.

fabricated from an aqueous precursor solution). Aqueous precursor solutions became hazy upon addition of hydrophobic $PDMS_{star}$-MA due to its water-insolubility [101] (**Figure 3.2**). Due to the improved solubility of $PDMS_{star}$-MA in DCM, precursor solutions were less hazy and the corresponding hydrogels were not as opaque. To validate photocrosslinking efficacy, hydrogel sol contents were measured. Sol content values of $PDMS_{star}$-PEG hydrogels fabricated from DCM precursor solutions (~2-11%) and aqueous precursor solutions (~0.5-8%) were similarly low (**Table 3.1**).

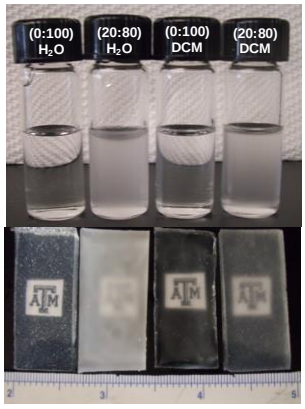

Figure 3.2. Precursor solutions [top] and corresponding hydrogels [bottom] formed from an aqueous precursor solution (left) and via SIPS (right) (i.e. with a DCM precursor solution followed by subsequent drying and hydration) with 6k g/mol PEG-DA.

Table 3.1. Sol Content of SIPS and analogous conventional hydrogels.

Hydrogel formed by SIPS	% sol content	Hydrogel formed in water	% sol content
PEG-DA: M_n = 3.4k g/mol		PEG-DA: M_n = 3.4k g/mol	
$PDMS_{star}$-PEG wt%		**$PDMS_{star}$-PEG wt%**	
0:100	3.9 ± 1.6	**0:100**	0.5 ± 0.7
1:99	2.0 ± 2.8	**1:99**	5.7 ± 1.2
10:90	4.0 ± 0.2	**10:90**	7.2 ± 1.4
20:80	6.7 ± 5.0	**20:80**	8.4 ± 0.7
PEG-DA: M_n = 6k g/mol		PEG-DA: M_n = 6k g/mol	
$PDMS_{star}$-PEG wt%		**$PDMS_{star}$-PEG wt%**	
0:100	3.2 ± 0.8	**0:100**	5.0 ± 0.8
1:99	2.8 ± 0.4	**1:99**	5.6 ± 0.4
10:90	5.0 ± 1.2	**10:90**	5.5 ± 1.9
20:80	10.8 ± 0.3	**20:80**	4.3 ± 1.7

[a] Prepared from an aqueous precursor solution
[b] Data taken from ref 60.

3.4.2. Morphology and Distribution of PDMS

Recently, macroporous PEG-DA hydrogels were prepared via SIPS by employing a DCM precursor solution [93]. During SIPS, macropores are produced by the separation of the growing polymer chains and network from the solvent into polymer rich and polymer lean domains (i.e. pores) that subsequently fill with water during hydration. Because pure PEG-DA hydrogels formed via SIPS did not significantly collapse during prior freeze-drying, their morphology could be examined by SEM [93]. However, SEM images of $PDMS_{star}$-PEG hydrogels revealed that they had significantly collapsed (**Figure 3.3**).

Thus, the porosity as well as $PDMS_{star}$-MA distribution of hydrated hydrogels was characterized with CLSM (**Figure 3.4**). Regions of the hydrogels containing the

hydrophobic $PDMS_{star}$-MA were stained by the hydrophobic dye whereas water-filled pores were unstained. With increased levels of $PDMS_{star}$-MA, hydrogel pore size increased and became macroporous at wt% ratios ≥ 10 wt%. Furthermore, the $PDMS_{star}$-MA is more uniformly distributed versus analogous $PDMS_{star}$-PEG hydrogels fabricated from an aqueous precursor solution in which discrete PDMS-enriched microparticles were observed [101]. Thus, SIPS is useful to achieve macroporous morphologies as well as a more uniform distribution of PDMS.

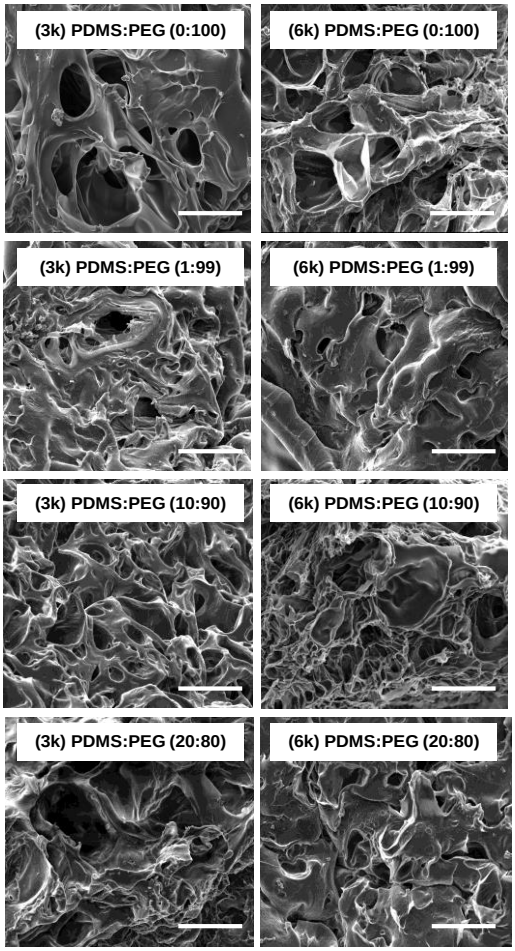

Figure 3.3. SEM images of $PDMS_{star}$-PEG hydrogels fabricated via SIPS. (scale bars = 50 μm)

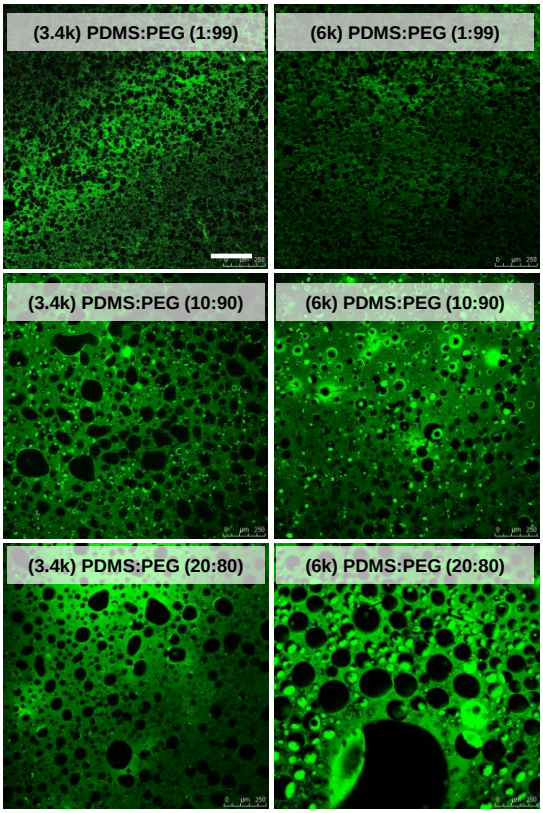

Figure 3.4. CLSM images of hydrated $PDMS_{star}$-PEG hydrogels prepared with different wt% ratios of $PDMS_{star}$-MA:PEG-DA from a DCM precursor solution (i.e. via SIPS). PDMS-enriched regions stained with hydrophobic dye (Nile Red). (scale bars = 250 μm)

3.4.3. Equilibrium Swelling

Swelling of $PDMS_{star}$-PEG hydrogels formed via SIPS was lower than that of the corresponding $PDMS_{star}$-PEG hydrogels produced from aqueous precursor solutions (**Table 3.2, Figure 3.5**). For "water fabricated" $PDMS_{star}$-PEG hydrogels, $PDMS_{star}$-MA content did not substantially alter hydration, likely due to the discrete nature of the

PDMS-enriched microparticles. Hydrophobic $PDMS_{star}$-MA is more soluble in DCM versus water and so becomes more evenly distributed throughout the hydrogels prepared via SIPS (**Figure 3.4**). As a result, increased $PDMS_{star}$-MA content produced a systematic decrease in swelling. While the macroporous nature of $PDMS_{star}$-PEG hydrogels formed via SIPS is expected to increase swelling [94, 154]. PEG-DA hydrogels prepared via SIPS likewise did not exhibit enhanced swelling versus PEG-DA hydrogels fabricated from aqueous precursor solutions [93] which may be due to reduced swelling of polymer-rich region. Thus, the distribution of water rather than total water uptake is changed by using SIPS to form $PDMS_{star}$-PEG hydrogels.

Table 3.2. Hydrogel Swelling Ratio and Adsorption of BSA Protein.

Hydrogel formed by SIPS	Swelling Ratio	mg BSA adsorbed per cm^2 (x 10^{-4})[b]	**Hydrogel formed in water**[a]	Swelling Ratio	mg BSA adsorbed per cm^2 (x 10^{-4})[b]
M_n = 3.4k g/mol (PEG-DA)			*M_n = 3.4k g/mol (PEG-DA)*		
$PDMS_{star}$-PEG wt%			**$PDMS_{star}$-PEG wt%**		
0:100	7.2 ± 0.01	2 ± 0.4	**0:100**	8.6 ± 0.02	5 ± 1
1:99	7.0 ± 0.04	25 ± 2	**1:99**	8.5 ± 0.03	14 ± 6
10:90	5.7 ± 0.04	10 ± 3	**10:90**	7.8 ± 0.02	6 ± 3
20:80	4.9 ± 0.09	19 ± 6	**20:80**	7.6 ± 0.09	19 ± 2
PEG M_n = 6k g/mol (PEG-DA)			*PEG M_n = 6k g/mol (PEG-DA)*		
$PDMS_{star}$-PEG wt%			**$PDMS_{star}$-PEG wt%**		
0:100	9.8 ± 0.09	10 ± 7	**0:100**	9.3 ± 0.2	12 ± 5
1:99	9.1 ± 0.10	16 ± 2	**1:99**	9.7 ± 0.1	15 ± 2
10:90	7.6 ± 0.06	11 ± 2	**10:90**	9.2 ± 0.1	13 ± 3
20:80	6.5 ± 0.13	19 ± 6	**20:80**	8.8 ± 0.1	10 ± 1

[a] Prepared from an aqueous precursor solution
[b] Data taken from ref 60.

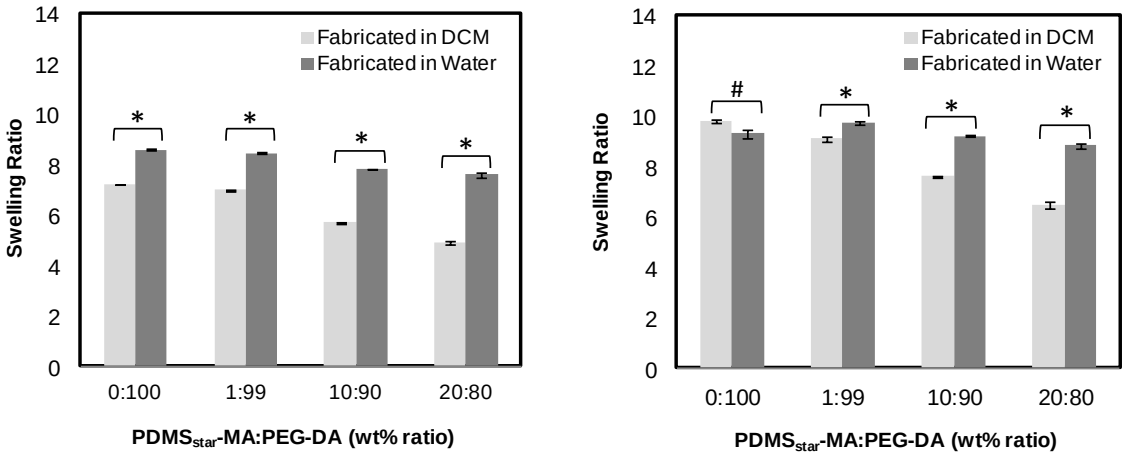

Figure 3.5. Swelling ratio of $PDMS_{star}$-PEG hydrogels fabricated with 3.4k g/mol (left) and 6k g/mol (right) PEG-DA from a DCM precursor solution (i.e. via SIPS) or from an aqueous precursor solution. Statistical significance was determined by student‟s t-test where (*): $p < 0.05$ and (#): $p > 0.05$.

3.4.4. Modulus

Hydrogel stiffness was quantified in term of the compressive storage modulus (G‟) obtained by DMA (**Figure 3.6**). As previously reported for PED-DA hydrogels,[98, 188] G‟ of $PDMS_{star}$PEG hydrogels prepared via SIPS increased with higher crosslink density (i.e. lower PEG-DA M_n). G‟ was substantially higher for hydrogels fabricated via SIPS compared to the corresponding hydrogels fabricated from aqueous precursor solutions. There are two contributing factors to this observation. First, for a given composition, $PDMS_{star}$-PEG hydrogels prepared via SIPS exhibited reduced swelling (**Figure 3.5**) which is typically associated with enhanced rigidity [175]. Second is the effect of the macroporous morphology of the hydrogels prepared via SIPS (**Figure 3.4**). Indeed, despite minor changes in swelling, pure PEG-DA hydrogels prepared via SIPS were macroporous and exhibited a pronounced increase in G‟ versus when fabricated in

water [93]. For hydrogels formed via SIPS, the associated thicker pore walls may be the source of the increase in G‟‟.

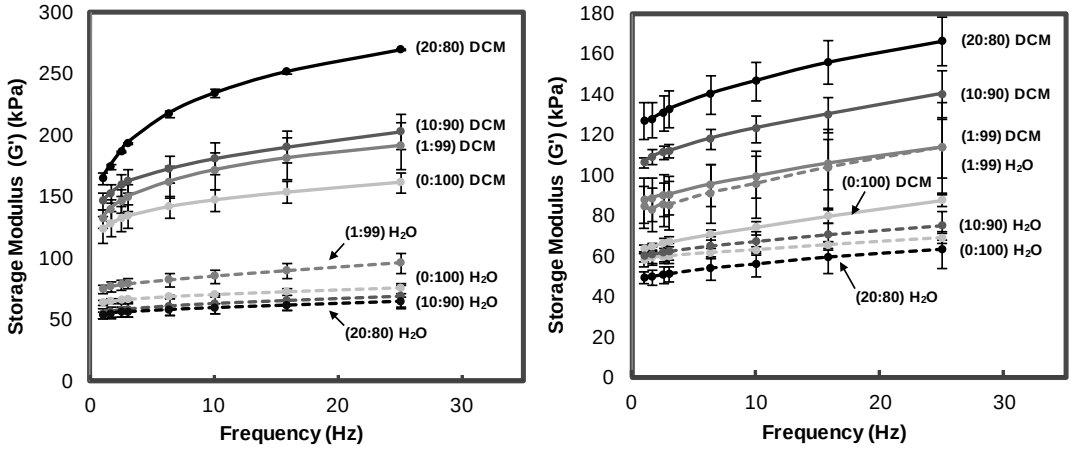

Figure 3.6. Storage modulus (G‟‟) of $PDMS_{star}$-PEG hydrogels fabricated with 3.4k g/mol (left) and 6k g/mol (right) from a DCM precursor solution (i.e. via SIPS) [solid lines] or from an aqueous precursor solution [dashed lines].

3.4.5. Degradation

Hydrolytic degradation of $PDMS_{star}$-PEG hydrogels was measured under accelerated (basic) conditions (**Figure 3.7**). Degradation was quantified in terms of the time to reach maximum swelling before loss of mechanical integrity as well as the time for complete dissolution [160]. For aliphatic polyesters, the rate of hydrolytic degradation increases with larger pore size and hence greater pore wall thickness [82] as well as film thickness [169] due to an autocatalytic effect of more slowly diffusing acidic degradation products. Under basic conditions, macroporous PEG-DA hydrogels

formed via SIPS likewise degraded faster than the corresponding hydrogel fabricated from aqueous precursor solutions [93]. For PEG-DA-based hydrogels, hydrolysis of ester bonds releases poly(acrylic acid) (PAA) kinetic chains [171] capable of inducing autoacceleration if diffusion is limited. However, under basic conditions, the increased degradation rate may be largely attributed to the limited diffusion of hydroxide ions through thicker pore walls which proceed to catalyze bond cleavage. Likewise, the observed increased degradation rate of $PDMS_{star}$-PEG hydrogels fabricated via SIPS versus the corresponding hydrogel fabricated in water is attributed to the former‟s increased pore size and thicker pore walls. As expected, degradation rate increased for hydrogels prepared with 6k g/mol PEG-DA versus from 3.4k g/mol PEG-DA due to the former‟s lower crosslink density. The effect of M_n was similarly observed for $PDMS_{star}$-PEG hydrogels fabricated from aqueous precursor solutions (**Figure 3.8**). Incorporation of $PDMS_{star}$-MA into hydrogels formed via SIPS led to an increased degradation time but did not necessarily coincide with $PDMS_{star}$-MA content. For these hydrogels, as $PDMS_{star}$-MA content increases, the degradation rate is influenced by both the increased hydrophobicity that reduces degradation [189] and the increased pore size that enhances degradation. Given the limited susceptibility to hydrolysis of PEG-DA-based hydrogels, their fabrication by SIPS to produce enhanced degradation rates as well as the ability to further increase degradation rates through the incorporation of $PDMS_{star}$-MA provide useful mechanisms to enhance the utility of PEG-DA hydrogels for tissue engineering.

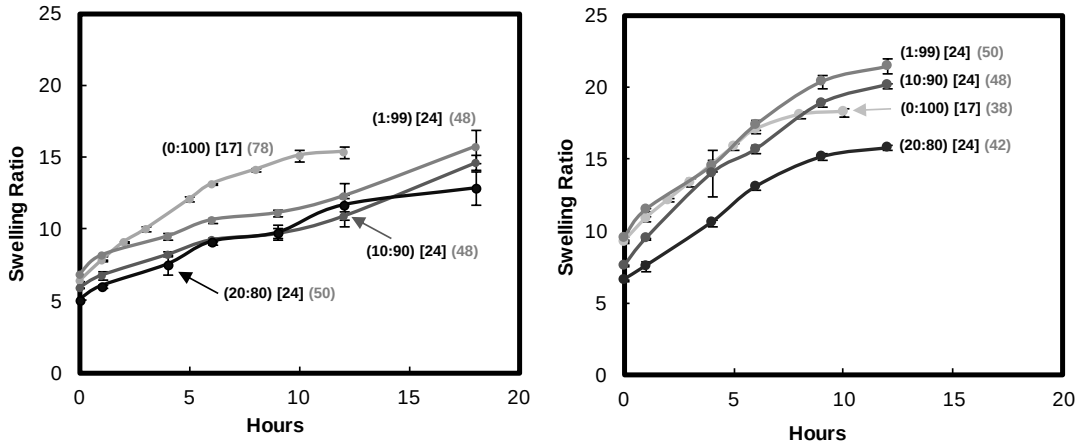

Figure 3.7. Swelling ratio under basic conditions (0.05 M NaOH) of $PDMS_{star}$-MA:PEG-DA hydrogels fabricated via SIPS with 3.4k g/mol (left) and 6k g/mol (right) PEG-DA. [ ] = hours to complete dissolution and ( ) = hours to complete dissolution of analogous hydrogel (i.e. fabricated from aqueous precursor solutions).

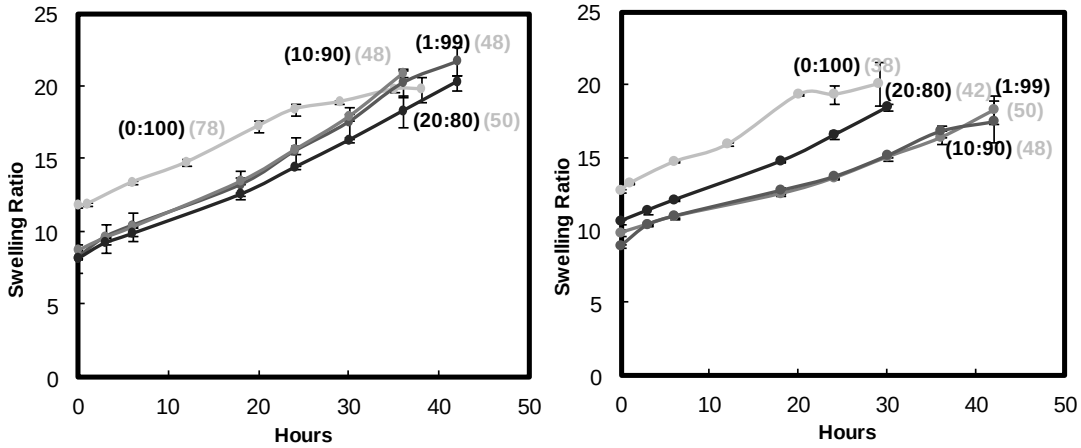

Figure 3.8. Swelling ratio under basic conditions (0.05 M NaOH) of $PDMS_{star}$-MA:PEG-DA hydrogels fabricated via SIPS with 3.4k g/mol (left) and 6k g/mol (right) PEG-DA. ( ) = hours to complete dissolution.

3.4.6. Bioactivity - Hydroxyapatite Formation

Bioactive materials chemically bond to bone via formation of a biological active hydroxyapatite (HAp) layer [190]. Calcium apatites such as HAp have also been shown to promote differentiation of mesenchymal stem cells (MSCs) to osteoblasts (i.e. are osteoinductive) [191]. Since inorganic, hydrophobic materials are associated with bioactivity,[105, 106, 173] it was anticipated that $PDMS_{star}$-PEG hydrogels prepared via SIPS would be bioactive. The degree of formation of HAp upon immersion into SBF is a qualitative indication of the level of scaffold bioactivity and has been correlated to the ability to bond to bone *in vivo* [192]. Thus, the extent of formation of HAp following SBF exposure was compared for a $PDMS_{star}$-PEG (3.4k g/mol) hydrogel (10:90 wt% ratio) versus the pure PEG-DA (3.4k g/mol) control (i.e. no PDMS) and $PDMS_{star}$-PEG (6k g/mol) hydrogel (20:80 wt% ratio) versus the pure PEG-DA (6k g/mol) control (i.e. no PDMS) (**Figure 3.9**). SEM images revealed a significant level of HAp on the $PDMS_{star}$-PEG hydrogel but its absence on the PEG-DA hydrogel. X-ray diffraction was performed on these hydrogel compositions to verify HAp formation and characteristic HAp peaks of 31.7, 45.5, and 56.5 were noted. These peaks indicate reflections from 112, 222, 004 crystal planes respectively and correspond to Bragg reflections of HAp (**Figure 3.10**) [193]. In previous studies, $PDMS_{star}$-PEG hydrogels prepared from aqueous precursor solutions demonstrated increased stimulation of osteogenic differentiation of encapsulated MSCs [108]. On the basis of these studies, $PDMS_{star}$-PEG hydrogels prepared via SIPS are bioactive and may increase the osteogenic potential of associated MSCs.

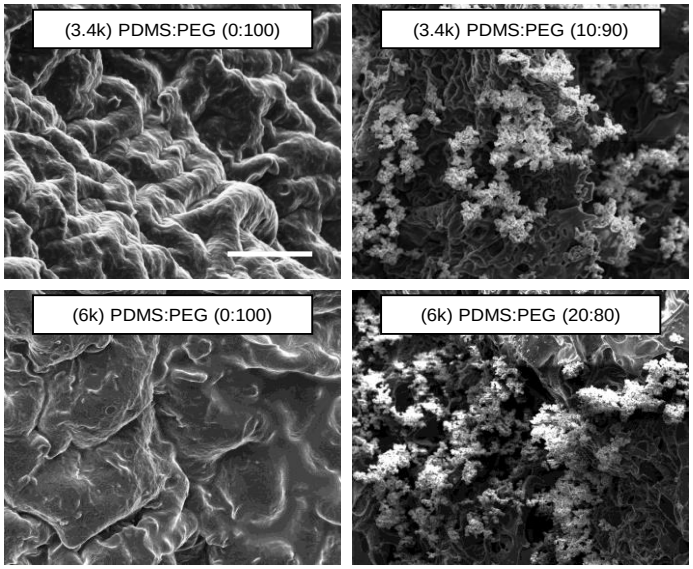

Figure 3.9. SEM images (following exposure to SBF for 2 weeks) of hydrogels fabricated with either 3.4k (top) or 6k g/mol (bottom) PEG-DA from a DCM precursor solution (i.e. via SIPS) with (right column) and without PDMS (left column) (scale bars = 50 μm).

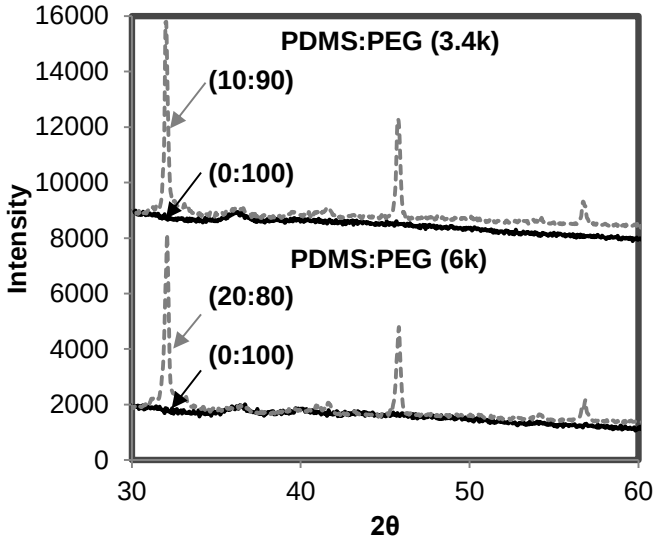

Figure 3.10. X-ray Diffraction of PDMS:PEG (3.4k and 6k g/mol) hydrogels soaked in SBF - revealing the formation of HAp within hydrogels when PDMS is incorporated (dotted line) and absence of HAp when no PDMS is incorporated (solid line).

3.4.7. Nonspecific Protein Adhesion

Because cell behavior is altered by adsorbed proteins (e.g. from serum),[89, 194] scaffolds useful to study materials-guided cell behavior must be significantly protein resistant. The adsorption of BSA onto $PDMS_{star}$-PEG hydrogels prepared via SIPS was compared to that of the corresponding PEG-DA hydrogels (**Table 3.2**). BSA adsorption on PEG-DA hydrogels has been shown to increase with reduced hydration [195]. As noted above, swelling was reduced with increased $PDMS_{star}$-MA content for $PDMS_{star}$-PEG hydrogels prepared via SIPS. When based on 6k g/mol PEG-DA, $PDMS_{star}$-PEG hydrogels formed via SIPS exhibited somewhat similar BSA adsorption versus the pure PEG-DA control. BSA adsorption was somewhat higher for hydrogels based on 3.4k g/mol PEG-DA versus the PEG-DA control. This may be due to the lower hydration of hydrogels based on 3.4k g/mol versus 6k g/mol PEG-DA. However, for all $PDMS_{star}$-MA:PEG-DA hydrogels, protein adsorption levels were within the range reported for PEG-DA hydrogels [195]. Furthermore, BSA adsorption was similar for $PDMS_{star}$-PEG hydrogels prepared by SIPS versus that of analogous hydrogels prepared in water, despite the former‟s reduced swelling. The increased pore size of $PDMS_{star}$-PEG hydrogels prepared by SIPS may enhance protein diffusion thereby reducing its adsorption.

3.4.8. Controlled Introduction of Cell Adhesion and Spreading

PEG-DA hydrogels‟ resistance to adsorption of bioactive serum proteins renders them “biological blank slates” as cells are subsequently unable to adhere and spread

[92]. Defined levels of cell adhesion may be introduced by covalent incorporation of acrylate-functionalized cell adhesive peptide RGDS into PEG hydrogels [88, 196, 197]. While minor changes in protein adsorption were observed, maintenance of the biological blank slate nature for $PDMS_{star}$-PEG hydrogels was assessed by evaluating cell adhesion onto hydrogels prepared with and without acrylate-RGDS (**Figure 3.11**). $PDMS_{star}$PEG hydrogels based on 3.4k g/mol PEG-DA were prepared via SIPS both with and without 1 μmol/mL of acrylate-derivatized RGDS. A PEG-DA hydrogel fabricated in water similarly prepared with and without RGDS served as a control ("PEG Control"). Incorporation of low levels of RGDS has been observed to cause only a minute change in hydrogel swelling [198]. As with the PEG control, cells did not adhere and spread in the absence of RGDS. However, modification of all hydrogels with RGDS did cause cell adhesion and spreading. Thus, as for "water fabricated" PEG-DA hydrogels, $PDMS_{star}$-PEG hydrogels prepared via SIPS permit the controlled introduction of cell adhesion and spreading which is critical for their utility to study cell-material interactions.

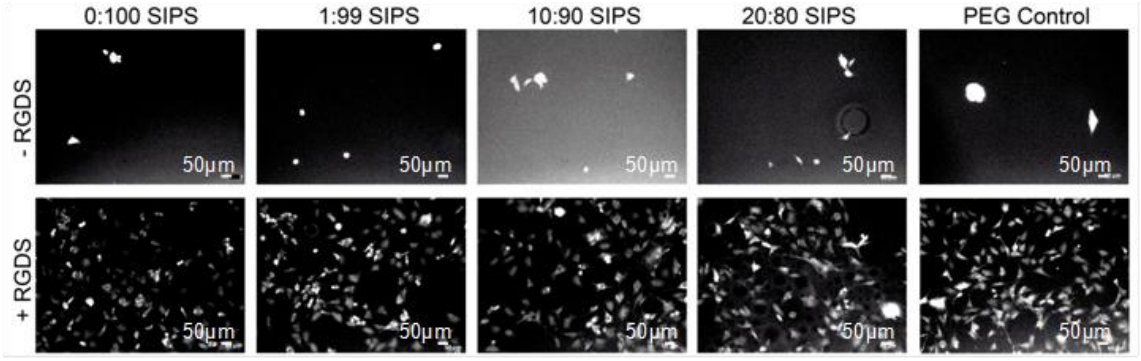

Figure 3.11. Cell spreading for PDMS-PEG hydrogels prepared without [top] and with [bottom] RGDS (cell-adhesive peptide). PEG Control = PEG-DA hydrogel (3.4k g/mol) prepared from an aqueous precursor solution. [Scale bars = 50 μm].

3.4.9. Cytocompatibility

Low cytotoxicity of $PDMS_{star}$-PEG hydrogels prepared via SIPS is essential for their utility as tissue engineering scaffolds. Cytocompatiblity was assessed by measuring LDH levels released by 10T½ cells 24 hr post-seeding onto RGDS-modified hydrogels based on 3.4k g/mol PEG-DA as a representative series (**Figure 3.12**). LDH is a soluble cytosolic enzyme that is released into the culture medium following membrane damage due to apoptosis or necrosis [199]. Thus, differences in the normalized levels of exogenous LDH across cell-laden hydrogels are indicative of the amount of cell death induced by the hydrogel composition. At all levels of $PDMS_{star}$-MA, the relative LDH activity associated with $PDMS_{star}$-PEG hydrogels prepared via SIPS were similar to pure PEG-DA hydrogels prepared via SIPS as well as PEG-DA hydrogels fabricated from aqueous precursor solutions. Thus, at these levels of $PDMS_{star}$-MA, $PDMS_{star}$-PEG hydrogels maintain the low cytotoxicity of PEG-DA hydrogels.

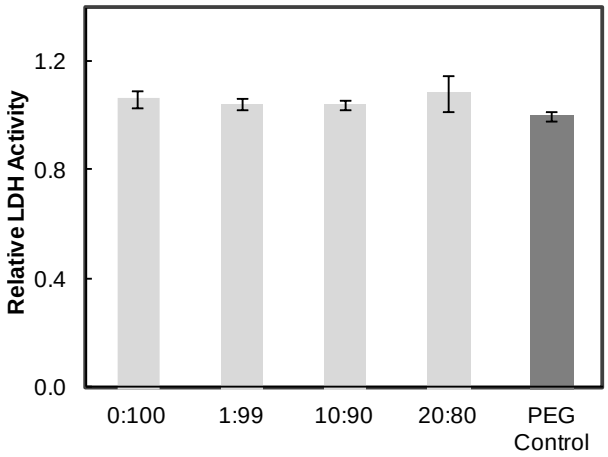

Figure 3.12. Relative LDH activity (24 hr) of $PDMS_{star}$-PEG hydrogels fabricated with 3.4k g/mol PEG-DA from a DCM precursor solution (i.e. via SIPS) with varying wt% ratio $PDMS_{star}$-MA:PEG-DA. PEG Control = PEG-DA hydrogel (3.4k g/mol) prepared from an aqueous precursor solution. All formulations were statistically similar versus each other (ANOVA, $p < 0.05$).

3.5. Conclusions

Hydrogels which maintain the useful properties of PEG-DA hydrogels but extend their physical and chemical properties would be useful for controlled cell-material interaction studies. In this study, $PDMS_{star}$-PEG hydrogels were fabricated via SIPS to produce macroporous morphologies and a more even distribution of bioactive PDMS versus when fabricated from an aqueous precursor solution. Hydrogel properties were tuned by adjusting the wt% ratio of $PDMS_{star}$-MA:PEG-DA (0:100, 1:99, 10:90 an 20:80) as well as PEG-DA M_n (3.4k or 6k g/mol). A pronounced increase in hydrogel stiffness (G‟) was observed for $PDMS_{star}$-PEG hydrogels fabricated via SIPS versus the corresponding hydrogel fabricated from an aqueous precursor solution and was shown to increase with $PDMS_{star}$-MA content. In addition, the degradation rate was enhanced for

hydrogels formed via SIPS. While PEG-DA hydrogels did not demonstrate bioactivity (i.e. formation of HAp upon submersion into SBF), $PDMS_{star}$-PEG hydrogels fabricated via SIPS were bioactive. This is attributed to the hydrophobic, inorganic nature of the PDMS. SIPS-produced $PDMS_{star}$-PEG hydrogels did substantially adsorb higher levels of BSA versus a PEG-DA hydrogel fabricated in water. As a result, cell adhesion and spreading onto $PDMS_{star}$-PEG hydrogels was observed only on hydrogels modified with the cell adhesive peptide RGDS. Thus, these $PDMS_{star}$-PEG hydrogels maintain the biological blank slate nature of "water fabricated" PEG-DA hydrogels. Thus, these new $PDMS_{star}$-PEG hydrogels formed by SIPS are useful to use, along with pure PEG-DA and $PDMS_{star}$-PEG hydrogels formed from aqueous precursor solutions, to study materials-guided cell behavior and tissue regeneration.

CHAPTER IV

CONTINUOUS GRADIENT SCAFFOLDS FOR RAPID SCREENING OF CELL-MATERIAL INTERACTIONS AND INTERFACIAL TISSUE REGENERATION*

4.1. Overview

In tissue engineering, the physical and chemical properties of the scaffold mediates cell behavior including regeneration. Thus, a strategy that permits rapid screening of cell-scaffold interactions is critical. Herein, eight "hybrid" hydrogel scaffolds have been prepared in the form of continuous gradients such that a single scaffold contains spatially varied properties (**Figure 4.1**). These scaffolds are based on combining an inorganic macromer [methacrylated star polydimethylsiloxane, $PDMS_{star}$-MA] and organic macromer [poly(ethylene glycol)diacrylate, PEG-DA] as well both aqueous and organic fabrication solvents.

*Reprinted with permission from "Continuous gradient scaffolds for rapid screening of cell-material interactions and interfacial tissue regeneration" by Brennan M. Bailey, Lindsay N. Nail and Melissa A. Grunlan, 2013. Acta Biomaterialia, in press online, Copyright [2013] by Acta Materialia Inc. Published Elsevier Ltd.

Having previously demonstrated its bioactivity and osteoinductivity, $PDMS_{star}$-MA is a particularly powerful component to incorporate into instructive gradient scaffolds based on PEG-DA. The following parameters were varied to produce the different gradients or gradual transitions in: (1) the wt% ratio of $PDMS_{star}$-MA to PEG-DA macromers, (2) the total wt% macromer concentration, (3) the number average molecular weight (M_n) of PEG-DA and (4) the M_n of $PDMS_{star}$-MA. Upon dividing each scaffold into four "zones" perpendicular to the gradient, it was found that spatial variation in morphology, bioactivity, swelling and modulus was demonstrated. Among these gradient scaffolds are those in which swelling and modulus are conveniently decoupled. In addition to rapid screening of cell-material interactions, these scaffolds are well-suited for regeneration of interfacial tissues (e.g. osteochondral tissues) that transition from one tissue type to another.

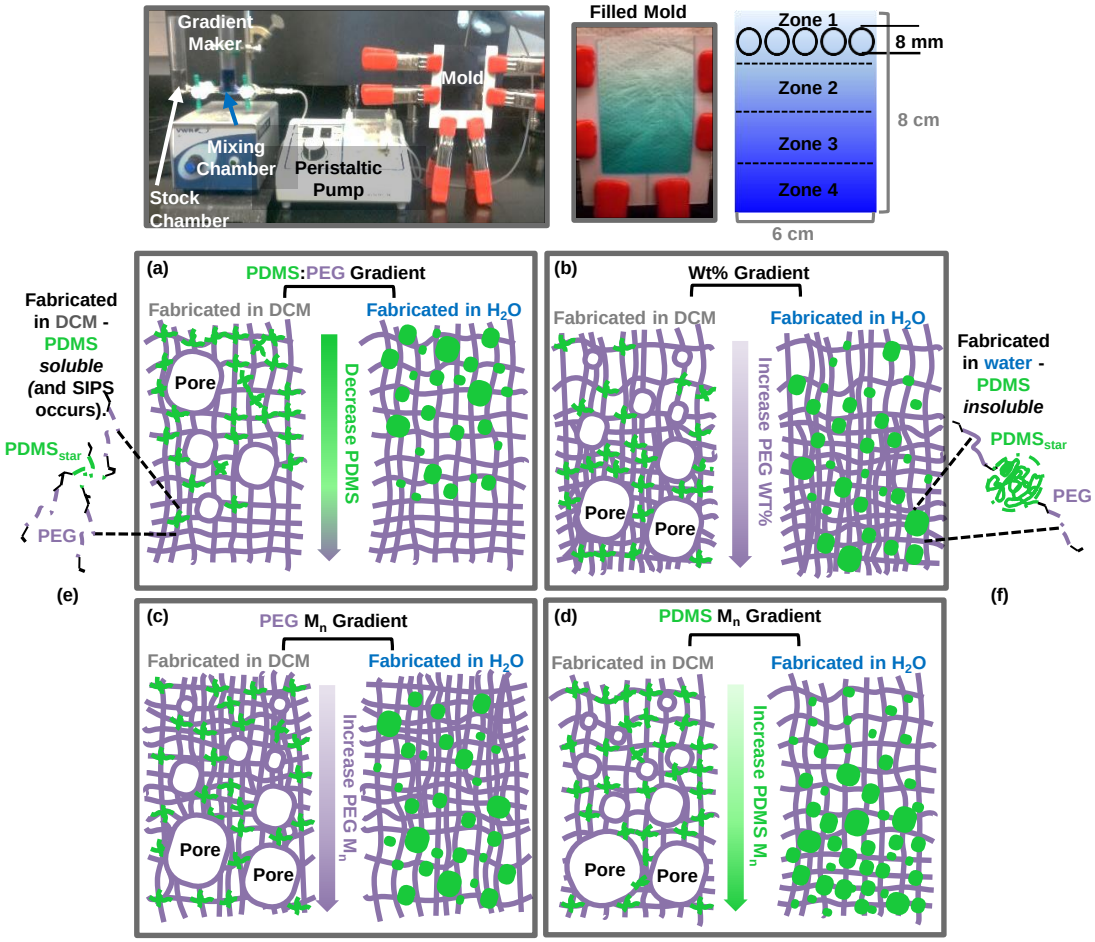

Figure 4.1. Gradient fabrication and compositions. The fabrication method (top) and eight resulting scaffolds possessing continuous gradients (bottom) based on a gradual transition in: (a) the wt% ratio of $PDMS_{star}$-MA to PEG-DA macromers, (b) the total wt% macromer concentration, (c) the M_n of PEG-DA and (d) the M_n of $PDMS_{star}$-MA. A constant wt% ratio of $PDMS_{star}$-MA to PEG-DA was maintained for b-d. Each scaffold was fabricated in both DI-H_2O and DCM to vary $PDMS_{star}$-MA distribution, scaffold porosity and modulus. Note, when fabricated from a DCM precursor solution, the resulting network was dried (i.e. DCM removal) and hydrated with water before testing.

4.2. Introduction

As with the extracellular matrix (ECM) in natural tissues, properties of the tissue engineering scaffold direct cell behavior and thus tissue regeneration [131, 132]. These include both physical properties (e.g. morphology or porosity[77, 81, 136] and modulus[86, 87, 140]) and chemical properties (e.g. chemical functionality,[75, 76, 105] hydrophobicity,[102, 174] hydration[87, 128, 175] and bioactivity[105, 106]). Importantly, recent studies suggest that these scaffold properties (e.g. modulus) may be as potent as growth factors in terms of directing stem cell fate [85, 86, 200]. As a result, scaffolds with properties precisely tuned for optimal cell regeneration have the potential to form tissues with properties closely resembling those of native tissues [1, 201]. Yet, scaffold-guided cell behavior is difficult to elucidate given the labor-intensive practice of evaluating a large number of individual scaffolds whose compositions and hence properties are iteratively varied. Thus, the development of a strategy that permits systematic and rapid screening of cell–scaffold interactions, particularly for a scaffold system with a broad range of properties, is critical. Combinatorial strategies have mainly been limited to two-dimensional (2D) culture in which arrays of isolated, individual scaffolds are rapidly produced and cells cultured on the surfaces [202-204]. However, three-dimensional (3D) culture is preferred as it better resembles the native tissue environment [205-207]. In this study, hydrogel scaffolds suitable for 3D culture have been prepared in the form of continuous gradients such that a single scaffold contains spatially varied properties. Thus, cell-material interaction studies may be conducted and compared among different "zones" defined along the gradient. These continuous

gradient hydrogel scaffolds not only allow for rapid screening of cell-material interactions, but scaffolds prepared in this way would ultimately be useful for regeneration of interfacial tissues which require scaffolds possessing spatially organized material compositions [114, 115].

Three-dimensional continuous gradients have been reported [110-113]. Recently, Chatterjee and co-workers used a gradient maker to produce continuous gradient hydrogel scaffolds based an organic macromer [poly(ethylene glycol)-diacrylate, PEG-DA] and an aqueous fabrication solvent [114]. In this study, this method has been applied to prepare "hybrid" continuous gradient hydrogel scaffolds based on combining an inorganic and organic macromer and using both aqueous and organic fabrication solvents. In previous work, introduction of inorganic, hydrophobic methacrylated star polydimethylsiloxane ($PDMS_{star}$-MA) to PEG-DA hydrogels prepared with aqueous solvent broadened both chemical and physical properties [101]. Later, it was demonstrated that both PEG-DA and $PDMS_{star}$-PEG hydrogels could be prepared via solvent-induced phase separation (SIPS) by employing dichloromethane as an organic fabrication solvent followed by sequential solvent removal and hydration after curing [100, 208]. SIPS produced hydrogels with low sol contents and low cytotoxicity as well as increased pore size, enhanced modulus and a more uniform distribution of $PDMS_{star}$-MA versus analogous hydrogels fabricated from aqueous precursor solutions. In addition, $PDMS_{star}$-PEG hydrogels fabricated from aqueous precursor solutions were bioactive, forming hydroxyapatite when exposed to simulated body fluid (SBF)[100] and furthermore resulted in an increase in osteogenic differentiation of encapsulated

mesenchymal stem cells (MSCs) in proportion to $PDMS_{star}$-MA content [108]. Based on these properties, this hybrid $PDMS_{star}$-PEG hydrogel scaffold system is particularly of interest for bone and osteochondral tissue engineering. More broadly speaking, this approach represents a general method by which a dual-component polymer scaffold system may be prepared as continuous gradients for rapid screening.

Herein, eight different continuous gradient hybrid scaffolds were prepared with spatially controlled chemical and physical properties (**Figure 4.1**). The following parameters were varied to produce the different "gradients" or gradual transitions in: (1) the wt% ratio of $PDMS_{star}$-MA to PEG-DA macromers, (2) the total wt% macromer concentration, (3) the number average molecular weight (M_n) of PEG-DA and (4) the M_n of $PDMS_{star}$-MA. Each gradient scaffold was made with both aqueous (distilled water, DI-H_2O) and organic (dichloromethane, DCM) fabrication solvents. These scaffolds were formed using a standard laboratory gradient maker (**Figure 4.1**). The stock and mixing chambers contained the designated precursor solutions (i.e. macromers, fabrication solvent and photocatalyst). A peristaltic pump and tubing were used to move the gradient maker output to a top-filling vertical mold (8 cm x 6 cm x 3 mm) consisting of two clamped rectangular glass slides separated by a U-shaped Teflon spacer. After filling, the mold was immediately exposed to UV light for 6 min (alternating sides after 3 min) to effect crosslinking. In the case of scaffolds prepared from a DCM precursor solution, the formed scaffold was dried to remove DCM and then hydrated in water. Each scaffold was divided into four "zones" along the length of the scaffold

(perpendicular to the gradient) and the morphology, bioactivity, swelling and modulus of each zone assessed.

4.3. Materials and Methods

4.3.1. Materials

Pt-divinyltetramethyldisiloxane complex (Karstedt‟s catalyst, 2 wt% in xylene), tetrakis(dimethylsiloxy)silane (tetra-SiH), and octamethylcyclotetrasiloxane (D_4) were obtained from Gelest. Allyl methacrylate, acryloyl chloride, triflic acid, 2,2-dimethyl-2-phenyl-acetophenone (DMPA), 1-vinyl-2-pyrrolidinone (NVP), triethylamine (Et_3N), $MgSO_4$, K_2CO_3, hexamethyldisilazane (HMDS), N3013 Nile Red (Nile Blue A Oxazone), NaOH, and solvents were obtained from Sigma Aldrich. HPLC grade toluene, CH_2Cl_2 (i.e. DCM) and NMR grade $CDCl_3$ were dried over 4Å molecular sieves. Poly(ethylene glycol) (PEG) [PEG-6000; MW = 5000-7000 g/mol and PEG-3400; MW = 3000-3700 g/mol per manufacturer‟s specifications] were obtained from Sigma Aldrich. The M_n of PEG-3400 (3371 g/mol) and PEG-6000 (6072 g/mol) were back-calculated from ^{1}H NMR end-group analysis of the corresponding diacrylated products. Phosphate buffered solution (PBS, pH = 7.4, without calcium and magnesium) was obtained from Mediatech.

4.3.2. $PDMS_{star}$-MA Synthesis

$PDMS_{star}$-MA (1.8k, 7k and 14k g/mol) were prepared as previously reported [209, 210].

4.3.3. PEG-DA (3.4k and 6k g/mol) Synthesis

PEG-DA (3.4k and 6k g/mol) were prepared as previously reported [101]. By ^{1}H NMR end-group analysis, M_n of PEG-DA, M_n of PEG-DA (3.4k g/mol) and PEG-DA (6k g/mol was determined to be 3382 g/mol (~3400 g/mol) and 5989 g/mol (~6000 g/mol), respectively.

4.3.4. NMR

^{1}H NMR spectra were obtained on a Mercury 300 300 MHz spectrometer operating in the Fourier transform mode. Five percent (w/v) $CDCl_3$ solutions were used to obtain spectra. Residual $CHCl_3$ served as an internal standard.

4.3.5. Continuous Gradient Hydrogel Scaffold Preparation

Macromer(s) and photocatalyst solution were combined with DI-H_2O or DCM and added to the stock and mixing chambers (the latter containing a stir bar) of a plastic gradient maker (Hoefer SG 15, Amersham Biosciences) or analogous glass gradient maker, respectively, atop a stir plate. The gradient maker output was pumped through PVC tubing (DI-H_2O-based precursor solution) or PharMed® BPT (Ryan Herco Flow Solutions) (DCM-based precursor solution) tubing at ~1 mL/min via a peristaltic pump (C.B.S. Scientific) into a single entry top-filling vertical mold (8 cm x 6 cm x 3 mm) comprised of two clamped rectangular glass slides and a U-shaped Teflon spacer. The filled mold was immediately exposed to UV light (UV-Transilluminator, 6 mW/cm^2, 365 nm) for 3 min per side. The water-based hydrogel sheets were rinsed with DI-H_2O and

soaked in a Petri dish containing DI-H_2O (60 mL) for 2 days with daily water changes. The DCM-based sheets were rinsed with DCM, air dried for 30 min and placed in a Petri dish containing DI-H_2O (60 mL). During the first hour of soaking, the water was changed every 15 min and thereafter daily for 2 days. All hydrogels were permitted to soak in DI-H_2O for a total of 72 hr prior to testing. Approximately 2 mm was removed from the perimeter to avoid any edge irregularities.

4.3.6. Confocal Laser Scanning Microscopy (CLSM)

An intact zone was soaked in 60 mL of a Nile Red solution for 24 hr and then 60 mL PBS for 3 days with daily water changes [211]. The Nile Red solution was prepared as follows: 75 μL of a Nile Red solution (20 mg per mL of methanol) was dissolved in 8 mL of DI-H_2O and combined with 120 mL of PBS. An 8 mm disc was punched from each zone along the strip, placed on a glass microscope slide and DI-H_2O dropped onto the disk to maintain hydration. Images were captured with a Leica TCS SP5 confocal microscope (Leica Microsystems, Bannockburn, IL; excitation filter of 488 nm and emission filter 490-570 nm). Images were obtained from 3 mm sections in the z-directions and assigned green for contrast.

4.3.7. Scanning Electron Microscopy (SEM)

Water-swollen hydrogels discs (8 mm diameter) were flash frozen in liquid nitrogen for 1 min and immediately lyophilized for 24 hr (Labconco Centri Vap Gel Dryer System). Specimens cross-sections were subjected to Pt-sputter coating and

viewed with a field emission scanning electron microscope (FEI Quanta 600 FE-SEM) at an accelerated electron energy of 10 keV.

4.3.8. Swelling Ratio

Five 8 mm discs from a given zone of five replicate hydrogel sheets were individually placed in a sealed vial containing 20 mL DI water and placed on a rocker table (250 rpm) for 48 hr at room temperature (RT). Discs were then removed, blotted with filter paper, and weighed (W_s). Equilibrium swelling ratio (SR) is defined as: $SR = (W_s - W_d)/W_d$, where W_s is the weight of the water-swollen hydrogel and W_d is the weight of the vacuum dried hydrogel (30 in. Hg, 60 ºC, 24 hr). The average value was calculated from the value of three individual discs representing median values.

4.3.9. Dynamic Mechanical Analysis (DMA)

Five 8 mm discs from a given zone of five replicate hydrogel sheets were collected. Their storage modulus (G‟) was measured in the compression mode with a dynamic mechanical analyzer (TA Instruments Q800) equipped with parallel-plate compression clamp with a diameter of 40 mm (bottom) and 15 mm (top). A water-swollen disc (8 mm diameter) was blotted with a Kim Wipe, clamped between the plates and silicone oil placed around the exposed hydrogel edge to prevent dehydration. Following equilibration at 25 °C (5 min), the samples were tested in a multi-frequency-strain mode (1 to 30 Hz). The average value was calculated from the value of three individual discs representing median values.

4.3.10. Bioactivity

An 8 mm disc from each zone was placed in a sealed centrifuge tube containing 20 mL of 1X SBF[186] for 14 days at 37 °C. The disc was then removed, blotted with a Kim Wipe and allowed to air dry for at least 24 hr. Next, the discs were flash frozen in liquid nitrogen (1 min) and immediately lyophilized (24 hr) (Labconco Centri Vap Gel Dryer System). To view HAp, specimen surfaces were subjected to Pt-sputter coating and viewed with a field emission scanning electron microscope (FEI Quanta 600 FE-SEM) at an accelerated electron energy of 10 keV.

4.3.11. X-ray Diffraction (XRD) Spectroscopy

Powder X-ray diffraction data was collected on a Bruker D8 diffractometer fitted with LynxEYE detector (Cu K_α; 40 kV, 40 mA; Bragg-Brentano geometry; scan range: 5 - 70°; step size: 0.05°; step time: 1 s).

4.4. Results and Discussion

4.4.1. $PDMS_{star}$:PEG Gradient

For the "$PDMS_{star}$:PEG gradient", the scaffolds were formed with a gradual transition from high (top) to low (bottom) amounts of inorganic, hydrophobic $PDMS_{star}$-MA using both DI-H_2O and DCM as the fabrication solvent (**Figure 4.1.a, Figure 4.2**). The total macromer concentration (10 wt%) and M_n of both $PDMS_{star}$-MA (7k g/mol) and PEG-DA (3.4k g/mol) were held constant. Two different precursor solutions were prepared with different wt% ratios of $PDMS_{star}$-MA to PEG-DA: 0:100 (mixing

solution) and 20:80 (stock solution). For every one mL of precursor solution was added 10 μL of photoinitiator solution (30 wt% solution of DMPA in NVP). The solutions were vortexed for 1 minute following addition of each component, poured into their respective chambers and the gradient hydrogel fabricated as stated above.

CLSM images confirmed the transition in $PDMS_{star}$-MA concentration among the different zones of the gradient (**Figure 2.a and 2.e**). Consistent with that previously observed for single composition scaffolds (i.e. "non-gradients" not formed with a gradient maker), the $PDMS_{star}$-MA formed discrete microspheres or was uniformly distributed when prepared from an DI-H_2O[127] or DCM[100] precursor solution, respectively. This was attributed to the improved solubility of $PDMS_{star}$-MA in DCM versus in DI-H_2O. As also previously noted with non-gradient scaffolds,[100] gradient scaffolds formed with a DCM precursor solution exhibited enhanced pore size, particularly in zones containing high levels of $PDMS_{star}$-MA. The increased pore size is attributed to SIPS [100, 208]. During SIPS, phase separation between the growing polymer network and solvent during cure leads to pore formation [37,[94, 95]. A macroporous morphology is generally useful due to enhanced diffusion of cellular waste and nutrients as well as for varying cell-cell proximity [79, 83]. Macroporous morphologies also contribute to an enhanced rate of degradation [36, 37, [82, 84]. In fact, faster rates of degradation were observed for non-gradient macroporous $PDMS_{star}$-PEG hydrogels (i.e. prepared from a DCM precursor solution) versus the analogous hydrogel prepared from an aqueous precursor solution [100]. It has also previously noted that non-gradient $PDMS_{star.}$PEG hydrogels exhibited both bioactivity[100] as well as

osteoinductivity [108]. Bioactive materials are attractive for bone regeneration as they chemically bond to adjacent native bone tissue via formation of a biologically active hydroxyapatite (HAp) layer [190]. Furthermore, the formation of HAp has also been shown to promote differentiation of mesenchymal stem cells (MSCs) to osteoblasts [191]. It was observed that non-gradient $PDMS_{star}$-PEG hydrogels increased stimulation of osteogenic differentiation of encapsulated MSCs in proportion to $PDMS_{star}$-MA content [108]. This behavior was attributed to the inorganic, hydrophobic nature of $PDMS_{star}$-MA, features commonly associated with other bioactive materials [105-107]. Thus, gradient scaffolds with a gradual change in bioactivity would be exceptionally useful, not only to screen cell-material interactions, but also for the ultimate regeneration of native-like osteochondral tissues which possess a gradual transition from osseous to cartilage tissue. The variation in bioactivity along the gradient scaffold was assessed via immersion in simulated body fluid (SBF, 1X) for two weeks followed by observing the amount of HAp formed via SEM. This protocol is considered to be a qualitative indication of the level of scaffold bioactivity and has also been correlated to the ability to bond to bone *in vivo* [192]. Indeed, it was found that the level of HAp gradually increased with the content of $PDMS_{star}$-MA along the gradient (**Figure 4.2.b and 4.2.f**). X-ray diffraction (XRD) was used to verify that the mineral deposits were HAp. Two zones exhibiting HAp with contrasting morphologies were examined (**Figure 4.3**). Characteristic HAp peaks of 31.7, 45.5, and 56.5 were noted. These peaks indicate reflections from 112, 222, 004 crystal planes respectively and correspond to Bragg

reflections of Hap [212]. The decreased amplitude of the peak at 31.7 for scaffold could be a result of the inhomogeneity of the HAp on the surface.

Given the known impact of swelling (i.e. hydration)[67] and modulus (i.e. stiffness)[86, 87, 140] on cell behavior, these properties were also assessed among the different zones of the gradient scaffolds (**Figure 4.2.c and 4.2.d**). For the gradient scaffold fabricated via SIPS, swelling increased (~5.5 to 6.8) and modulus decreased (~400 to 325 kPa) as the level of hydrophobic $PDMS_{star}$-MA decreased. In contrast, since $PDMS_{star}$-MA formed discrete microspheres in an "unperturbed" PEG matrix when fabricated in DI-H_2O,[101] resulting in swelling that remained very consistent (~8.6 to 8.9) across the entire gradient while modulus decreased modestly (~110 to 80 kPa). In this way, swelling and modulus are uniquely decoupled such that the effect of each parameter on cell behavior may be studied independent of one another. Notably, modulus was substantially higher for the gradient scaffold fabricated in DCM versus in DI-H_2O. As noted previously, the enhanced modulus may be due to the decreased hydration arising from a more homogeneous distribution of hydrophobic $PDMS_{star}$-MA as well as well as the increased pore size and hence pore wall thickness when fabricated via SIPS [213, 214]. For most zones, the SIPS gradient exhibits a substantial change in modulus (and hydration) within the range that has been shown to impact cell behavior [86, 215-217]. In contrast, the gradient fabricated in DI-H_2O exhibited seemingly minor zone-to-zone changes in modulus and hydration. This may afford the opportunity to decouple the effect of swelling and modulus from, for instance, PDMS content on cell behavior.

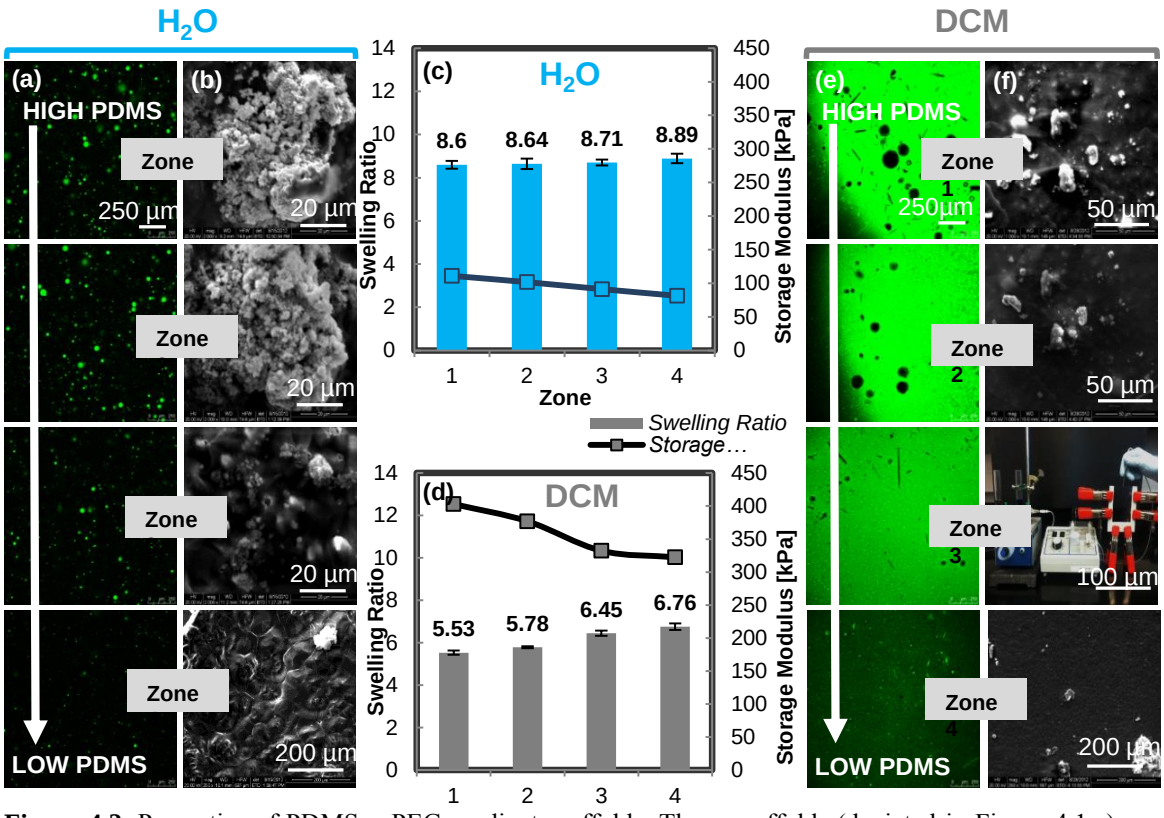

Figure 4.2. Properties of $PDMS_{star}$:PEG gradient scaffolds. These scaffolds (depicted in Figure 4.1.a) were formed with a gradual transition from high (top) to low (bottom) amounts of $PDMS_{star}$-MA using both DI-H_2O and DCM as the fabrication solvent. The total macromer concentration (10 wt%) and M_n of both $PDMS_{star}$-MA (7k g/mol) and PEG-DA (3.4k g/mol) were held constant. For gradient scaffolds prepared from an aqueous and DCM precursor solution, respectively: (a, e) CLSM images of $PDMS_{star}$-MA distribution and scaffold porosity, (b, f) SEM images of HAp formation following exposure to SBF (i.e. "bioactivity") and (c, d) swelling and modulus.

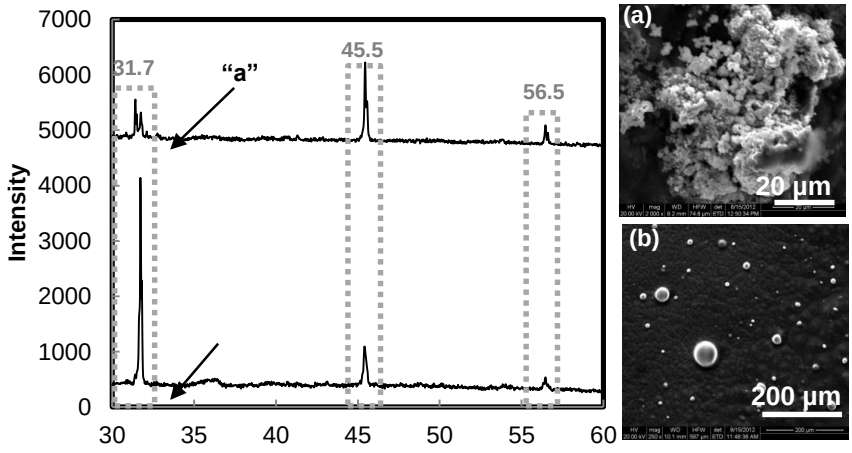

Figure 4.3. Right: SEM of HAp formation on (a) $PDMS_{star}$:PEG gradient (fabricated in DI-H_2O); zone 1 and (b) PEG-DA M_n gradient (fabricated in DI-H_2O); zone 4. Left: XRD of "a" and "b" exhibit characteristic HAp peaks of 31.7, 45.5, and 56.5.

4.4.2. Total Wt% Macromer Concentration Gradient

For the "total wt% macromer concentration gradient", scaffolds were formed with a gradual transition in the total wt% of macromer from low (top) to high (bottom) with a constant 9:91 wt% ratio of $PDMS_{star}$-MA (7k g/mol) to PEG-DA (3.4k g/mol) (**Figure 4.1.b, Figure 4.4**). Two precursor solutions were prepared at two different concentrations: 20 wt% (mixing solution) and 5 wt% (stock solution). First, 20 wt% PEG-DA (mixing solution) and 5 wt% PEG-DA (stock solution) were each dissolved in DCM or DI-H_2O and the appropriate amount of $PDMS_{star}$-MA was added to achieve a 9:91 wt% ratio. This wt% ratio was selected as it represents an intermediate wt% ratio as was utilized the "$PDMS_{star}$:PEG gradients". Formation of the gradient scaffolds proceeded as noted above. However, for gradients fabricated from a DCM precursor solution, the mold was exposed to UV light while it was filled. This was done after

observing that scaffolds exposed to UV light only after the mold was filled did not maintain the wt% gradient, perhaps due to substantial interdiffusion of these particular solutions. After filling, the mold continued to be exposed to UV light for an additional 6 min.

CLSM imaging visually confirmed constant levels of $PDMS_{star}$-MA along the gradient but with the same distribution features based on precursor solution solvent as per the $PDMS_{star}$:PEG gradient scaffolds (**Figures 4.4.a and 4.4.e**). For the scaffold gradient made from a DCM precursor solution, pore size generally increased with wt% macromer concentration due to an enhanced SIPS process. The constant levels of $PDMS_{star}$-MA produced similar levels of HAp formation along the gradient (**Figures 4.4.b and 4.4.f**).

For gradient scaffolds prepared in DI-H_2O, the increase in total wt% of macromer led to an expected dramatic decrease in swelling ratio (~12 to 5.6) (**Figure 4.4.c**). This was the widest range of swelling ratio values observed for a given scaffold composition. The substantial decrease in swelling was accompanied by a considerable increase in modulus values (~90 to 280 kPa). In contrast, swelling ratios were very similar (~5.8) among zones of the gradient scaffold fabricated with DCM (**Figure 4.4.d**). This may be attributed to the larger pore size that accompanied the increased wt% macromer concentration. Modulus values were distributed over a narrow range (~290 to 350 kPa). Thus, this latter gradient has utility for screening the impact of pore size uncoupled from both hydration and modulus.

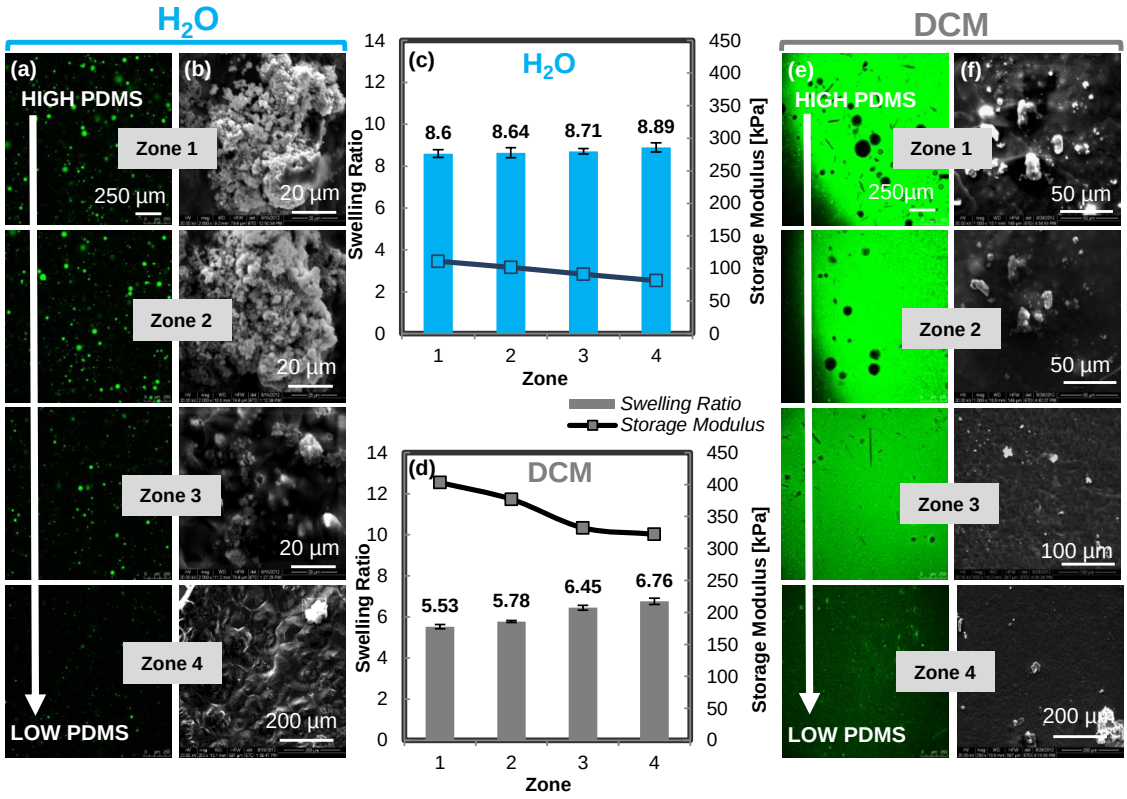

Figure 4.4. Properties of total wt% macromer concentration gradient scaffolds. These scaffolds (depicted in Figure 4.1.b) were produced with a gradual transition from low (top) to high (bottom) total wt% macromer concentrations. A constant 9:91 wt% ratio of $PDMS_{star}$-MA (7k g/mol) to PEG-DA (3.4k g/mol) was maintained. For gradient scaffolds prepared from an aqueous and DCM precursor solution, respectively: (a, e) CLSM images of $PDMS_{star}$-MA distribution and scaffold porosity, (b, f) SEM images of HAp formation following exposure to SBF (i.e. "bioactivity") and (c, d) swelling and modulus

4.4.3. PEG-DA M_n Gradient

For the "PEG-DA M_n gradient", scaffolds were formed with a gradual transition in the PEG-DA M_n from low (top) to high (bottom) with a constant 9:91 wt% ratio of $PDMS_{star}$-MA (7k g/mol) to PEG-DA (**Figure 4.1.c, Figure 4.5**). In this way, the crosslink density of the scaffold varies from high (top) to low (bottom). Two precursor solutions were prepared with two different M_n(s) of PEG-DA: 6k g/mol (mixing

solution) and 3.4k g/mol (stock solution). Both solutions were prepared at a constant concentration of 10 wt% PEG-DA in either DCM or DI-H_2O and the appropriate amount of $PDMS_{star}$-MA added to achieve a 9:91 wt% ratio ($PDMS_{star}$-MA to PEG-DA). Formation of the gradient scaffolds proceeded as noted above.

CLSM imaging visually confirmed constant levels of $PDMS_{star}$-MA along the gradient but with the same distribution features based on precursor solution solvent as noted above (**Figures 4.5.a and 4.5.e**). For the scaffold gradient made from a DCM precursor solution, higher PEG-DA M_n produced a somewhat higher concentration of pores and larger pore sizes. Similar levels of HAp formed along the gradient were observed due to the constant levels of $PDMS_{star}$-MA (**Figures 4.5.b and 45.f**).

Because of the corresponding decrease in crosslink density, an increase in PEG-DA M_n resulted in an increase in swelling and a decrease in modulus (**Figures 4.5.c and 4.5.d**). For gradient scaffolds prepared in DI-H_2O, the swelling ratio varied moderately (~8.4 to 9.6) and produced a likewise moderate decrease in modulus (~105 to 75 kPa). Scaffolds fabricated in DCM produced a wider range of swelling ratios (~6.6 to 8.3) as well as modulus values (~205 to 130 kPa).

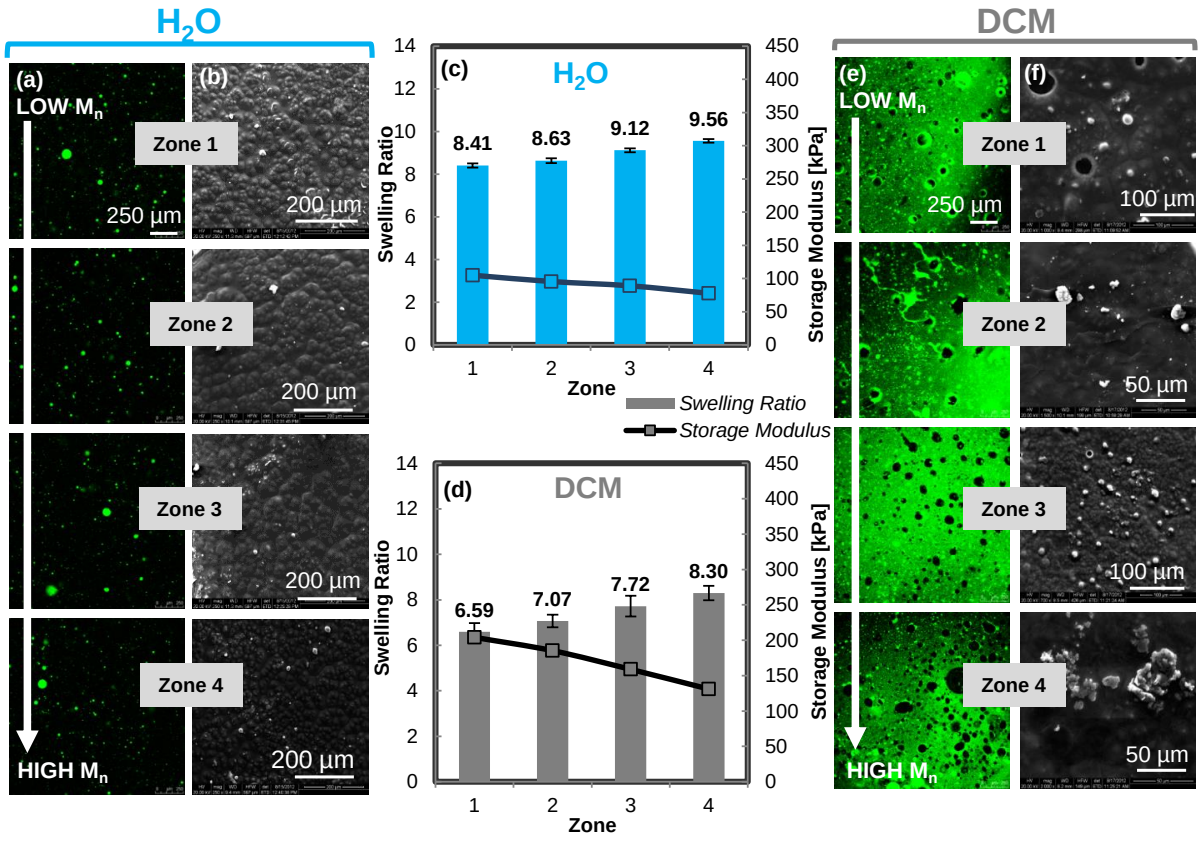

Figure 4.5. Properties of PEG-DA M_n gradient scaffolds. These scaffolds (depicted in Figure 4.1.c) were produced with a gradual transition from low (3.4k g/mol) (top) to high (6k g/mol) (bottom) PEG-DA M_n with a constant 9:91 wt% ratio of $PDMS_{star}$-MA (7k g/mol) to PEG-DA. For gradient scaffolds prepared from an aqueous and DCM precursor solution, respectively: (a, e) CLSM images of $PDMS_{star}$-MA distribution and scaffold porosity, (b, f) SEM images of HAp formation following exposure to SBF (i.e. "bioactivity") and (c, d) swelling and modulus.

4.4.4. $PDMS_{star}$-MA M_n Gradient

For the "$PDMS_{star}$-MA M_n gradient", scaffolds were formed with a gradual transition in $PDMS_{star}$-MA M_n from low (top) to high (bottom) with a constant 9:91 wt% ratio of $PDMS_{star}$-MA to PEG-DA (3.4k g/mol) (**Figure 4.1.d, Figure 4.6**). Two precursor solutions were prepared with two different M_n"s of $PDMS_{star}$-MA: 14k g/mol

(mixing solution) and 1.8k g/mol (stock solution). Both solutions were prepared at a constant concentration of 10 wt% PEG-DA in either DCM or DI-H_2O and the appropriate amount of $PDMS_{star}$-MA added to achieve a 9:91 wt% ratio ($PDMS_{star}$-MA to PEG-DA). Thus, in contrast to the "PEG-DA M_n gradient", here, the M_n of the minor component ($PDMS_{star}$-MA) is varied. Formation of the gradient scaffolds proceeded as noted above.

When DI-H_2O was used as the fabrication solvent, CLSM images showed increased $PDMS_{star}$-MA M_n enhanced its insolubility in water and led to an increase in PDMS-microparticle number and size (**Figures 4.6.a**). When DCM was used as the fabrication solvent, the increase in $PDMS_{star}$-MA M_n enhanced the effects of SIPS, leading to the general increase in pore size (**Figures 4.6.e**). For both gradient scaffolds, HAp was observed in all zones due to the constant level of $PDMS_{star}$-MA (**Figures 4.6.b and 4.6.f**).

For both gradient scaffolds, swelling ratio was quite constant and modulus remained varied within a tight range across the different zones (**Figures 4.6.c and 4.6.d**). Again, this is expected since it was the M_n of the minor component ($PDMS_{star}$-MA) that was continuously varied. However, the fabrication solvent had a notable impact on these properties. When prepared from an aqueous precursor solution, swelling and modulus (~10 and ~65 to 40 kPa) were substantially higher and lower, respectively, versus the gradient scaffolds prepared from DCM precursor solution (~7 and ~205 to 175 kPa). Thus, these scaffolds would permit the evaluation of subtle changes in scaffold modulus independent of hydration.

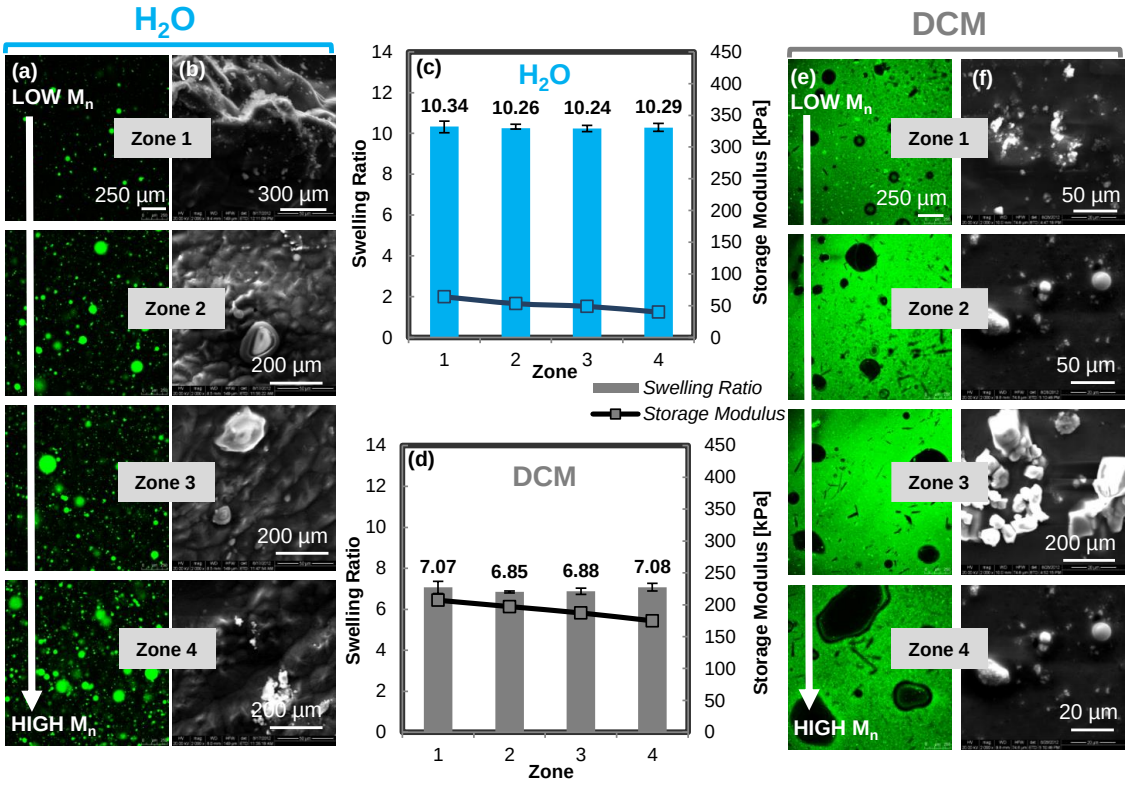

Figure 4.6. Properties of $PDMS_{star}$-MA M_n gradient scaffolds. These scaffolds (depicted in Figure 4.1.d) were produced with a gradual transition from low (top) to high (bottom) $PDMS_{star}$-MA M_n with a constant 9:91 wt% ratio of $PDMS_{star}$-MA to PEG-DA (3.4k g/mol). For gradient scaffolds prepared from an aqueous and DCM precursor solution, respectively: (a, e) CLSM images of $PDMS_{star}$-MA distribution and scaffold porosity, (b, f) SEM images of HAp formation following exposure to SBF (i.e. "bioactivity") and (c, d) swelling and modulus.

4.5. Conclusions

Herein, "hybrid" continuous gradient hydrogel scaffolds have been prepared based on combining an inorganic ($PDMS_{star}$-MA) and organic macromer (PEG-DA) and using both aqueous and organic fabrication solvents. The previously established bioactivity[100] and osteoinductivity[108] of $PDMS_{star}$-MA makes it a particularly

powerful component to incorporate into gradient scaffolds based on PEG-DA. These scaffolds were quickly produced and exhibited spatially varied chemical and physical properties. Specifically, the ability to spatially control $PDMS_{star}$-MA distribution, pore size, bioactivity, swelling and modulus within a single scaffold was demonstrated. The eight gradient scaffolds reported herein exhibited swelling values from ~5.5 to 12 and modulus values from ~40 to 405 kPa. Their rapid production and achievable range of properties not only allow for rapid screening of cell-material interactions, but would also prove useful towards the regeneration of interfacial tissues which require scaffolds comprised of spatially organized material compositions [114, 115]. Given the bioactivity and osteoinductivity of $PDMS_{star}$-MA, these hybrid scaffolds are particularly of interest for bone and osteochondral tissue engineering. In the case of hydrogel gradients produced via SIPS, direct photoencapsulation obviously is prohibited. Thus, pore interconnectivity, essential for 3D penetration of seeded cells will require modification of fabrication with a poragen strategy (e.g. salt leaching).

CHAPTER V

SYNTHESIS OF AMINATED AND PHOSPHONATED POLY(DIMETHYL SILOXANE) METHACRYLATE FOR ENHANCED BIOACTIVITY AND OSTEOINDUCTIVITY

5.1. Introduction

Similar to the extracellular matrix (ECM) in natural tissues, properties of the tissue engineering scaffold direct cell behavior and accordingly tissue regeneration [131, 132]. These include both physical properties (e.g. morphology or porosity [77, 81, 136] and modulus [86, 87, 140]) as well as chemical properties (e.g. chemical functionality, [75, 76, 105] hydrophobicity, [102, 174] hydration [87, 128, 175] and bioactivity [105, 106]). Thus, scaffolds with properties modified for optimal cell regeneration have the potential to form tissues with properties closely resembling those of native tissues [1, 201].

In previous work, physical and chemical properties of poly(ethylene glycol) diacrylate (PEG-DA)-based hydrogel scaffolds were altered via both incorporation of methacrylated star poly(dimethyl siloxane) ($PDMS_{star}$-MA) and fabrication with solvent-induced phase separation (SIPS) [100, 208]. SIPS produced hydrogels with low sol contents and low cytotoxicity as well as increased pore size, enhanced modulus and a more uniform distribution of $PDMS_{star}$-MA versus analogous hydrogels fabricated from aqueous precursor solutions. In addition, $PDMS_{star}$-PEG hydrogels fabricated from aqueous precursor solutions were bioactive, forming hydroxyapatite when exposed to

simulated body fluid (SBF) [100] and furthermore resulted in an increase in osteogenic differentiation of encapsulated mesenchymal stem cells (MSCs) corresponding to $PDMS_{star}$-MA content [108]. This is ideal as bioactive, osteoinductive scaffolds improve regeneration of and integration into bone tissue [218].

The focus of this study is further enhancement of the bioactivity and osteoinductivity of a PDMS macromer via functionalization with amine and phosphonate groups. Well-defined (2D) models have been used to study the effects of amine and phosphonate on cell behavior [116-119]. Keselowsky et al. demonstrated that surfaces grafted with amine groups up-regulated osteoblast-specific gene expression, alkaline phosphatase enzymatic activity, and matrix mineralization [117]. The positive charge on these functional groups at neutral pH may explain this phenomenon [117]. Increasing phosphonate content of graft copolymers on the surfaces of biomaterials increased osteoblast-like cell adhesion and proliferation [120]. Also, the functionalization of polymers with phosphorous-containing pendant groups has shown to result in more complete mineralization and at a faster rate [121]. Recent findings suggest phosphate-containing polymers possess an affinity for calcium ions necessary for the development of biomaterial-associated calcification [219, 220]. Thus, it was expected that amine and phosphonate functionalized PDMS would exhibit enhanced bioactivity and osteoinductivity.

Phosphorous-based scaffolds are of particular interest for bone tissue regeneration given the ideal osteoinductive environment they are able to provide [123-125]. Saltzman et al. found that the adhesion and growth of osteoblast-like cells within

acrylamide gels increased with increasing phosphonate content [123]. While, Anseth et al. incorporated pendant phosphate groups into PEG hydrogels and saw an increased rate and degree of mineralization within the hydrogel even in the absence of hMSCs [126]. Amines have not been incorporated into hydrogel scaffolds for cell behavior studies with regard to osteoinductivity and bioactivity, providing further motivation for the study herein.

In this work, amine functionalized PDMS has been synthesized. Also, a protocol and rationale for further functionalization with phosphonate has been established (**Figure 5.1**). Based on the osteoinductivity and bioactivity of PDMS [99, 108] it is expected that amine and phosphonate groups would further enhance these properties. Future methacrylation and incorporation of these macromers into the previously described PEG-DA scaffold system is expected to provide a method of study regarding their effects on cell behavior in a 3D environment. These scaffolds are also anticipated to be valuable for osteochondral tissue regeneration.

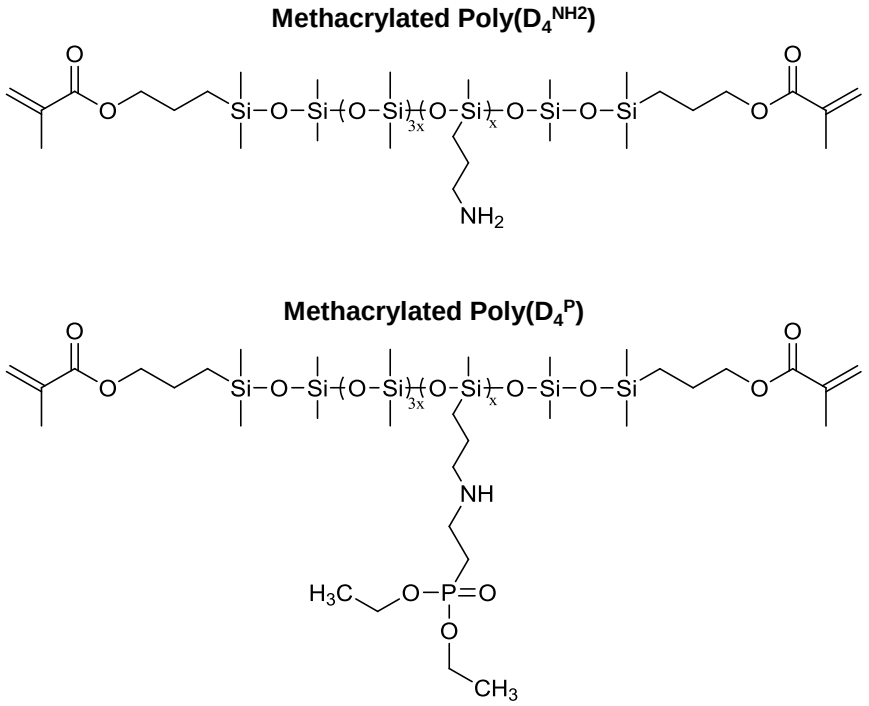

Figure 5.1. Amine and phosphonate functionalized PDMS-MA described herein for subsequent incorporation into PEG-DA hydrogels towards enhanced bioactivity and osteoinductivity of tissue engineering scaffolds.

5.2. Materials and Methods

5.2.1. Materials

Heptamethyl-cyclotetrasiloxane (D_4^{H1}), 1,1,3,3,5,5,7,7,9,9-decamethylpenta-siloxane, 95% (DMPS), and tetramethylammonium siloxanolate (TMAS) were obtained from Gelest. Activated carbon was obtained from Fisher Scientific. Platinum (IV) oxide (PtO_2), allyl amine, and NMR grade $CDCl_3$ were obtained from Sigma Aldrich. $CDCl_3$ was dried over 4Å molecular sieves.

5.2.2. Aminotrimethyleneheptamethylcyclo-tetrasiloxane (D_4^{NH2}) Synthesis (**Figure 5.2.a**)

D_4^{NH2} was prepared as previously reported [221]. Briefly, D_4^{H1} (5.1 g, 18 mmol), allyl amine (1.55 g, 27 mmol) and a small amount of PtO_2 were added in a pressure vessel under nitrogen. The vessel was sealed and heated at 85°C for 24 h. The product was then removed, allowed to cool, and analyzed with NMR. In the case of incomplete reaction, additional allyl amine and PtO_2 was added, the reaction purged with nitrogen, and allowed to proceed at 85°C for 4 h. After cooling to room temperature, the crude product was combined with two identical reactions to improve yield, and activated carbon added. The reaction was then purified by vacuum distillation and vacuum dried at 60 ºC overnight to afford product D_4^{NH2} (11g, yield 56%, bp: 78°C/0.8 mm Hg). ^{1}H-NMR (δ ppm): 2.65–2.61 (m, 2H, NH_2–C*H*$_2$–CH_2–CH_2), 1.49–1.39 (m, 2H, NH_2–CH_2–C*H*$_2$–CH_2), 0.51–0.46 (m, 2H, NH_2– CH_2–CH_2–C*H*$_2$), 0.04 (s, 21H, Si–C*H*$_3$).

5.2.3. Amine Functionalized Poly(dimethyl siloxane) (Poly (D_4^{NH2})) Synthesis (**Figure 5.2.b**)

D_4^{NH2} (2.75 g, 8.1 mmol), DMPS 0.23 g (0.63 mmol) and TMAS (0.1 wt %) were combined in a round bottom flask equipped with a magnetic stir bar and rubber septum. The air in the flask was exchanged with nitrogen and the reaction temperature increased to 90°C. After 10 h, the reaction was heated at 140 ºC for 3 h while bubbling nitrogen through to decompose the catalyst. The reaction mixture was then heated at 125 ºC under vacuum for 5 h to remove cyclics [222]. Colorless oil was given (1.7 g, yield 57%).

^{1}HNMR (δ ppm): 2.66–2.61 (m, 32H, NH_2–C*H*$_2$–CH_2– CH_2), 1.49–1.39 (m, 32H, NH_2–CH_2–C*H*$_2$–CH_2), 0.52– 0.46 (m, 32H, NH_2–CH_2–CH_2–C*H*$_2$), 0.05 (s, 431H, Si–C*H*$_3$); M_n (g/mol): 5700.

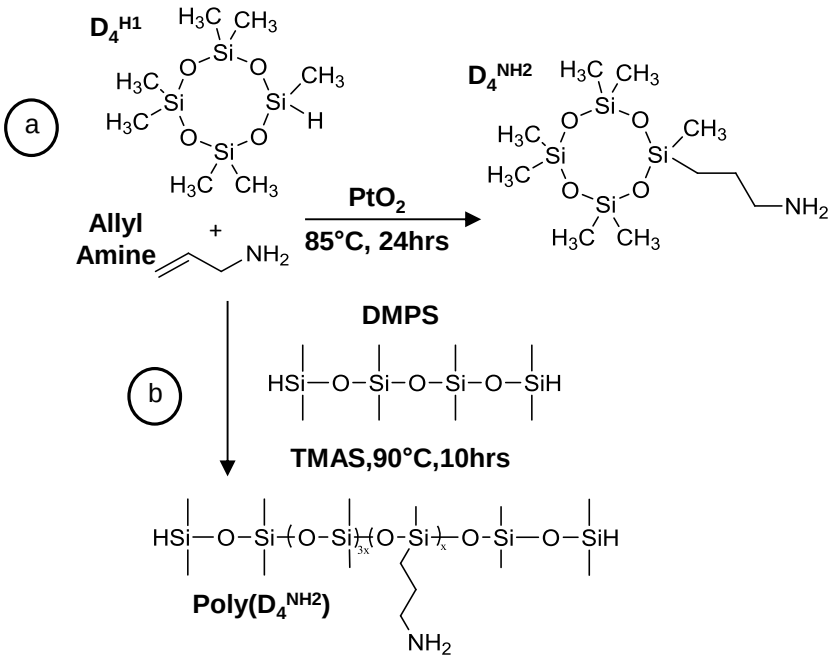

Figure 5.2. (a) Platinum catalyzed hydrosilylation of D_4^{H1} with allyl amine to yield D_4^{NH2} and (b) base catalyzed ring opening polymerization of D_4^{NH2} to yield silane terminated, amine functionalized PDMS (Poly(D_4^{NH2})).

5.2.4. NMR

^{1}H NMR spectra were obtained on a Mercury 300 300 MHz spectrometer operating in the Fourier transform mode. Five percent (w/v) $CDCl_3$ solutions were used to obtain spectra. Residual $CHCl_3$ served as an internal standard.

5.3. Results and Discussion

Materials which promote mineralization can be incorporated into tissue engineering scaffolds for improved regeneration of bone tissue [218]. The bioactivity of PDMS, [100, 109] phosphonates, [116, 125] and amines [117, 118] has been established. Thus, it was expected that PDMS functionalized with amine and phosphonate would result in significantly enhanced bioactivity and osteoinductivity. Therefore, a straightforward synthesis for the functionalization of PDMS with either amine (**Figures 5.2 and 6.2**) or phosphonate (**Figures 5.2 and 6.3**) has been described herein. A linear PDMS polymer has been synthesized as a more complex synthesis is required compared to previous studies involving $PDMS_{star}$-MA. Linear PDMS will provide a more simplistic approach for analysis of these novel polymers.

5.3.1. Amine Functionalized Poly(dimethyl siloxane) (Poly (D_4^{NH2})) Synthesis

Functionalization of PDMS with amine (Poly (D_4^{NH2})) is a two-step synthesis (**Figure 5.2**). First, a siloxane ring possessing one functional silane underwent hydrosilylation with the vinyl of allyl amine (**Figure 5.2.a**). The product was black due to the use of a platinum catalyst. The catalyst was subsequently removed by distilling with activated carbon, yielding a clear product. Thorough removal of the catalyst is expected to be important for subsequent synthesis.

Next, the siloxane ring was opened using a base catalyzed ring opening polymerization with a short silane terminated dimethylsiloxane as an end capping agent (**Figure 5.2.b**). This resulted in a silane terminated, amine functionalized PDMS

polymer. The polymer is such that every third siloxane repeat unit possesses a functional amine (assuming complete reaction). The molecular weight of the polymer synthesized herein was determined to be 5700 g/mol by end-group analysis This gives an "x" value of 16 (**Figure 5.2.b**). Molecular weight may be increased or decreased with longer and shorter reaction times, respectively. The silane groups on each end of the PDMS will allow for the subsequent hydrosilylation with allyl methacrylate thereby permitting subsequent photo-crosslinking with PEG-DA (**Figures 6.1 and 6.2**). NMR spectroscopy was used to confirm each synthetic step as well as determine molecular weight of the polymer.

5.3.2. Phosphonate Functionalized Poly(dimethyl siloxane) (Poly(D_4^P)) Proposed Synthesis

The synthesis of phosphonate functionalized PDMS (Poly(D_4^P)) began in the same way as that of Poly(D_4^{NH2}) (**Figure 5.2**). However, an additional subsequent step is required to attach the phosphonate. This can be done by reacting the vinyl group of DEVP with the functional amine on Poly(D_4^{NH2}) via an aza-Michael Addition (**Figure 6.3.a**). Similar to the synthesis of Poly(D_4^{NH2}), the silane side groups can then be reacted with allyl methacrylate to introduce photo-crosslinking capabilities (**Figure 6.3.b**).

5.4. Conclusions

Herein, the synthesis of amine functionalized poly(dimethyl siloxane) was reported (**Figure 5.2**). In addition, a protocol for phosphonate functionalized PDMS was

established (**Figures 5.2 and 6.3.a**). Based on the previously established bioactivity of PDMS, [100, 109] phosphonates, [116, 125] and amines [117, 118] it is expected that these hybrid materials will exhibit significant bioactivity and osteoinductivity.

Future addition of methacrylate end groups will allow incorporation into hydrogel scaffolds. This is expected to deliver a tissue engineering scaffold capable of regenerating more native-like bone tissue. It is expected that these novel macromers combined with previously described fabrication processes (i.e. SIPS and continuous gradients) will provide a platform for the rapid assessment of a broad range of properties. These studies are anticipated to result in the establishment of an ideal environment for bone, cartilage, and bone – cartilage interfacial tissue regeneration.

CHAPTER VI

CONCLUSIONS AND FUTURE DIRECTIONS

6.1. Conclusions

Herein, "hybrid" continuous gradient hydrogel scaffolds have been prepared based on combining an inorganic and organic macromer and using both aqueous and organic fabrication solvents. This research resulted in the establishment of a "library" of 3D scaffolds useful for both the study of cell-material interactions as well as interfacial tissue regeneration.

In Chapter II, the ability to greatly enhance and alter the physical properties of PEG-DA hydrogels based solely on varying fabrication solvent was demonstrated [93]. The SIPS fabrication process produced hydrogels with macroporous morphologies and increased modulus values versus analogous PEG-DA hydrogels fabricated from an aqueous precursor solution. Particularly, certain properties were uncoupled, such as morphology and hydration or modulus and hydration such that their impact on cell behavior may be isolated. In addition, PEG-DA hydrogels prepared via SIPS exhibited enhanced degradation rates. In total, these SIPS PEG-DA hydrogel scaffolds possess properties beneficial for tissue engineering applications and cell-material interaction studies.

In Chapter III, modification of hydrogel chemistry and bioactivity of the scaffold was explored via incorporation of inorganic, hydrophobic $PDMS_{star}$-MA into PEG-DA hydrogels [100]. When fabricated via SIPS (rather than with an aqueous precursor

solution), the enhanced solubility of $PDMS_{star}$-MA resulted in a more homogenous distribution. In addition, modulus and pore size were increased. Bioactivity was confirmed with *in vitro* assessment of HAp formation on the scaffolds in the presence of SBF. Thus, it was expected that these scaffolds would specifically enhance outcomes for bone tissue regeneration. Also, the unique combination of properties presented by $PDMS_{star}$-PEG hydrogels formed by SIPS renders them useful to study both physical and chemical properties-guided cell behavior.

In Chapter IV, continuous gradient scaffolds were prepared to spatially control $PDMS_{star}$-MA distribution, pore size, bioactivity, swelling and modulus within a single PEG-DA hydrogel scaffold [109]. The rapid production and broad range of properties would permit prompt screening of cell-material interactions. Furthermore, with controlled distribution of bioactive $PDMS_{star}$-MA, these hybrid scaffolds are of particular interest for bone and osteochondral tissue engineering [114, 115].

Chapter V is focused on enhancing the bioactivity and osteoinductivity of PDMS-MA by incorporating amine and phosphonate functional groups. Both of these functional groups have shown the ability to promote mineralization and osteoblast differentiation [116, 117]. Thus, PDMS polymer was functionalized with an amine (Poly (D_4^{NH2})). Also, motivation for and a synthetic approach towards further functionality of Poly(D_4^{NH2}) with phosphonate was given. The subsequent attachment of cross-linkable side groups will allow for the incorporation of these polymers into a hydrogel scaffold. Such macromers can be used in systems like those of Chapters III and IV to further modify and enhance PEG-DA scaffold properties.

6.2. Future Directions

6.2.1. Poly(D_4^{NH2}) and Poly(D_4^{P}) – PEG-DA Hydrogel Scaffolds

Future studies will combine the synthetic and fabrication techniques described in the preceding chapters to create a library of scaffolds based on the incorporation of Poly(D_4^{NH2}) and Poly(D_4^{P}) into PEG-DA hydrogel scaffolds. Similarly to the methods described in Chapter IV, these functionalized polymers can be incorporated into PEG-DA scaffolds along a continuous gradient (**Figure 6.1**). This will allow for the rapid screening of cell-material interactions. It is also expected that this will provide an improved scaffold for the regeneration of osteochondral tissue due to the additional bioactivity of the amine and phosphonate moieties on bioactive, osteoinductive PDMS. The use of both DCM and DI-H_2O is expected to further alter the properties (e.g. porosity, stiffness, and hydration) based on the combination of phosphonate and amine with hydrophobic PDMS.

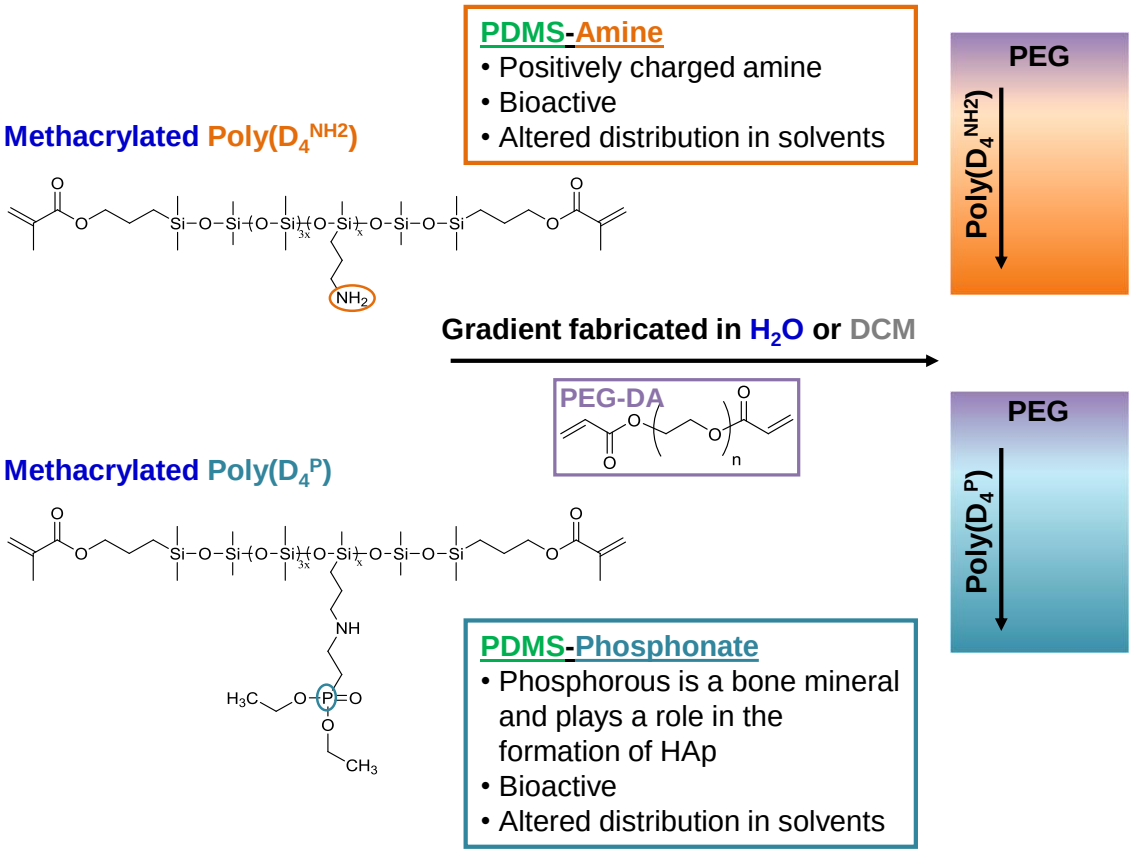

Figure 6.1. Methacrylated Poly(D_4^{NH2}) and Poly(D_4^{P}) can be subsequently incorporated into the "gradient platform technology" established in Chapter IV allowing for rapid screening and potentially the fabrication of more native-like osteochondral interface. Amine and phosphonate moieties on PDMS are expected to enhance properties of PEG-DA hydrogel scaffolds, including bioactivity.

6.2.1.1. Methacrylated Poly(D_4^{NH2}) and Methacrylated Poly(D_4^{P}) Synthesis

The synthesis from Chapter V will be completed in future studies yielding two bioactive polymers capable of crosslinking within a hydrogel scaffold (**Figure 6.1**). First, the completion of the synthesis of Poly(D_4^{NH2}) requires the attachment of photo-crosslinkable end groups. The silane side groups can be reacted with the vinyl group of allyl methacrylate via a "Pt" catalyzed hydrosilylation reaction (**Figure 6.2**). When

combined with a photo-catalyst, this provides a means for photo-crosslinking this polymer into a PEG-DA hydrogel (**Figure 6.1.**).

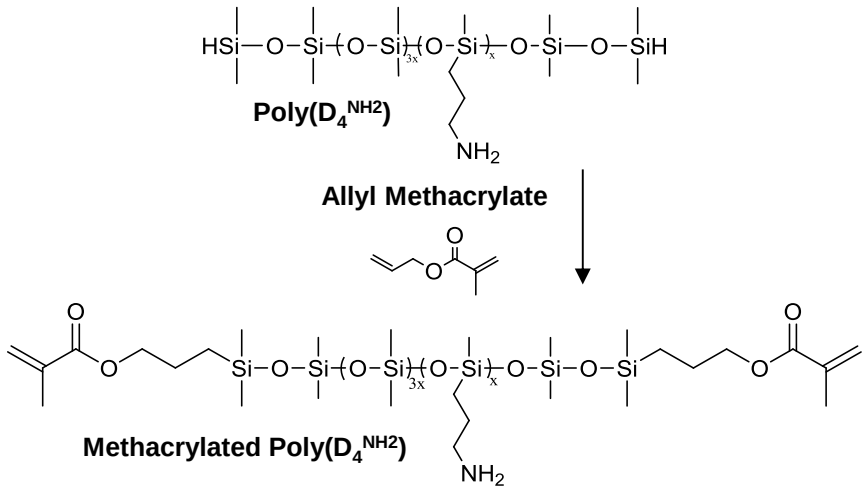

Figure 6.2. Hydrosilylation of D_4^{NH2} with allyl methacrylate to yield an amine functionalized polymer capable of photo-crosslinking into a PEG-DA hydrogel scaffold.

The synthesis of Poly(D_4^{P}) requires an additional step in which the phosphonate is attached to the amine moiety. This can be done by reacting the vinyl group of DEVP with the functional amine on Poly(D_4^{NH2}) via an aza Michael Addition (**Figure 6.3.a**). Similar to the synthesis of Poly(D_4^{NH2}), the silane terminated polymer can then be reacted with allyl methacrylate to introduce a mechanism for photo-crosslinking the polymer into a hydrogel (**Figure 6.3.b**).

6.2.1.2. Spatially Controlled Incorporation of Poly(D_4^{NH2}) and Poly(D_4^{P}) into PEG- DA Hydrogels

Based on previous studies, altered scaffold properties are expected as a result of varied dissolution and distribution of these materials dependent on solvent polarity [100]. The use of solvent is also expected to alter physical properties (i.e. increased pore size and modulus) [93]. Utilizing the recently established gradient fabrication platform [109] will allow for rapid assessment of cell – material interactions. The combination and spatial control of properties such as bioactivity (e.g. mineral deposition), modulus, porosity, and hydrophilicity is expected provide an ideal environment for osteochondral interface tissue regeneration.

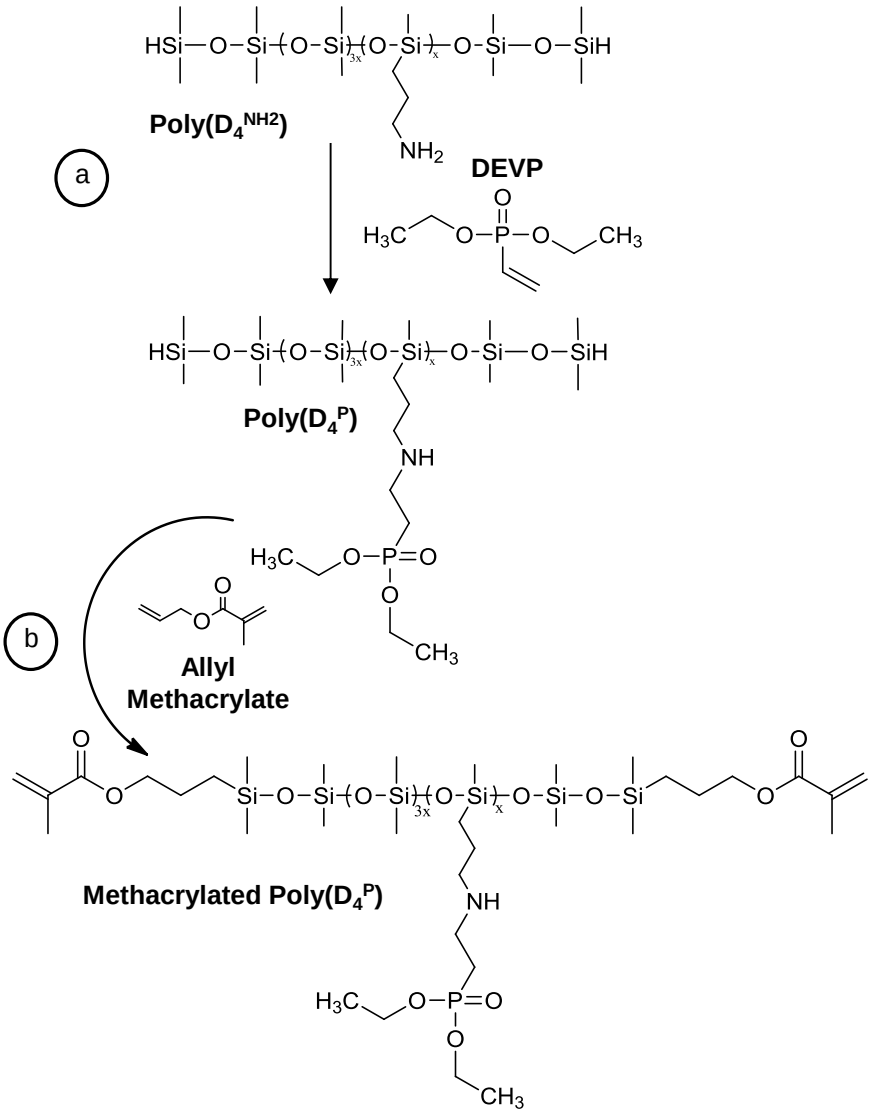

Figure 6.3. (a) Platinum catalyzed hydrosilylation of Poly(D_4^{NH2}) with DEVP to yield a phosphonate functionalized polymer and (b) platinum catalyzed hydrosilylation of Poly(D_4^{P}) to yield a phosphonate functionalized polymer capable of photo-crosslinking within a PEG-DA hydrogel.

6.2.2. Enhanced Osteoconductivity and Biodegradability

In the case of hydrogel scaffolds produced via SIPS, direct photoencapsulation is obviously prohibited. Thus, to permit cell seeding resulting in full thickness delivery, the requisite pore interconnectivity can be achieved by incorporation of a poragen (e.g. salt leaching). Grunlan et al. recently fabricated inorganic–organic shape memory polymer foams with tunable pore size and high interconnectivity. This was done via a refined solvent-casting/particulate-leaching (SCPL) method [223]. Briefly, salt particles were fused by the addition of water. A solution of acrylated polymer in DCM was then photo-cured around the fused salt matrix and the salt matrix removed via leaching resulting in interconnected pores.

In addition, biodegradation of the scaffolds could be further enhanced and altered as the scaffold‟s degradation rate should parallel that of the regeneration of tissue. This can be done via substitution of PDMS with poly(silyl ether) (PSE). Due to its more hydrophilic nature and the hydrolytic instability of silyl ether bonds, faster degradation is expected. Thus, degradation rate can be altered based on the choice of macromere (i.e. PDMS or PSE) incorporated into the SIPS fabricated PEG-DA hydrogel.

REFERENCES

[1] Khan IM, Gilbert SJ, Singhrao SK, Duance VC, Archer CW. Cartilage integration: Evaluation of the reasons for failure of integration during cartilage repair. A review. Eur Cells Mater. 2008;16:26-39.

[2] Emans PJ, Hulsbosch M, Wetzels G, Bulstra SK, Kuijer R. Repair of osteochondral defects in rabbits with ectopically produced cartilage. Tissue Eng. 2005;11:1789-96.

[3] Barrie HJ. Osteochondritis dissecans 1887-1987. J Bone Joint Surg. 1987;69B:693-5.

[4] Gelber AC, Hochberg MC, Mead LA, Wang N, Wigley FM, Klag MJ. Joint injury in young adults and risk for subseequent knee and hip osteoarthritis. Ann Intern Med. 2000;133:321-8.

[5] Lawrence RC, Helmick CG, Arnett FC, Deyo RA, Felson DT, Giannini EH, et al. Estimates of the prevalence of arthritis and selected musculoskeletal disorders in the United States. Arthrit Rheum. 1998;41:778-99.

[6] Lohmander LS, Englund PM, Dalhl LD, Roos EM. The long-term consequence of anterior cruciate ligament and meniscus injuries: osteoarthritis. Am J Sports Med. 2007;35:1756-69.

[7] Buckwalter JA, Brown TD. Joint injury, repair, and remodeling. Clin Orthop Relat Res. 2004;423:7-16.

[8] Gross AE, Shasha N, Aubin P. Long-term followup of the use of fresh osteochondral allografts for posttraumatic knee defects. Clin Orthop. 2005;435:79-87.

[9] Aubin P, Cheah HK, Davis AM, Gross AE. Long-term followup of fresh femoral osteochondral allografts for posttraumatic knee defects. Clin Orthop Relat Res. 2001;391:S318-S27.

[10] Scopp JM, Mandelbaum BR. Hospital Physician Orthopaedic Sports Medicine Board Review Manual: Turner White; 2005.

[11] Buckwalter JA, Lane NE. Athletics and osteoarthritis. Am J Sports Med. 2000;25:159-68.

[12] Buckwalter JA, Mankin HJ. Articular cartilage: II. Degeneration and osteoarthritis, repair, regeneration and transplantation. J Bone Joint Surg. 1997;79A:612-32.

[13] Buckwalter JA, Martin JA, Mankin HJ. Synovial joint degeneration and teh syndrome of osteoarthritis. Instr Course Lect. 2000;49:481-9.

[14] Buckwalter JA, Stanish WD, Rosier RN, Schenck RC, Dennis DA, Coutts RD. The increasing need for nonoperative treatment of osteoarthritis. Clin Orthop. 2001;385:36-45.

[15] Buckwalter JA, Ballard TW. Primer on the rheumatic diseases. Arthritis Foundation. Atlanta2001. p. 613-23.

[16] Dieppe P, Buckwalter JA. Management of limb osteoarthritis. In: J.H. K, Dieppe PA, editors. Rheumatology. London: Mosby; 1997. p. 9.1-10.

[17] Sant S, Hancock MJ, Donnelly JP, Iyer D, Khademhosseini A. Biomimetic gradient hydrogels for tissue engineering. Can J Chem eNG. 2010;88:899-911.

[18] Inoue G. Bilateral osteochondritis dissecans of the elbow treated by Herbert screw fixation. Br J Sports Med. 1991;25:142-4.

[19] Angel MJ, Razzano P, Grande DA. Defining the challenge - the basic science of articular cartilage repair and response to injury. Sports Med Arthroscopy Rev. 2003;11:168-81.

[20] Shapiro F, Koide S, Glimcher MJ. Cell origin and differentiation in the repair of full-thickness defects of articular cartilage. J Bone Joint Surg Am. 1993;75:532-53.

[21] Bentley G, Biant LC, Carrington RWJ, Akmal M, Goldberg A, Williams AM, et al. A prospective, randomised comparison of autologous chondrocyte implantation versus mosaicplasty for osteochondral defects in the knee. J Bone Joint Surg. 2003;85-B:223-30.

[22] Knutsen G, Engebretsen L, Ludvigsen TC, Drogset JO, Grontvedt T, Solheim E, et al. Autologous chondrocyte implantation compared with microfracture in the knee. A randomized trial. J Bone Joint Surg Am. 2004;86A:455-64.

[23] Steadman JR, Rodkey WG, Rodrigo JJ. Microfracture:surgical technique and rehabilitation to treat chondral defects. Clin Orthop Relat Res. 2001;391:S362-9.

[24] van der Kooy D, Weiss S. Why stem cells? Science. 2000;287:1439-41.

[25] Outerbridge HK, Outerbridge AR, Outerbridge RE. The use of a lateral patellar autologous graft for the repair of a large osteochondral defect in the knee. J Bone Joint Surg Am. 1995;77:65-72.

[26] Attmanspacher W, Dittrich V, Stedtfeld HW. Our experience with the arthroscopic therapy of chondral and osteochondral defects of the knee with the OATS. Zentralbl Chirug. 2000;125:494-9.

[27] Stone KR, Walgenbach AW, Freyer A, Turek TJ, Speer DP. Articular cartilage paste grafting to full-thickness articular cartilage knee joint lesions: a 2- to 12-year follow-up. Arthroscopy. 2006;22:291-9.

[28] O' Driscoll SW. The healing and regeneration of articular cartilage. J Bone Joint Surg Am. 1998;80:1795-812.

[29] Carranza-Bencano A, Perez-Tinao M, Ballesteros-Vazquez P, Armas-Padron JR, Hevia-Alonso A, Martos Crespo F. Comparitive study of the reconstruction of articular cartilage defects with free costal perichondral grafts and free tibial periosteal grafts: an experimental study on rabbits. Calcified Tissue Int. 1999;65:402-7.

[30] Bauer TW, Muschler GF. Bone graft materials: An overview of the basic science. Clin Orthop 2000;371:10-27.

[31] Kartus J, Movin T, Karlsson J. Donor-site morbidity and anterior knee problems after anterior cruciate ligament reconstruction using autografts. Arthroscopy. 2001;17:971-80.

[32] Stapleton TR. Complications in anterior cruciate ligament reconstructions with patellar tendon grafts. Sports Med Arthrosc Rev. 1997;5:156-62.

[33] Jackson DW, Windler GE, Simon TM. Intraarticular reaction associated with the use of freeze-dried, ethylene oxide-sterilized bone-patella tendon-bone allografts in the reconstruction of the anterior cruciate ligament. Am J Sports Med. 1990;18:1-11.

[34] Coughlin MJ, Mann R, Saltzman CL. Arthritis, postural disorders, and tendon disorders. Surgery of the Foot and Ankle. 8th ed. Maryland Heights, MO: Mosby; 2006. p. 1087-123.

[35] Brittberg M, Lindahl A, Nilsson A, Ohlsson C, Isaksson O, Peterson L. Treatment of deep cartilage defects in the knee with autologous chondrocyte transplantation. N Engl J Med. 1994;331:889-95.

[36] Peterson L, Brittberg M, Kiviranta I, Akerlund EL, Lindahl A. Autologous chondrocyte transplantation. Biomechanics and long-term durability. Am J Sports Med. 2002;30:2-12.

[37] Peterson L, Minas T, Brittberg M, Nilsson A, Sjogren-Jansson E, Lindahl A. Two- to 9-year outcome after autologous chondrocyte transplantation of the knee. Clin Orthop. 2000;374:212-34.

[38] Hunziker EB. Articular cartilage repair: basic science and clinical progress. A review of the current status and prospects. Osteoarthitis and Cartilage. 2002;10:432-63.

[39] Dell'Accio F, Vanlauwe J, Bellemans J, Neys J, De Bari C, Luyten FP. Expanded phenotypically stable chondrocytes persist in the repair tissue and contribute to cartilage matrix formation and structural integration in a goat model of autologous chondrocyte implantation. J Orthop Res. 2003;21:123-31.

[40] Brittberg M, Peterson L, Sjogren-Jansson E, Tallheden T, Lindahl A. Articular cartilage engineering with autologous chondrocyte transplantation. A review of recent developments. J Bone Joint Surg Am. 2003;85-A(Suppl 3):3109-15.

[41] HCUPnet. National statistics on all stays: 2005 outcomes by patient and hospital characteristics for ICD-9-CM principal procedure code 81.54 total knee replacement.

[42] Kurtz S, Ong K, Schmier MA, Mowat F, Saleh K, Dybvik E, et al. Future clinical and economic impact of revision total hip and knee arthroplasty. J Bone Joint Surg. 2007;89:144-51.

[43] Schmalzried TP, Callaghan JJ. Wear in total hip and knee replacements. J Bone Joint Surg Am. 1999;81:115-36.

[44] Fabi DW, Mohan V, Goldstein WM, Dunn JH, Murphy BP. Unilateral vs bilateral total knee arthroplasty risk factors increasing morbidity. J Arthroplasty. 2011;26:668-73.

[45] Thorey F, Stukenborg-Colsman C, Windhagen H, Wirth CJ. The effect of tourniquet release timing on perioperative blood loss in simultaneous bilateral cemented total knee arthroplasty: A prospective randomized study. Technol Health Care. 2008;16:85-92.

[46] Cram PL, Lu X, Kates SL, Singh JA, Li Y, Wolf BR. Total knee arthroplasty volume, utilization, and outcomes among medicare beneficiaries, 1991-2010. J Am Med Assoc. 2012;308.

[47] HCUPnet National statistics on all stays: 2005 outcomes by patient and hospital characteristics for ICD-9-CM principal procedure code 81.54 total knee replacement.

[48] Laurencin CT, Ambrosio AMA, Borden MD, Cooper JA, Jr. Tissue engineering: orthopedic applications. Annu Rev Biomed Eng. 1999;01:19-46.

[49] Langer R, Vacanti JP. Tissue Engineering. Science. 1993;260:920-6.

[50] Baksh D, Song L, Tuan RS. Adult mesenchymal stem cells: characterization, differentiation, and application in cell and gene therapy. J Cell Molec Med. 2004;8:301-16.

[51] Young RG, Butler DL, Weber W, Caplan AI, Gordon SL, Fink DJ. Use of mesenchymal stem cells in a collagen matrix for achilles tendon repair. J Orthopaedic Res. 1998;16:406-13.

[52] Caplan AI. Mesenchymal stem cells. J Orthopedic Res. 1991;9:641-50.

[53] Gao JZ, Dennis JE, Solchaga LA, Awadallah AS, Goldberg VM, Caplan AI. Tissue-engineered fabrication of an osteochondral composite graft using rat bone marrow-derived mesenchymal stem cells. Tissue Eng. 2001;7:363-71.

[54] Niederauer GG, Slivka MA, Leatherbury NC, Korvick DL, Harroff HH, Ehler WC, et al. Evaluation of multiphase implants for repair of focal osteochondral defects in goats. Biomaterials. 2000;21:2561-74.

[55] Schaefer D, Martin I, Shastri P, Padera RF, Langer R, Freed LE, et al. *In vitro* generation of osteochondral composites. Biomaterials. 2000;21:2599-606.

[56] Kreklau B, Sittinger M, Mensing MB, Voigt C, Berger G, Burmester GR, et al. Tissue engineering of biphasic joint cartilage transplants. Biomaterials. 1999;20:1743-9.

[57] Malafaya PB, Pedro AJ, Peterbauer A, Gabriel C, Redl H. Chitosan particles agglomerated scaffolds for cartilage and osteochondral tissue engineering approaches with adipose tissue derived stem cells. J Mater Sci Mater Med. 2005;16:1077-85.

[58] Schek RM, Taboas JM, Segvich SJ. Engineered osteochondral grafts using biphasic composite solid free-form fabricated scaffolds. Tissue Eng. 2004;10:1376-85.

[59] Nooeaid P, Salih V, Beier JP, Boccaccini AR. Osteochondral tissue engineering: scaffolds, stem cells and applications. J Cell Mol Med. 2012;16:2247-70.

[60] Balint L, Park SH, Bellyei A, Luck JV, Jr., Sarmiento A, Lovasz G. Repair of steps and gaps in articular cartilage fracture models. Clin Orthop Relat Res. 2005;430:208-18.

[61] Hunziker EB. Articular cartilage repair: basic science and clinical progress. A review of the current status and prospects. Osteoarthritis Cartilage. 2002;10:432-63.

[62] Karp JM, Dalton PD, Shoichet MS. Scaffolds for tissue engineering. MRS Bulletin. 2003:301-6.

[63] Khan Y, Yaszemski MJ, Mikos AG, Laurencin CT. Tissue engineering of bone: Material and matrix considerations. J Bone Joint Surg Am. 2008;90:36-42.

[64] Chen G, Ushida T, Tateishi T. Scaffold design for tissue engineering. Macromol Biosci. 2002;2:67-77.

[65] Liu C, Xia Z, Czernuszka JT. Design and development of three dimensional scaffolds for tissue engineering. Chem Eng Res Design. 2007;85:1051-64.

[66] Lavik E, Langer R. Tissue engineering: current state and perspectives. Appl Microbiol Biotechnol. 2004;65:1-8.

[67] Drury JL, Mooney DG. Hydrogels for tissue engineering: Scaffold design variables and applications. Biomaterials. 2003;24:4337-51.

[68] Lee KY, Mooney DJ. Hydrogels for tissue engineering. Chem Rev. 2001;101:1869-79.

[69] Cushing MC, Anseth KS. Hydrogel cell cultures. Science. 2007;316:1133-4.

[70] Hoffman AS. Hydrogels for biomedical applications. Adv Drug Delivery Rev. 2002;54:3-12.

[71] Hennink WE, van Nostrum CF. Novel crosslinking methods to design hydrogels. Adv Drug Deliv Rev. 2002;54:3-12.

[72] Peppas NA, Bures P, Leobandung W, Ichikawa H. Hydrogels in pharmaceutical formulations. Eur J Pharm Biopharm. 2000;50:27-46.

[73] Peppas NA, Hilt JZ, Khademhosseini A, Langer R. Hydrogels in biology and medicine. Adv Mater. 2006;18 1345–60.

[74] Dado D, Levenberg S. Cell-scaffold mechanical interplay within engineered tissues. Sem Cell Dev Biol. 2009;20:656-64.

[75] Kim BS, Nikolovski J, Bonadio J, Smiley E, Mooney DJ. Engineered smooth muscle tissues: regulating cell phenotype with the scaffold. Exp Cell Res. 1999;251:321-8.

[76] Benoit DSW, Schwartz MP, Durney AR, Anseth KS. Small functional groups for controlled differentiation of hydrogel-encapsulated human mesenchymal stem cells. Nat Mater. 2008;7:816-23.

[77] Crouch AS, Miller D, Luebke KJ, Hu W. Correlation of anisotropic cell behaviors with topographic aspect ratio. Biomaterials. 2009;30:1560-7.

[78] Khademhosseini A, Langer R. Microengineered hydrogels for tissue engineering. Biomaterials. 2007;28:5087.

[79] Keskar V, Marion NW, Mao JM, Gemeinhart RA. In vitro evaluation of macroporous hydrogels to facilitate stem cell infliltration, growth, and mineralization. Tissue Eng A. 2009;15:1695-707.

[80] Khetan S, Burdick JA. Patterning hydrogels in three dimensions towards controlling cellular interactions. Soft Matter. 2011;5:830-8.

[81] Glawe JD, Hill JB, Mills DK, McShane MJ. Influence of channel width on alignment of smooth muscle cells by high-aspect-ratio microfabricated elastomeric cell culture scaffolds. J Biomed Mater Res. 2005;75A:106-14.

[82] Odelius K, Hoeglund A, Kumar S, Hakkarainen M, Ghosh AK, Bhatnagar N. Porosity and pore size regulate the degradation product profile of polylactide. Biomacromolecules. 2011;12:1250-8.

[83] Woodfield TBF, Malda J, de Wign J, Peters F, Riesle J, van Blitterswijk CA. Design of porous scaffolds for cartilage tissue engineering using a three-dimensional fiber-deposition technique. Biomaterials. 2004;25:4149-61

[84] Wu L, Ding J. Effects of porosity and pore size on *in vitro* degradation of three-dimensional porous poly(D,L-lactide-*co*-glycolide) scaffolds for tissue engineering. J Biomed Mater Res. 2005;75A:767-77.

[85] Engler AJ, Tse JR. Stiffness gradients mimicking *in vivo* tissue variation regulate mesenchymal stem cell fate. PLoS One. 2011;6:e15978.

[86] Discher DE, Janmey P, Wang Y-L. Tissue cells feel and respond to the stiffness of their substrate. Science. 2005;310:1139-43.

[87] Liao H, Munoz-Pinto D, Qu X, Hou Y, Grunlan MA, Hahn MS. Influence of hydrogel mechanical properties and mesh size on vocal fold fibroblast extracellular matrix production and phenotype. Acta Biomater. 2008;4:1161-71.

[88] Hahn MS, Miller JS, West JL. Three-dimensional biochemical and biomechanical patterning for guiding cell behavior. Adv Mater. 2006;18:2679-84.

[89] Mann BK, Gobin AS, Tsai AT, Schmedlen RH, West JL. Smooth muscle cell growth in photopolymerized hydrogels with cell adhesive and proteolytically degradable domains: Synthetic ECM analogs for tissue engineering. Biomaterials. 2001;22:3045-51.

[90] Burdick JA, Anseth KS. Photoencapsulation of osteoblasts in injectable RGD-modified PEG hydrogels for bone tissue engineering. Biomaterials. 2002;23:4315-23.

[91] Yang F, Williams CG, Wang D-A, Lee H, Manson PN, Eliseef J. The effect of incorporating RGD adhesive peptide in polyethylene glycol diacrylate hydrogel on osteogenesis of bone marrow stromal cells. Biomaterials. 2005;26:5991-8.

[92] Gombotz WR, Guanghui W, Horbett TA, Hoffman AS. Protein adsorption to poly(ethylene oxide) surfaces. J Biomed Mater Res. 1991;25:1547-62.

[93] Bailey BM, Hui V, Fei R, Grunlan MA. Tuning PEG-DA hydrogel properties via solvent-induced phase separation (SIPS). J Mater Chem. 2011;21:18776-82.

[94] Zhang X-Z, Yang Y-Y, Chung T-S. Effect of mixed solvents on characteristics of poly(*N*-isopropylacrylamide) gels. Langmuir. 2002;18:2538-42.

[95] Shibayama M, Morimoto M, Nomura S. Phase separation induced mechanical transition of poly(*N*-isopropylacrylamide)/water isochore gels. Macromolecules. 1994;27:5060-6.

[96] Ford MC, Bertram JP, Hynes SR, Michaud M, Li Q, Young M, et al. A macroporous hydrogel for the coculture of neural progenitor and endothelial cells to form functional vascular networks in vivo. PNAS. 2006;103:2512-7.

[97] Yoon DM, Fisher JP. Chondrocyte signaling and artificial matrices for articular cartilage engineering. Adv Exp Med Biol. 2006;585:67-86.

[98] Bryant SJ, Anseth KS. Hydrogel properties influence ECM production by chondrocytes photoencapsulated in poly(ethylene glycol) hydrogels. J Biomed Mater Res. 2002;59:63-72.

[99] Hutmacher DW. Scaffold design and fabrication technologies for engineering tissues: State of the art and future perspectives. J Biomater Sci, Polym Ed. 2001;12:107-24.

[100] Bailey BM, Fei R, Munoz-Pinto D, Hahn MS, Grunlan MA. $PDMS_{star}$-PEG hydrogels prepared via solvent-induced phase separation (SIPS) and their potential utility as tissue engineering scaffolds. Acta Biomater. 2012;8:4324-33.

[101] Hou Y, Schoener CA, Regan KR, Munoz-Pinto D, Hahn MS, Grunlan MA. Photo-cross-linked $PDMS_{star}$-PEG Hydrogels: Synthesis, characterization, and potential application for tissue engineering scaffolds. Biomacromolecules. 2010;11:648-56.

[102] Ayala R, Zhang C, Yang D, Hwang Y, Aung A, Shroff SS, et al. Engineering the cell-material interface for controlling stem cell adhesion, migration, and differentiation. Biomaterials. 2011;32:3700-11.

[103] Fisher JP, Lalani Z, Bossano CM, Brey EM, Demian N, Johnston CM, et al. Effect of biomaterial properties on bone healing in a rabbit tooth extration socket model. J Biomed Mater Res Part A. 2004;68:428-38.

[104] Jansen EJP, Sladek REJ, Bahar H, Yaffe A, Gijbels MJ, Kuijer R, et al. Hydrophobicity as a design criterion for polymer scaffolds in bone tissue engineering. Biomaterials. 2005;26:4423-31.

[105] Song J-H, Yoon B-H, Kim Y-E, Kim H-W. Bioactive and degradable hybridized nanofibers of gelatin-siloxane for bone regeneration. J Biomed Mater Res. 2008;84:875-84.

[106] Ning CQ, Mehta J, El-Ghannam A. Effect of silica on the bioactivity of calcium phosphate composites *in vitro*. J Mater Sci Mater Med. 2005;16:355-60.

[107] Gupta G, El-Ghannam A, Kirakodu S, Khraisheh M, Zbib H. Enhancement of osteoblast gene expression by mechanically compatible porous Si-rich nanocomposite. J Biomed Mater Res 2007;81B:387-96.

[108] Munoz-Pinto D, Jimenez-Vergara AC, Hou Y, Hayenga HN, Grunlan MA, Hahn MS. Osteogenic potential of poly(ethylene glycol)-poly(dimethylsiloxane) hybrid hydrogels. Tissue Eng Part A. 2012;18:1-10.

[109] Bailey BM, Nail LN, Grunlan MA. Continuous gradient scaffolds for rapid screening of cell-material interactions and interfacial tissue regeneration. Acta Biomater. 2013;Accepted.

[110] Lo CT, Throckmorton DJ, Singh AK, Herr AE. Photopolymerized diffusion-defined polyacrylamide gradient gels for on-chip protein sizing. Lab Chip. 2008;8:1273-9.

[111] Dubruel P, Unger R, Vlierberghe SV, Cnudde V, Jacobs PJ, Schacht E, et al. Porous gelatin hydrogels: 2. *In vitro* cell interaction study. Biomacromolecules. 2007;8:338-44.

[112] Harley BA, Hastings AZ, Yannas IV, Sannino A. Fabricating tubular scaffolds with a radial pore size gradient by a spinning technique. Biomaterials. 2006;27:866-74.

[113] Nemir S, Hayenga HN, West JL. PEGDA hydrogels with patterned elasticity: novel tools for the study of cell response to substrate rigidity. Biotechnol Bioeng. 2010;105:636-44.

[114] Chatterjee K, Lin-Gibson S, Wallace WE, Parekh SH, Lee YJ, Cicerone MT, et al. The effect of 3D hydrogel scaffold modulus on osteoblast differentiation and mineralization revealed by combinatorial screening. Biomaterials. 2010;31:5051-62.

[115] Singh M, Tech B, Berkland C, Detamore MS. Strategies and applications for incorporating physical and chemical signal gradients in tissue engineering. Tissue Eng Part B. 2008;14:341-66.

[116] Tanahashi M, Matsuda T. Surface functional group dependence on apatite formation on self-assembled monolayers in a simulated body fluid. J Biomed Mater Res. 1997;34:305-15.

[117] Keselowsky BG, Collard DM, Garcia AJ. Integrin binding specificity regulates biomaterial surface chemistry effects on cell differentiation. Proc Natl Acad Sci USA. 2005;102:5953-7.

[118] Keselowsky BG, Collard DM, Garcia AJ. Surface chemistry modulates fibronectin conformation and directs integrin binding and specificity to control cell adhesion. J Biomed Mater Res A. 2003;66:247-59.

[119] Tretinnikov ON, Kato K, Ikada Y. *In vitro* hydroxyapatite deposition onto a film surface-grafted with organophosphate polymer. J Biomed Mater Res. 1994;28:1365-73.

[120] Gemeinhart RA, Bare CM, Haasch RT, Gemeinhart EJ. Osteoblast-like cell attachment to and calcification of novel phosphonate-containing polymeric substrates. J Biomed Mater Res Part A. 2006;78:433-40.

[121] Stancu IC, Filmon R, Cincu C, Marculescu B, Zaharia C, Tourman Y, et al. Synthesis of methacryloyloxyethyl phosphate copolymers and in vitro calcification capacity. Biomaterials. 2004;25:205-13.

[122] Yin YJ, Luo XY, Cui JF, Wang CY, Guo XM, Yao KD. A study on biomineralization behavior of n-methylene phosphochitosan scaffolds. Macromol Biosci. 2004;4:971.

[123] Tan J, Gemeinhart RA, Ma M, Saltzman WM. Improved cell adhesion and proliferation on synthetic phosphonic acid-containing hydrogels. Biomaterials. 2005;26:3663-71.

[124] Wang D-A, Williams CG, Li Q, Sharma B, Eliseef J. Synthesis and characterization of a novel degradable phosphate-containing hydrogel. Biomaterials. 2003;24:3969-80.

[125] Nuttelman CR, Benoit DS, Tripodi MC, Anseth KS. The effect of ethylene glycol methacrylate phosphate in PEG hydrogels on mineralization and viability of encapsulated hMSCs. Biomaterials. 2006;27:1377-86.

[126] Nuttelman CR, Benoit DSW, Tripodi MC, Anseth KS. The effect of ethylene glycol methacrylate phosphate in PEG hydrogels on mineralization and viability of encapsulated hMSCs. Biomaterials. 2006;27:1377-86.

[127] Hou Y, Schoener CA, Regan KR, Munoz-Pinto D, Hahn MS, Grunlan MA. Photo-crosslinked PEO-PDMSstar hydrogels: Synthesis, characterization, and potential application for tissue engineering scaffolds. Biomacromolecules. 2010;11:648-56.

[128] Lin S, Sangaj N, Razafiarison T, Zhang C, Varghese S. Influence of physical properties of biomaterials on cellular behavior. Pharm Res. 2011;28:1422-30.

[129] Klawitter J, Hulbert SJ. Biomed Mater Res Symp. 1983;2:161.

[130] Spector M, Michno MJ, Smarook WH, Kwiakowski GT. Biomed Mater Res Symp. 1978;12:655.

[131] Dutta RC, Dutta AK. Cell-interactive 3D-scaffold; advances and applications. Biotech Adv. 2009;27:334-9.

[132] Kleinman HK, Philp D, Hoffman MP. The role of the extracellular matrix in morphogenesis. Curr Opin Biotechnol. 2003;14:526-32.

[133] Lutolf MP, Hubbell JA. Synthetic biomaterials as instructive extracellular microenvironments for morphogensis in tissue engineering. Nature Biotech. 2005;23:47-55.

[134] Brandl F, Sommer F, Goepferich A. Rational design of hydrogels for tissue engineering: Impact of physical factors on cell behavior. Biomaterials. 2007;28:134-6.

[135] Pennesi C, Scaglione S, Gionnoni P, Quarto R. Regulatory influence of scaffolds on cell behavior: How cells decode biomaterials. Curr Pharm Biotech. 2011;12:151-9.

[136] Nichol JW, Khademhosseini A. Modular tissue engineering: Engineering biological tissues from the bottom up. Soft Matter. 2009;5:1312.

[137] Khetan S, Burdick JA. Patterning hydrogels in three dimensions towards controlling cellular interactions. Soft Matter. 2011;7:830-8.

[138] Woodfield TBF, Moroni L, Malda J. Combinatorial approaches to controlling cell behaviour and tissue formation in 3D via rapid-prototyping and smart scaffold design. Comb Chem High Throuput Screen. 2009;12:562-79.

[139] McGlohorn JB, W.D. Holder J, Grimes LW, Thomas CB, Burg KJL. Evaluation of smooth muscle cell response using two types of porous polylactide scaffolds with differing pore topography. Tissue Eng. 2004;10:505-14.

[140] Engler AJ, Sen S, Sweeney HL, Discher DE. Matrix elasticity directs stem cell lineage specification. Cell. 2006;126:677-89.

[141] Paxton JZ, Donnelly K, Keatch RP, Baar K. Engineering the bone-ligament interface using polyethylene glycol diacrylate incorporated with hydroxyapatite. Tissue Eng. 2009;15:1201-9.

[142] Bryant SJ, Nicodemus GD, Vallanueva I. Designing 3D photopolymer hydrogels to regulate biomechanical cues and tissue growth for cartilage tissue engineering. Pharm Res. 2008;25:2379-86.

[143] Hahn MS, McHale MK, Wang E, Schmedlen RH, West JL. Physiological pulsatile flow bioreactor conditioning of poly(ethylene glycol)-based tissue engineering grafts. Ann Biomed Eng. 2007;35:190-200.

[144] Mahoney MJ, Anseth KS. Three-Dimensional growth and function of neural tissue in degradable polyethylene glycol hydrogels. Biomaterials. 2006;27:2265-74.

[145] Zhang H, Wang L, Song L, Niu G, Cao H, Wang G, et al. Controllable properties and microstructure of hydrogels based on crosslinked poly(ethylene glycol) diacrylates with different molecular weights. J Appl Polym Sci. 2011;121:531-40.

[146] Munoz-Pinto D, Bulick AS, Hahn MS. Inorganic-organic hybrid scaffolds for osteochondral regeneration. Biomed Mat Res A. 2009;90A:303-16.

[147] Malda J, Woodfield TBF, Vloodt Fvd, Wilson C, Martens DE, Tramper J, et al. The effect of PEGT/PBT scaffold architecture on the composition of tissue engineered cartilage. Biomaterials. 2006;26:63-72.

[148] Wang H, Pieper J, Peters F, Blitterswijk CAv, Lamme EN. Synthetic scaffold morphology controls human dermal connective tissue formation. J Biomed Mat Res. 2005;74A:523-32.

[149] Zeltinger J, Sherwood JK, Graham DA, Muller R, Griffith LG. Effect of pore size and voice fraction on cellular adhesion, proliferation, and matrix deposition. Tissue Eng. 2001;7:557-72.

[150] Khetan S, Katz JS, Burdick JA. Sequential crosslinking to control cellular spreading in 3 dimensional hydrogels. Soft Matter. 2009;5:1601-6.

[151] Ford MC, Bertram JP, Hynes SR, Michaud M, Li Q, Young M, et al. A macroporous hydrogel for the coculture of neural progenitor and endothelial cells to form functional vascular networks *in vivo*. Proc Nat Acad Sci. 2006;103:2512-7.

[152] Wu L, Ding J. Effects of porosity and pore size on *in vitro* degradation of three-dimensional porous poly(D,L-lactide-*co*-glycolide) scaffolds for tissue engineering. J Biomed Mat Res. 2005;75A:767-77.

[153] Chen C-W, Betz MW, Fisher JP, Paek A, Chen Y. Macroporous hydrogel scaffolds and their characterization by optical coherence tomography. Tissue Eng C. 2011;17:101-12.

[154] Chiu Y-C, Larson JC, A. Isom J, Brey EM. Generation of porous poly(ethylene glycol) hydrogels by salt leaching. Tissue Eng Part C. 2010;16:905-12.

[155] Hwang Y, Sangaj N, Varghese S. Interconnected macroporous poly(ethylene glycol) cryogels as a cell scaffold for cartilage tissue engineering. Tissue Eng A. 2010;16:3033-41.

[156] Hwang Y, Zhang C, Varghese S. Poly(ethylene glycol) cryogels as potential cell scaffolds: Effect of polymerization conditions on cryogel microstructure and properties. J Mater Chem. 2010;20:345-51.

[157] Sannino A, Netti PA, Madaghiele V, Coccoli V, Luciani A, Maffezzoli A, et al. Synthesis and characterization of macroporous poly(ethylene glycol)-based hydrogels for tissue engineering application. J Biomed Mater Res A. 2006:229-36.

[158] Annabi N, Nichol JW, Zhong X, Ji C, Koshy S, Khademhosseini A, et al. Controlling porosity and microarchitecture of hydrogels for tissue engineering. Tissue Eng B. 2010;16:371-83.

[159] Ulery BD, Nair LS, Laurencin CT. Biomedical applications of biodegradable polymers. J Polym Sci 2011;49B:832-64.

[160] Metters AT, Anseth KS, Bowman CN. Fundamental studies of a novel, biodegradable PEG-*b*-PLA hydrogel. Polymer. 2000;41:3993-4004.

[161] Bryant SJ, Durand KL, Anseth KS. Manipulations in hydrogel chemistry control photoencapsulated chondrocyte behavior and their extracellular matrix production. J Biomed Mater Res. 2003;67A:1430-6.

[162] Sawhney AS, Pathak CP, Hubbell JA. Bioerodible hydrogels based on photopolymerized poly(ethylene glycol)-*co*-poly(α–hydroxy acid) diacrylate macromers. Macromolecules. 1993;26:581-7.

[163] McBath RA, Shipp DA. Swelling and degradation of hydrogels synthesized with degradable poly(β-amino ester) crosslinkers. Polym Chem. 2010;1:860-5.

[164] Metters A, Hubbell J. Network formation and degradation behaviors of hydrogels formed by Michael-type addition reactions. Biomacromolecules. 2005;6:290-301.

[165] Halstenberg S, Panitch A, Rizzi S, Hall H, Hubbell JA. Biologically engineered protein-*graft*-poly(ethylene glycol) hydrogels: a cell adhesive and plasmin-degradable biosynthetic material for tissue repair. Biomacromolecules. 2002;3:710-23.

[166] West JL, Hubbell JA. Polymeric biomaterials with degradation sites for proteases involved in cell migration. Macromolecules. 1999;32:241-4.

[167] Joy A, Cohen DM, Luk A, Anim-Danso E, Chen C, Kohn J. Control of surface chemistry, substrate stiffness, and cell function in a novel terpolymer methacrylate library. Langmuir. 2011;27:1891-9.

[168] Escobar-Ivirico JL, Salmeron-Sanchez M, Gomez-Ribelles JL, Monleon-Pradas M, Soria JM, Gomes ME, et al. Proliferation and differentiation of goat bone marrow stromal cells in 3D scaffolds with tunable hydrophilicity. J Biomed Mater Res. 2009;91B:277-86.

[169] Lu L, Garcia CA, Mikos AG. *In vitro* degradation of thin poly(DL-lactic-*co*-glycolic acid) films. J Biomed Mat Res. 1999;46:236-44.

[170] Odelius K, Hoglund A, Kumar S, Hakkarainen M, Ghosh AK, Bhatnagar N, et al. Porosity and pore size regulate the degradation product profile of polylactide. Biomacromolecules. 2011;12:1250-8.

[171] Peters R, Litvinov VM, Steeman P, Dias AA, Mengerink Y, Benthem Rv, et al. Characterisation of UV-cured acrylate networks by means of hydrolysis followed by aqueous size-exclusion combined with reversed-phase chromatography. J Chromatography 2007;11A:111-23.

[172] Woodfield TBF, Moroni L, Malda J. Combinatorial approaches to controlling cellular interactions. Soft Matter. 2009;12:562-79.

[173] Ren L, Tsuru K, Hayakawa S, Osaka A. Novel approach to fabricate porous gelatin-siloxane hybrids for bone tissue engineering. Biomaterials. 2002;23:4765-73.

[174] Escobar-Ivirico JL, Salmeron-Sanchez M, Gomez-Ribelles JL, Monleon-Pradas M, Soria JM, Gomes ME, et al. Proliferation and differentiation of goat bone marrow stromal cells in 3D scaffolds with tunable hydrophilicity. J Biomed Mater Res. 2009;91B:277-86.

[175] Anseth KS, Bowman CN, Brannon-Peppas L. Mechanical properties of hydrogels and their experimental determination. Biomaterials. 1996;17:1647-57.

[176] Munoz-Pinto D, Bulick AS, Hahn MS. Uncoupled investigation of scaffold modulus and mesh size on smooth muscle cell behavoir J Biomed Mater Res. 2009;90A:303-16.

[177] Gudipati CFG, Greenlief CM, Johnson JA, Prayongpan P, Wooley KL. Hyperbranched fluoropolymer (HBFP) and linear poly(ethylene glycol) (PEG) based on amphiphilic crosslinked networks as efficeint anti-fouling coatings: An insight into the surface compositions, topographies and morphologies. J Polym Sci Part A: Polym Chem. 2004;42:6193-208.

[178] McGlohorn JB, Holder J, Grimes LW, Thomas CB, Burg KJL. Evaluation of smooth muscle cell response using two types of porous polylactide scaffolds with differing pore topography. Tissue Eng. 2004;10:505-14.

[179] Sarkar S, Dadhania M, Rourke P, Desai TA, Wong JY. Vascular tissue engineering: microtextured scaffold templates to control organization of vascular smooth muscle cells and extracellular matrix. Acta Biomater. 2005;1:93-100.

[180] Kim B-S, Nikolovski J, Bonadio J, Smiley E, Mooney DJ. Engineered smooth muscle tissues: regulating cell phenotype with the scaffold. Exp Cell Res. 1999;251:321-8.

[181] Lin NJ, Lin-Gibson S. Osteoblast response to dimethacrylate composites varying in composition, conversion and roughness using a combinatorial approach. Biomaterials. 2009;30:4480-7.

[182] Ning CQ, Mehta J, El-Ghannam A. Effect of silica on the bioactivity of calcium phosphate composites *in vitro*. J Mater Sci Mater Med. 2005;16:355-60.

[183] Song J-H, Yoon B-H, Kim Y-E, Kim H-W. Bioactive and degradable hybridized nanofibers of gelatin-siloxane for bone regeneration. J Biomed Mater Res. 2008;84:875.

[184] McBath RA, Shipp DA. Swelling and degradation of hydrogels synthesized with degradable poly(β−amino ester) crosslinkers. Polym Chem. 2010;1:860-5.

[185] Grunlan MA, Lee NS, Mansfield F, Kus E, Finlay JA, Callow JA, et al. Minimally invasive polymer surfaces prepared from star oligosiloxanes and star oligofluorosiloxanes. J Polym Sci, Part A: Polym Chem. 2006;44.

[186] Kokubo T, Takadama H. How useful is SBF in predicting in vivo bone bioactivity? Biomaterials. 2006;27:2907-15.

[187] Lynn AD, Kyriakides TR, Bryant SJ. Characterization of the *in vitro* macrophage response and *in vivo* host response to poly(ethylene glycol)-based hydrogels. J Biomed Mater Res. 2010;93A:941-53.

[188] Zhang H, Wang L, Song L, Niu G, Cao H, Wang G, et al. Controllable properties and microstructure of hydrogels based on crosslinked poly(ethylene glycol) diacrylates with different molecular weights. J Appl Polym Sci. 2011;121:531-40.

[189] Griffith LG. Polymeric biomaterials. Acta Mater. 2000;48:263-77.

[190] Hench LL. Bioceramics. J Amer Ceram Soc. 1998;81:1705-28.

[191] Habibovic P, deGroot K. Osteoinductive biomaterials - properties and relavence in bone repair. J Tissue Eng Regen Med. 2007;1:25-32.

[192] Kokubo T, Kushitani H, Sakka S, Kitugi T, Yamanuro T. Solutions able to reporduce in vivo surface-structure changes in bioactive glass-ceramic. J Biomed Mater Res Part A. 1990;24:721-34.

[193] Liji Sobhana SS, Sundaraseelan J, Sekar S, Sastry TP, Mandal AB. Gelatin-chitosan composite capped gold nanoparticles: a matrix for the growth of hydroxyapatite. J Nanopart Res. 2009;11:333-40.

[194] Kim BS, Nikolovski J, Bonadio J, Smiley E, Mooney DJ. Engineered smooth muscle tissues: regulating cell phenotype with the scaffold. Exp Cell Res. 199;251:321-8.

[195] Ju H, McCloskey BD, Sagle AC, Kusuma VA, Freeman BD. Preparation and characterization of crosslinked poly(ethylene glycol) diacrylate hydrogels as fouling - resistant membrane coatings. J Membr Sci. 2009;330:180-8.

[196] Yang F, Williams CG, Wang D-A, Lee H, Manson PN, Elisseeff J. The effect of incorporating RGD adhesive peptide in polyethylene glycol diacrylate hydrogel on osteogenesis of bone marrow stromal cells. Biomaterials. 2005;26:5991-8.

[197] Burdick JA, Anseth KS. Photoencapsulation of osteoblasts in injectable RGD-modified PEG hydrogels for bone tissue engineering. Biomaterials 2002;23:4315-23.

[198] Munoz-Pinto DJ, Bulick AS, Hahn MS. Uncoupled investigation of scaffold modulus and mesh size on smooth muscle cell behavior. J Biomed Mater Res Part A. 2009;90A:303-16.

[199] Renner K, Amberger A, Konwalinka G, Kofler R, Gnaiger E. Changes of mitochondrial respiration, mitochondrial content and cell size after induction of apoptosis in leukemia cells. Biochim Biophys Acta. 2003;1642:115-23.

[200] Subramony SD, Dargis BR, Castillo M, Azeloglu EU, Tracey MS, Su A, et al. The guidance of stem cell differentiation by substrate alignment and mechanical stimulation. Biomaterials. 2013;34:1942-53.

[201] Ziats NP, Miller KM, Anderson JM. *In vitro* and *in vivo* interactions of cells with biomaterials. Biomaterials. 1988;9:5-13.

[202] Simon CG, Yang Y, Thomas V, Dorsey SM, Morgan AW. Cell interactions with biomaterials gradients and arrays. Comb Chem High Throughput Screen. 2009;12:544-53.

[203] Meredith JC, Sormana JL, Keselowsky BG, Garcia AJ, Tona A, Karim A, et al. Combinatorial characterization of cell interactions with polymer surfaces. J Biomed Mater Res A. 2003;66:483-90.

[204] Anderson DG, Levenberg S, Langer R. Nanoliter-scale synthesis of arrayed biomaterials and application to human embryonic stem cells. Nat Biotechnol. 2004;22:863-6.

[205] Fischbach C, Chen R, Matsumoto T, Schmelze T, Brugge JS, Polverini PJ, et al. Engineering tumors with 3D scaffolds. Nat Methods. 2007;4:855-60.

[206] Tanaka H, Murphy CL, Kimura M, Kawai S, Polak JM. Chondrogenic differentiation of murine embryonic stem cells: Effects of culture conditions and dexamethasone. J Cell Biochem. 2004;93:454-62.

[207] Tibbitt MW, Anseth KS. Hydrogels as extracellular matrix mimics for 3D cell culture. Biotechnol Bioeng. 2009;103:655-63.

[208] Bailey BM, Hui V, Fei R, Grunlan MA. Tuning PEG-DA hydrogel properties *via* solvent-induced phase separation (SIPS). J Mater Chem. 2011;21:18776-82.

[209] Grunlan MA, Lee NS, Mansfeld F, Kus E, Finlay JA, Callow JA, et al. Minimally adhesive polymer surfaces prepared from star oligosiloxanes and star oligofluorosiloxanes. J Polym Sci, Part A: Polym Chem. 2006;44:2551-66.

[210] Hou Y, Regan KR, Schoener CA, Hahn MS, Grunlan MA. Inorganic-organic hydrogels with tunable properties. POLY Preprints (Amer Chem Soc, Div Poly Chem). 2007;48:900-1.

[211] Bailey BM, Fei R, Munoz-Pinto D, Hahn MS, Grunlan MA. $PDMS_{star}$-PEG hydrogel scaffolds prepared via solvent-induced phase separation (SIPS). Acta Biomaterialia. 2012;in press on-line.

[212] Sobhana SS, Sundaraseelan J, Sekar S, Sastry TP, Mandal AB. Gelatin-chitosan composite capped gold nanoparticles: a matrix for the growth of hydroxyapatite. J Nanopart Res. 2009;11:333-40.

[213] Bailey BM, Hou Y, Grunlan MA. Tailoring the properties of PDMS-PEG hydrogel scaffolds. POLY Preprints (Amer Chem Soc, Div Chem),. 2012;53:480.

[214] Bailey BM, Hou Y, Grunlan MA. Photo-crosslinked $PDMS_{star}$-PEG hydrogels: Fabrication and use as tissue engineering scaffolds. POLY Preprints (Amer Chem Soc, Div Chem),. 2010;51:18-9.

[215] Toh WS, Lim TC, Kurisawa M, Spector M. Modulation of mesenchymal stem cell chondrogenesis in a tunable hyaluronic acid hydrogel microenvironment. Biomaterials. 2012;33:3835-45.

[216] Kloxin AM, Benton JA, Anseth KS. *In situ* elasticity modulation with dynamic substrates to direct cell phenotype. Biomaterials. 2010;31:1-8.

[217] Huebsch N, Arany PR, Mao AS, Shvartsman D, Ali OA, Bencherif SA, et al. Harnessing traction-mediated manipulation of the cell-matrix interface to control stem cell fate. Nat Mater. 2010;9:518-26.

[218] Mitra J, Tripathi G, Sharma A, Basu M. Scaffolds for bone tissue engineering: role of surface patterning on osteoblast response. RSC Adv. 2013:1-22.

[219] Vijayasekaran S, Chirila TV, Robertson TA, Lou X, Fitton JH, Hicks CR, et al. Calcification of poly(2-hydroxyethyl methacrylate) hydrogel sponges implanted in the rabbit cornea: a 3-month study. J Biomater Sci Polym Ed. 2000;11:599-615.

[220] Wu Y, Ackerman JL, Strawich ES, Rey C, Kim H-M, Glimcher MJ. Phosphate ions in bone: identification of a calcium-organic phosphate complex by ^{31}P solid-state NMR spectroscopy at early stages of mineralization. Calcif Tissue Int. 2003;72:610-26.

[221] Zhou CJ, Guan RF, Feng SY. The preparation of a new polysiloxane copolymer with glucosylthioureylene groups on the side chains. European Polymer Journal. 2004;40:165-70.

[222] Ragheb RT. Synthesis and characterization of polylactide-siloxane block copolymers as magnetite nanoparticle dispersion stabilizers: Virginia Polytechnic Institute and State University; 2005.

[223] Zhang D, Burkes WL, Schoener CA, Grunlan MA. Porous inorganic-organic shape memory polymers. Polymer. 2012;53:2935-41.

APPENDIX

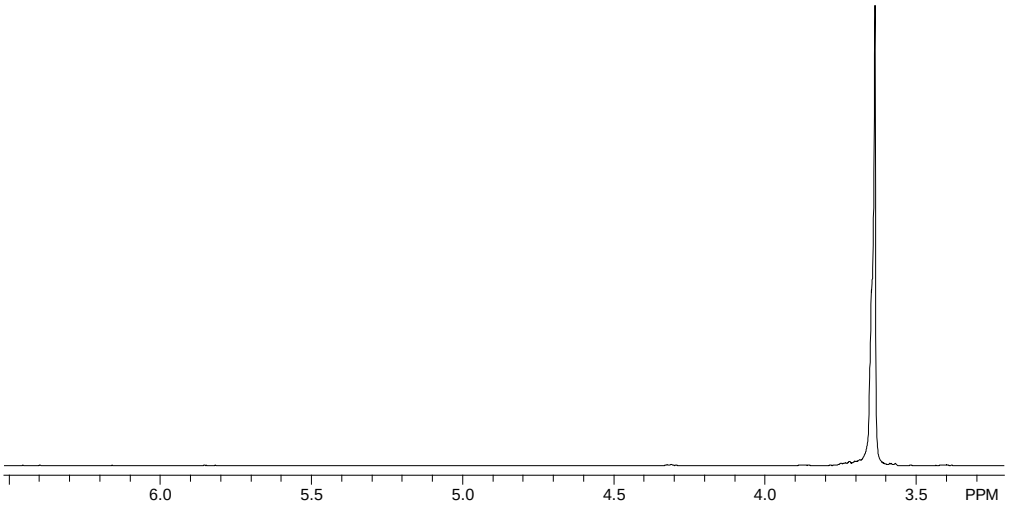

^{1}H-NMR of PEG-DA (3.4k g/mol) [From Chapters II and III]

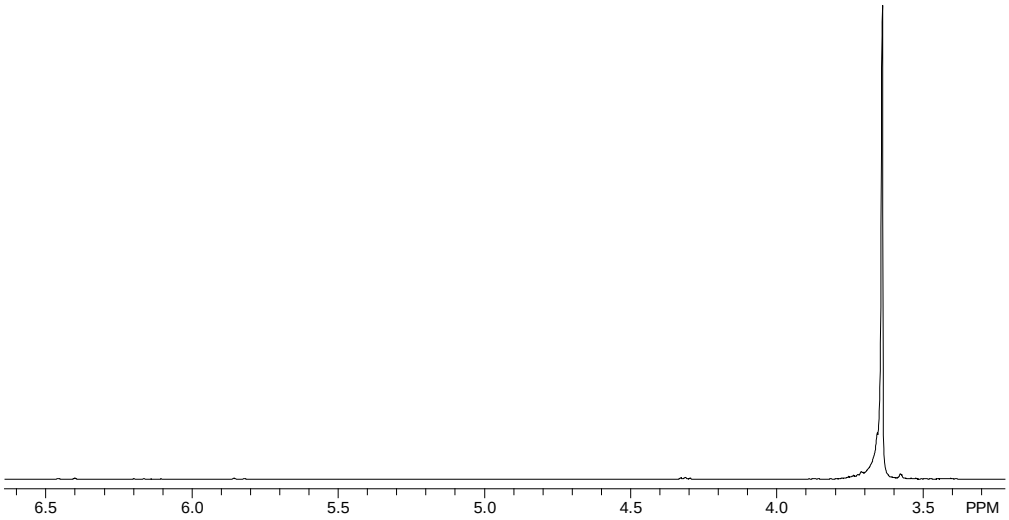

^{1}H-NMR of PEG-DA (6k g/mol) [From Chapters II and III]

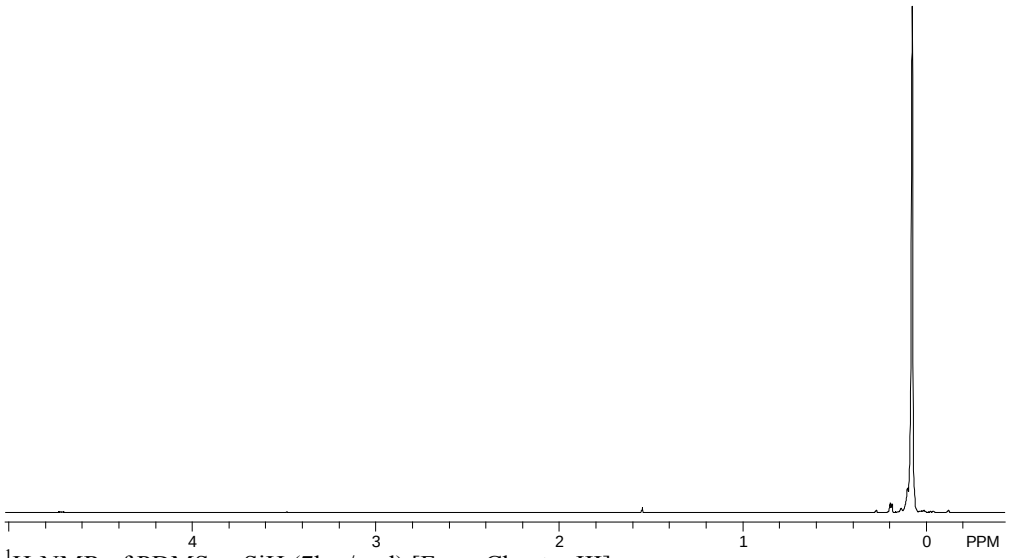

^{1}H-NMR of PDMS$_{star}$-SiH (7k g/mol) [From Chapter III]

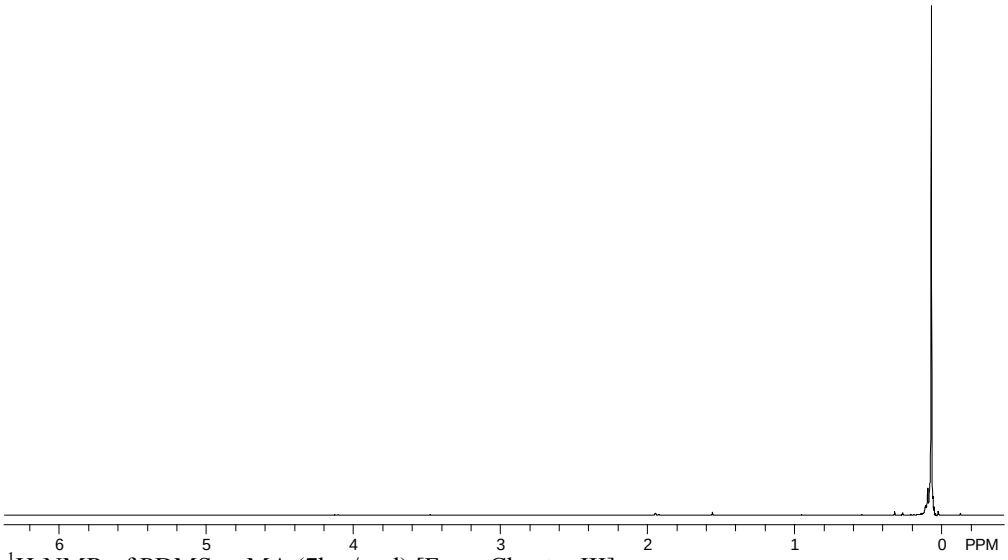

^{1}H-NMR of PDMS$_{star}$-MA (7k g/mol) [From Chapter III]

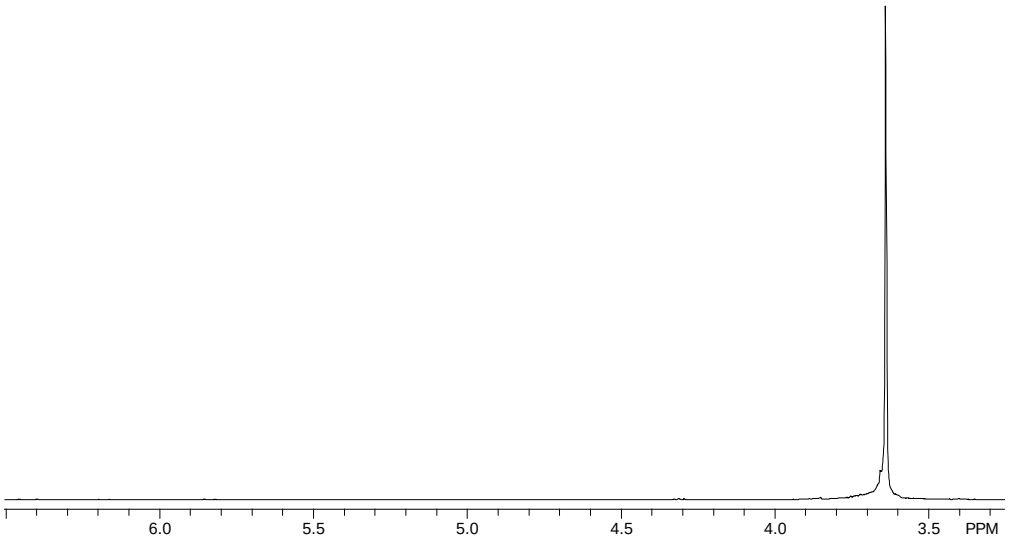

^{1}H-NMR of PEG-DA (3.4k g/mol) [From Chapter IV]

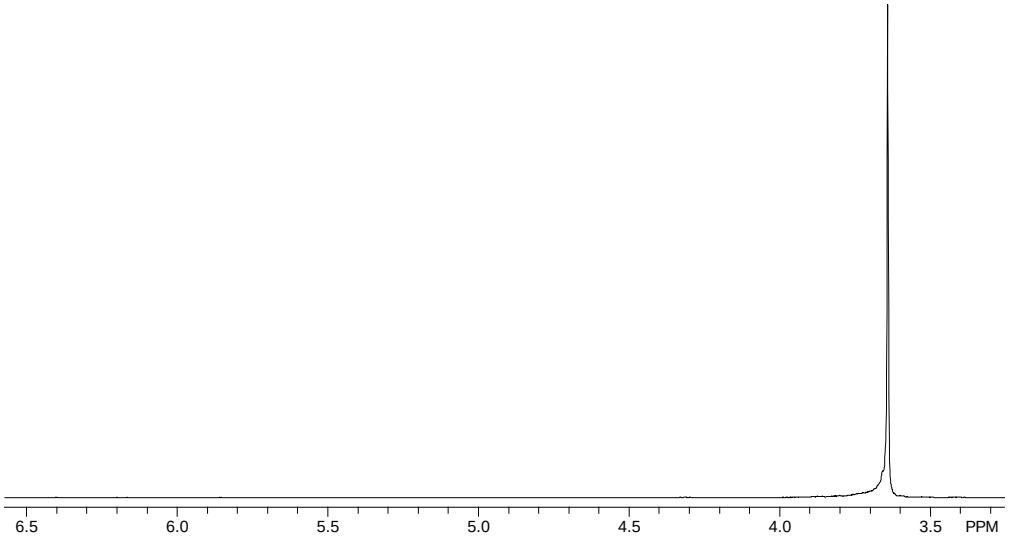

^{1}H-NMR of PEG-DA (6k g/mol) [From Chapter IV]

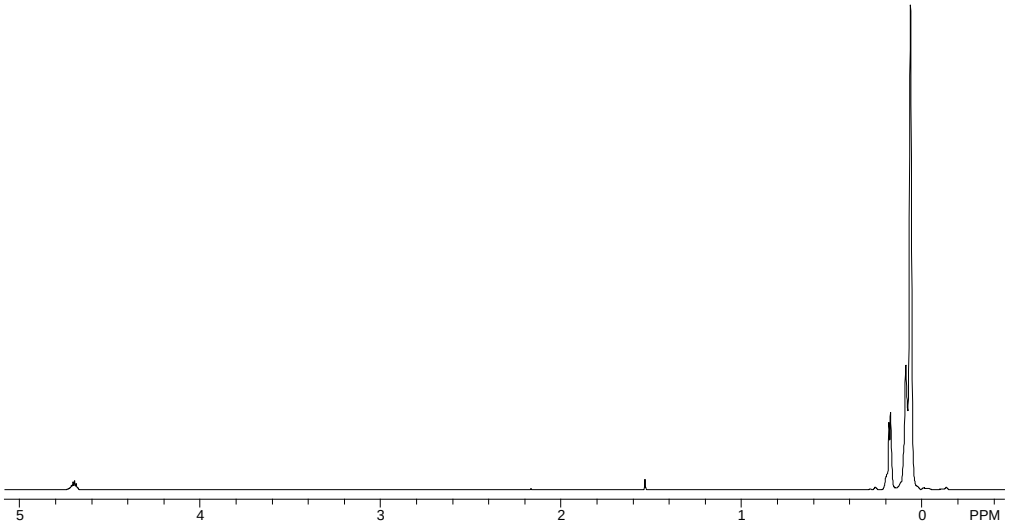

^{1}H-NMR of PDMS$_{star}$-SiH (1.8k g/mol) [From Chapter IV]

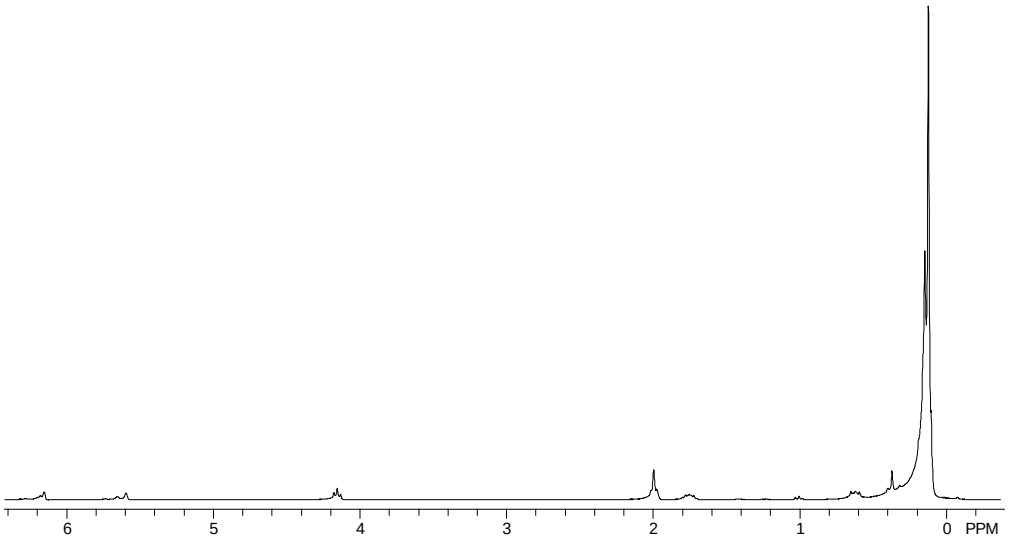

^{1}H-NMR of PDMS$_{star}$-MA (1.8k g/mol) [From Chapter IV]

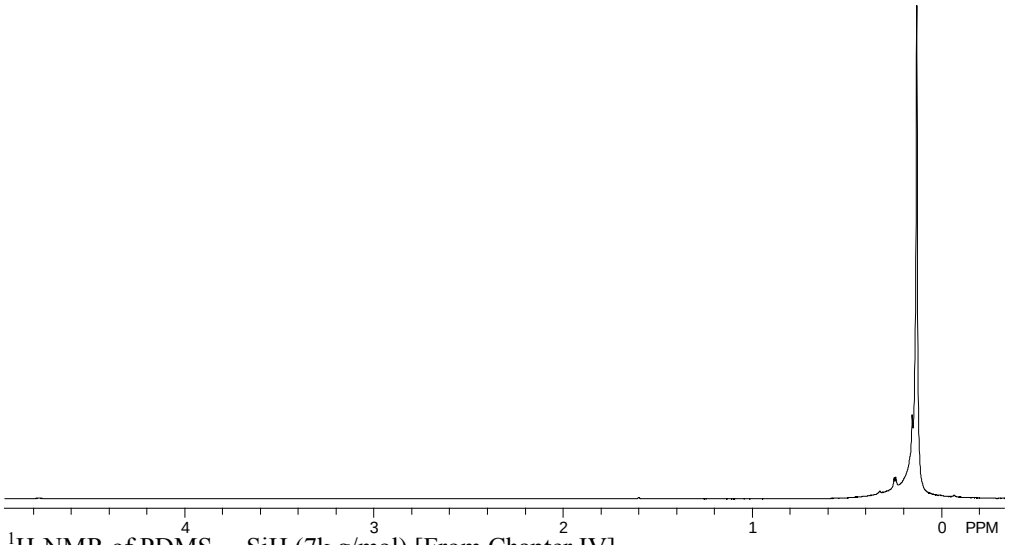

^{1}H-NMR of PDMS$_{star}$-SiH (7k g/mol) [From Chapter IV]

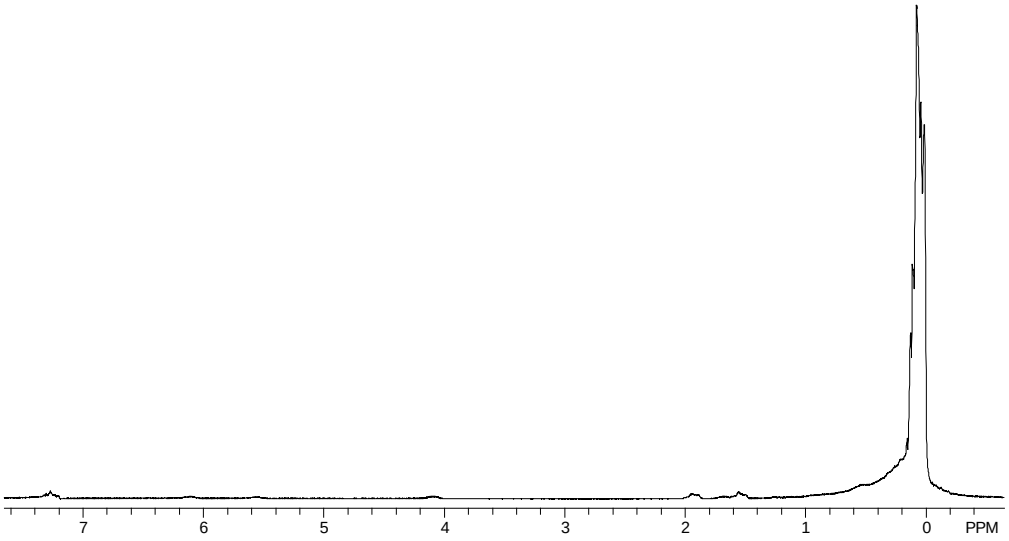

^{1}H-NMR of PDMS$_{star}$-MA (7k g/mol) [From Chapter IV]

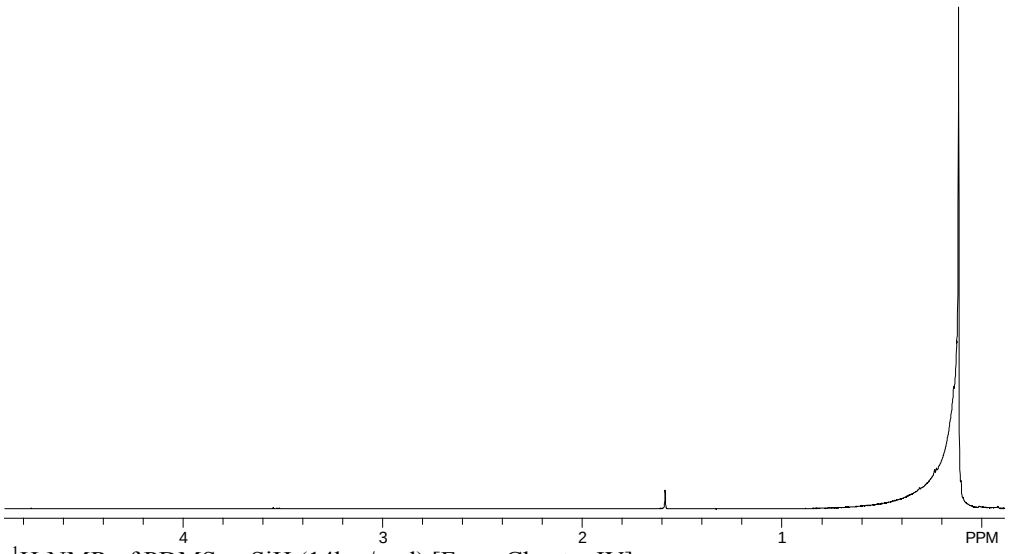

^{1}H-NMR of PDMS$_{star}$-SiH (14k g/mol) [From Chapter IV]

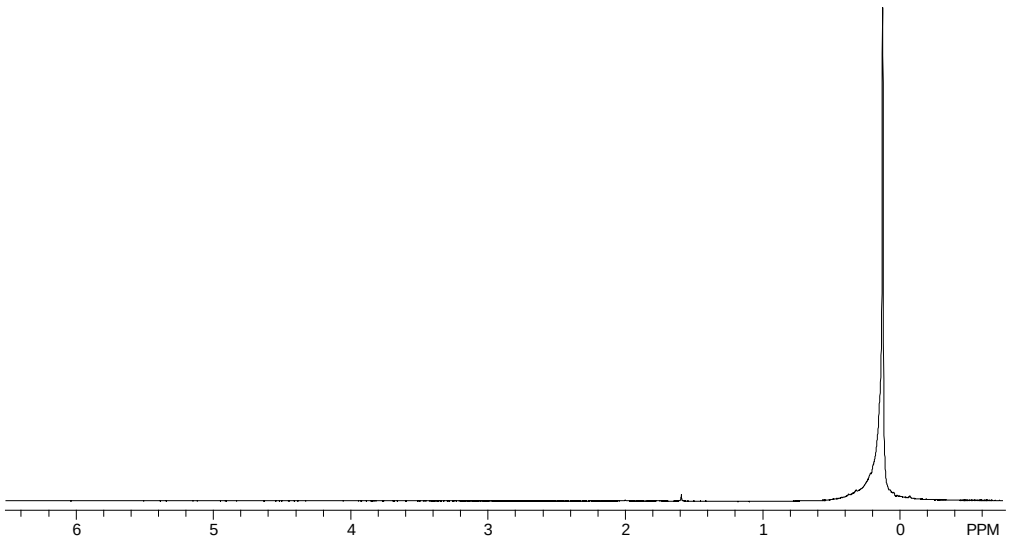

^{1}H-NMR of PDMS$_{star}$-SiH (14k g/mol) [From Chapter IV]

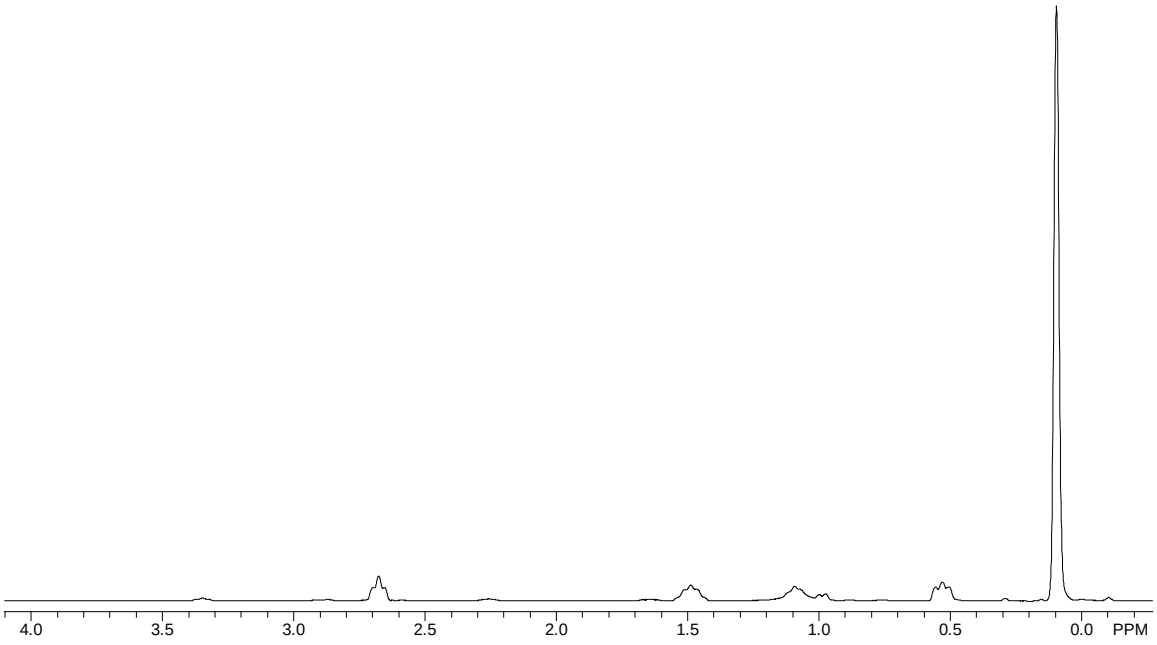

^{1}H-NMR of D_4^{NH2} [From Chapter V]

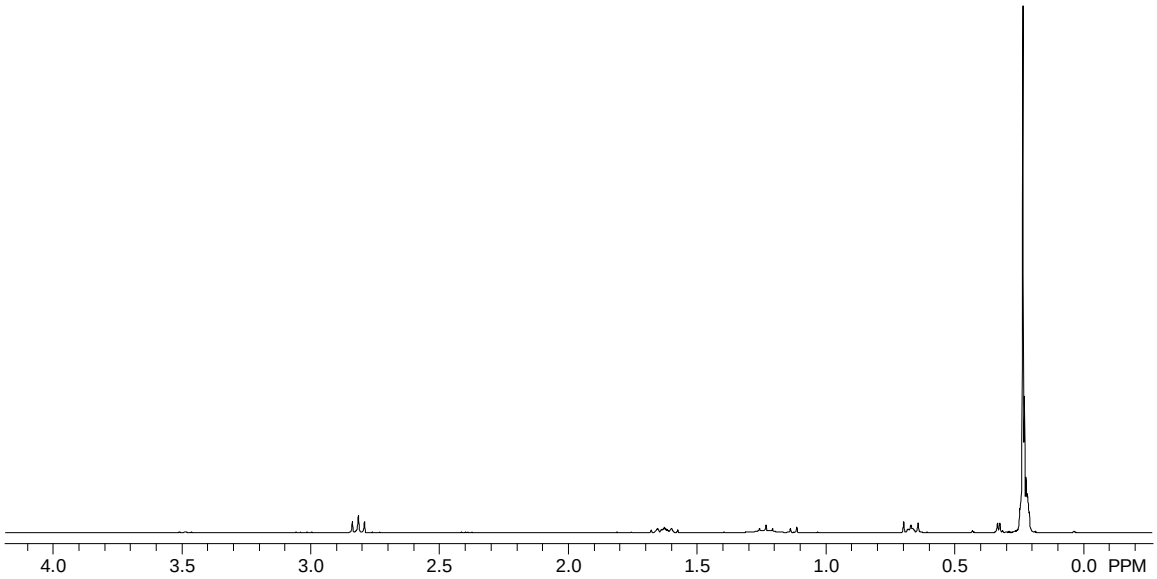

^{1}H-NMR of P-D_4^{NH2} [From Chapter V]